ANALYSIS OF BINARY PHOSPHOLIPID BILAYERS WITH A SELF-CONSISTENT FIELD THEORY

NAN ZHENG

Analysis of Binary Phospholipid Bilayers with a Self-Consistent Field Theory

by

© Nan Zheng

A thesis submitted to the
School of Graduate studies
in partial fulfillment of the
requirements for the degree of
Master of Science

Department of Physics and Physical Oceanography,
Memorial University of Newfoundland

August, 2005

St. John's Newfoundland

Your file Votre référence
ISBN: 978-0-494-19410-2
Our file Notre référence
ISBN: 978-0-494-19410-2

Abstract

This thesis applies a self-consistent field theory of compressible, fully hydrated phospholipid binary mixtures to an idealized model of binary bilayers. The theory is extended to calculate the average order parameter and gauche isomer number on each layer, as well as distributions of the chain-segments. It then makes calculations for a series of mixtures to present systematically the effects of composition and chain length mismatch on the structural properties, and to make comparison with experiments. In the theory, the effective fields, and the inhomogeneous particle and bond distributions throughout the bilayer interior are related self-consistently. This allows numerical calculation of all these properties.

Experimental results for binary mixtures such as distearoylphosphatidylcholine (DSPC)/ dimyristoylphosphatidylcholine (DMPC) and galactosylceramide (GalCer)/1-stearoyl-2-oleoyl phosphatidylcholine (SOPC) show the influence of chain length mismatch and composition on each component, in particular a feature called the "second plateau" in the order parameter profile near the tail of the long chain. To interpret and compare with these systems and phenomena are the foci of this work

Acknowledgements

I would like to take this opportunity to express my deep gratitude to my supervisor Professor Mark Whitmore for his kind patience, valuable guidance, and continuous support throughout my research, and for giving me the opportunity to work and learn new things in his research group. I really appreciate all he has taught me and all he has done for me during these two years of graduate study.

I also wish to express my particular gratitude to Professor John Whitehead and Professor Michael Morrow for their advices on my thesis and instructions on my seminar.

Besides, I would like to thank Professor Jolantal Lagowski, Professor John Lewis, Professor Michael Morrow and Professor Mark Whitmore (according to alphabetic sequence of last name) for their courses, which greatly deepened my understanding of physics.

I also wish to thank Ian Skanes. He helped me a lot in understanding quickly the former work of the research group.

I am grateful to the School of Graduate Studies at the Memorial University of Newfoundland, the Physics Department, and my supervisor for financial support.

Contents

List of Tables

List of Figures

Chapter 1

Introduction

1.1 Phospholipid Membranes

A major element of cell membranes belongs to a chemical class called phospholipids. These macromolecules are usually composed of a phosphate headgroup and two attached hydrocarbon chains. If the hydrocarbon chains have no double bonds, C=C, then such phospholipids are saturated, otherwise they are unsaturated.

Water molecules are extremely polar and form strong hydrogen-bond (H-bond) networks. Because the headgroups of phospholipids are polar, they interact electrostatically with surrounding water molecules. This interaction leads to a reduction in electrostatic energy that can compensate for the entropic penalty associated with the fact that they may not form H-bonds with surrounding water. Thus, the headgroups of phospholipids incur no significant free energy cost when immersed in water, and are hydrophilic. In contrast, the hydrocarbon tails of phospholipids are not polar. When immersed in water, they disturb the H-bond network of the water molecules, and thus cause an increase in the electrostatic energy and a loss in entropy, i.e., increase the free energy of the system. Hence, the hydrocarbon tails are hydrophobic. In order to reach the minimum free energy, phospholipids in water usually form bilayers so that hydrocarbon tails and water are separated by surfaces of headgroups. In this thesis we concentrate on modeling and simulating bilayers of Diacyl phosphatidylcholines (PC's), a kind of phospholipid, because they are very common in cell membranes, and because the

experimental results by Morrow and Lu [2, 3] on binary mixtures of PC's provide an excellent opportunity for comparison with our theoretical work. However, it should be noted that while diacyl PCs have been useful for simple bilayers and model membranes, biological membranes are rich in unsaturated lipids, phospholipids with headgroups other than phosphatidylcholine, and with lipids other than phospholipids.

Fully hydrated single-component bilayers usually have a well-defined phase transition in which the lipids transfer from a relatively ordered gel state to liquid crystal state. Generally the phase behavior of single-component bilayers is as follows [4]: At low enough temperature, the lipids are in a lamellar crystalline state conventionally designated $l_{C'}$ or l_C depending on whether the lipids are tilted or not; as temperature is increased to some temperature $T = T_S$, the lipids undergo a subtransition to a lamellar gel state denoted as $l_{\beta'}$ or l_β, also depending on whether the chains are tilted or not; then with the further increase of temperature, some bilayers may pass through a ripple phase $P_{\beta'}$ or P_β in which the surface of the bilayer breaks up into a series of periodic, quasilamellar segments so that the bilayer surfaces may be modeled as sawtooth like, partly melted or sinusoidal. The hydrocarbon chains in all the phases mentioned to this point are well ordered and almost fully stretched. If we further increase the temperature to a certain point $T = T_t$, the chains undergo the cooperative gel/fluid transition (or chain-melting phase transition) in which the chains lose their order and come into liquid crystal phase designated l_α. For different kinds of lipids and different water contents, the main phase transition temperature T_t and phase behavior are also different. In general, the

main phase transition temperature increases with chain length and hydrostatic pressure, but decreases with degree of unsaturation.

The phase behavior of mixtures is much more complicated. For binary mixtures, which are the focus of this thesis, if the chain length difference is equal to or larger than four [5], there may be phase separation in addition to these phase transitions. For example, in some membranes of living cells, some component lipids are in the gel phase and are not miscible with the surrounding lipids in the fluid phase, so they form small domains in the gel phase. Such small domains may have important biological functions. In this thesis, we concentrate on bilayers in the liquid crystal phase, and the systems are all at high enough temperature so that there is no phase separation.

1.2 NMR and the Order Parameter

An important method of studying these systems is Deuterium Nuclear Magnetic Resonance (^2H-NMR) experiments, in which some hydrogen atoms at specific positions or all the hydrogen atoms along each lipid are replaced by deuterium atoms. This is called deuteration. For fast, axially symmetric reorientation of a lipid molecule about the bilayer normal, the ^2H NMR spectrum of a deuteron of a hydrocarbon chain is a pair of lines split by a frequency proportional to

$$\left(\frac{3\cos^2\beta-1}{2}\right)\left\langle\frac{3\cos^2\theta_{CD}-1}{2}\right\rangle \tag{1.1}$$

where β is the angle between the bilayer normal and the magnetic field, and θ_{CD} is the angle between the C–D bond axis and bilayer normal. The average is over motions of the chain.

Bilayers formed by dispersing lipids into water tend to form closed multi-lamellar vesicle assemblies in which all orientations of bilayer normal are equally likely. The result of this effective spherical distribution is that orientations of the bilayer normal perpendicular to the magnetic field $(\beta = 90^o)$ are most likely and orientations of the bilayer normal parallel to the magnetic field $(\beta = 0^o)$ are the least likely. The resulting superposition of splittings gives rise to the characteristic Pake doublet powder pattern.

Relative to the magnetic field, the largest density of bilayer normal orientations is near $\beta = 90^o$ for which the splitting is proportional to

$$\left(\frac{3\cos^2 90^o - 1}{2}\right)\left\langle\frac{3\cos^2\theta - 1}{2}\right\rangle = \left(-\frac{1}{2}\right)\left\langle\frac{3\cos^2\theta - 1}{2}\right\rangle \tag{1.2}$$

The lowest density of bilayer normal orientations is near $\beta = 0^o$ for which the splitting is proportional to

$$\left(\frac{3\cos^2 0^o - 1}{2}\right)\left\langle\frac{3\cos^2\theta - 1}{2}\right\rangle = (+1)\left\langle\frac{3\cos^2\theta - 1}{2}\right\rangle \tag{1.3}$$

The Pake doublet powder pattern is thus characterized by prominent edges, corresponding to the splitting for lipids reorienting about bilayer normals perpendicular to the magnetic field. The splitting of these prominent edges is proportional to the orientational order parameters,

$$S_{CD} = \left\langle \frac{3\cos^2 \theta_{CD} - 1}{2} \right\rangle \tag{1.4}$$

For lipids deuterated at each position along the hydrocarbon chain, the spectrum is a superposition of Pake powder doublets scaled by the orientational order parameters corresponding to each position along the chain. The de-Paking technique developed by Bloom and coworkers [6, 7] is used to extract orientational order parameter for each hydrocarbon unit from the superposed Pake Doublet powder patterns, and then the smoothed orientational order parameter profile can be further obtained. ("Smoothed" is used because the orientational order parameters are ordered according to their relative magnitudes, not necessarily according to their positions along a chain, so the profile is a smoothed monotonic curve.)

The smoothed orientational order parameter profiles for all single-component bilayers are similar: there is a plateau from the beginning to the middle of the chain, followed by a fast decrease from the middle to the end of the chain. However, almost all real membranes are mixtures of lipids of different chain lengths. Chain length mismatch causes changes in the smoothed order parameter profiles from the corresponding single-component bilayers [2, 3]. In mixtures, with the decrease in the fraction of one component, its order parameter profile tends to approach that of the major component in its single-component bilayer. If the long chains are in the minority, near their free end, the slope of the order parameter profile becomes less negative. This gives rise to a feature called the second plateau by Lu, Morrow and Grant [2]. This second plateau becomes more prominent with increases in the chain length difference and short chain percentage.

Chain length mismatch can cause a very fluid central region in bilayers. The second plateau can provide information about this region where the largest density fluctuations may occur to facilitate ion permeation [8] or information transmission across the bilayer.

1.3 Theoretical Approaches

A number of approaches have been developed to model the bilayers. Among them, the molecular dynamics (MD) and Monte Carlo (MC) methods are used extensively.

In molecular dynamics calculations [4], the various interactions involved are modeled as near to the true interactions as possible; the CH_2 groups and CH_3 groups in many cases are considered as "single-atom" centers. By using Newtonian equations of motion combined with physically-motivated constraints such as $\left\langle \frac{1}{2}\sum_{i=1}^{N} m_i v_i^2 \right\rangle = \frac{3}{2}k_B T$, one can simulate the evolution of the system from a given initial state over a series of tiny time intervals. After each time interval, a new state of the system can be obtained. Then after long enough time, the time and ensemble average over the entire trajectory will give the various observable properties of the system. MD is one of the simulations nearest to real bilayer systems. Many of its results agree with the experiments very well. For example, Robinson et al. [32] made MD calculations for DMPC bilayer. From a starting state with interdigitation of the chains at the bilayer center, after 200 *ps* of simulation, the system behaved as in a liquid crystal phase: the lipid chains were melted, most of the free volume between lipids was filled, and the interdigitation was greatly reduced. They also observed the fluctuation of the headgroup regions. The mean frequency of gauche

isomers per myristoyl chain of dimyristoylphosphatidylcholine (DMPC) from their simulation was about 2.6, which is in excellent agreement with the experimental results of Mendelsohn et al. [33]. Their calculated orientational order parameter profiles were also in good agreement with the experimental results of Seelig et al. [30] and Oldfield et al. [34]. Zaraiskaya et al. [44] made MD simulations for galactosylceramide /dipalmitoylphosphoglycerol (GalCer/DPPG) lipid bilayers. Their results for orientational order parameters, area per lipid and bilayer thickness are in good agreement with experiments. They also revealed the cooperative bilayer undulations, which are expected in the liquid crystalline phase. Gurtovenko et al. [45] also applied MD method to bilayers of DMPC and the cationic lipid dimyristoyltrimethylammonium propane (DMTAP). Their simulation revealed the electrostatic origin of the dependence of the area per lipid on the DMTAP concentration, and explained the change of the electrostatic properties of the bilayer with changing DMTAP concentration and the influence of this change on the surrounding water and ions. However, in MD, the calculation complexity will increase quickly with the size of the system and the complexity of the molecules, so MD is usually applied to systems with limited number of lipid molecules, and periodic boundary conditions are used.

In Monte Carlo (MC) simulations for equilibrium systems [9], starting from a selected initial state, the system samples in sequence a series of states according to various strategies reflecting the Boltzmann distribution (in fact, the efficiency of MC usually depends on these strategies). In this way, a collection of sampling states satisfying the Boltzmann distribution is generated, and the ensemble averages over all these states will

give the various statistical quantities we want. For example, Xu and Cafiso [35] detected terminal methyls in the vicinity of the headgroup/hydrocarbon interface. This result suggests the existence of backward pointing bonds, which are called the "stepping back"-type of bonds in the paper of Whitmore et al. [1]. However, it is difficult to give quantitative description of such bonds through experiments. Monte Carlo simulations of H. L. Scott [36] provided the probability of such bonds at each carbon atom along a DMPC chain. Their results are comparable to the values obtained by Whitmore et al. [1]. Using a two-state, two-component, Ising-type model, Sugár et al. [42] made MC simulations for DMPC/DSPC bilayers. They found that when the temperature is between the main transition temperatures of DMPC and DSPC, there can form domains of gel-phase DSPC in a fluid phase continuum of DMPC. They also obtained the excess heat capacity curves, the fluorescence recovery after photobleaching (FRAP) threshold temperatures, the most frequent center-to-center distances between the DSPC domains, and the fractal dimensions of DSPC domains. Based on the same model, the MC simulations of Ekaterina et al. [43] gave a quantitative description of phase separation and formation of small domains in the DMPC/DSPC bilayers. Compared with MD, the dynamic strategies in MC are based not on Newtonian equations, but directly on Boltzmann distribution. This may help MC to acquire enough states to reflect Boltzmann distribution faster than MD does, so MC can deal with larger systems than can MD. However, MD can give more details about a system, especially those beyond equilibrium statistics. Besides, in MC, sampling only a small number of possible states may lead to

statistical noise in the partition function, which makes it problematic to calculate expectation values by taking the derivative of partition function.

The theoretical approach used in this thesis is a lattice-based, self-consistent field (SCF) theory. Leermakers and Scheutjens [10, 11] may be the first to apply a lattice-based self-consistent field theory to bilayer, after which Meijer et al. [12, 13] made important extensions. In their theory, the lipids and the solvent can distribute throughout the system, which makes the separation of the potential energy into separate surface and interior contributions inappropriate. All the interactions between these constituents are modeled as contact forces, and then further expressed as the interaction between a component and a self-consistent, spatially inhomogeneous effective field, which also incorporates the constraint that the average total occupancy of each lattice site sums to unity. Besides, the hard-core repulsions were also realized in the theory. The systems in their model can self-organize into a stable bilayer [10]. Then by further incorporating the spatial correlations between successive units of the lipid molecules in the statistical weight of each configuration, they [11] obtained an anisotropic effective field, and saw a phase transition in their improved model, which maintains the ability of self-organizing bilayers. The theory is also in resonable qualitative agreement with many experimental results. For example, it predicts that the phase transition temperature increases with chain length, although the increase is not as much as shown by experiments. However, in their theory [10 – 13], there remain some problems such as full intercalation in the gel phase, too small bilayer thickness, too large solvent content in bilayer interior, and neglect of vacancies in bilayer interior.

By incorporating vacancies in the model and by adopting a more realistic lattice, Whitmore et al. [1] addressed the above problems and developed a SCF theory of compressible single-component bilayers. The theory incorporates the effects of hydrostatic pressure. Their quantitative results such as bilayer thickness, water content in bilayer interior, density change on passing through the main phase transition, and average orientational order parameter, are in considerable agreement with experiments. They also showed that the thickness of a bilayer in liquid crystal phase increases with applied hydrostatic pressure, which may be somewhat counter-intuitive, but agrees with experiments [39, 40, 41]. Then Geehan and Whitmore [14] extended this theory to deal with binary mixtures. The work presented in this thesis follows from the work of Geehan [14], and Whitmore et al. [1].

We can make the following general comments on the application of SCF theories to fully hydrated lipid systems [1, 10 – 13, 15, 16, 17 – 22]. SCF theories can explain the self-organization of phospholipids into bilayers. Incorporation of the connectivity within the lipids in SCF theories leads to anisotropy of the effective field, which is crucial in modeling the gel/liquid main phase transition. Existence of vacancies in the model enables simulating the behavior of bilayers under hydrostatic pressure. SCF theories have strong ability to give microscopic and detailed physical pictures of the systems being modeled. Although SCF theory, MD and MC can all give results in good qualitative agreement with experiments for a number of structural properties, SCF theory can make detailed treatment of those aspects of their behavior currently beyond MD and MC simulations.

1.4 Goals and Outline of Thesis

The goal of this thesis is to use the SCF theory to understand the behavior of lipids in binary mixtures, with a focus on the orientational order parameter. In the second chapter we present the SCF theory for fully hydrated binary mixtures. We apply it to a simplified bilayer model in the third chapter. Then, in the fourth chapter, the equation of state and the partial lipid Gibbs free energy are given. In the fifth chapter, the equations and methods for calculating the orientational order parameter, the order parameter by layer, the gauche isomers by layer, and the segment distributions are derived and explained. Finally, in the sixth chapter, we make calculations for a series of systems to understand the behavior of lipids in binary mixtures, and to compare with experiments. Our foci are on how short and long chains affect each other, how the order parameter profiles compare and change, how they are influenced by the local environment, and in particular the nature and cause of the second plateau.

Chapter 2

Self-Consistent Field Theory

The self-consistent field theory presented here is based on the work of Whitmore et al. [1] and the thesis of Geehan [14]. The theory in this chapter applies to any fully hydrated lipid/solvent mixture that is planar and periodic. In the next chapter, we apply it to a particular model of a bilayer.

In this chapter, we first write down the partition function of a mixture based on a model of lipids, water molecules, vacancies and interactions, then transform it to a functional integration using a standard method. To proceed further, the functional integral is approximated by the maximum of the integrand, and then the resulting formulas are applied to layered structures.

2.1 Partition Function

Consider a system of lipids and solvent molecules at a temperature T and ambient pressure P_0. There are two kinds of lipids. Each lipid has a headgroup and two chains of the same length. Since in this paper we are mainly concerned with the effects of mixing hydrocarbon chains with different length, instead of with different headgroups, we require in our model that the two kinds of lipids have identical headgroups, but different length chains. The solvent should be mainly water because the highly polar water molecules play a dominant role in the formation of bilayer structures. In real systems, there are often other ingredients. For example, in experimental studies, lipids are

typically hydrated in various buffers. In biological objects, the cell bilayers exist in much more complicated environments. In our model, we assume there is only a single solvent.

We are interested in the fully hydrated phase, so in our model the solvent molecules are in excess. In the equilibrium state, such a system should separate into two macroscopic phases, namely, a mixture of lipid and solvent, and a solvent phase having negligible lipid concentration due to strong hydrophobic interactions, and thus playing the role of a solvent reservoir for the mixture. In the lipid/solvent phase, the lipids can form periodic structures. We will be interested in periodic layered structures. We want to calculate the equilibrium phases and structural properties of these layers. The two kinds of lipids in each layer could be mixed or separate into two "macrophases", with one of them rich in long-chain lipids, and the other rich in short-chain lipids. The phase, or phases, could be liquid crystal or gel. Our ultimate goal is to determine this, and the properties of each phase. The fundamental approach is to calculate the minimum free energy under the assumption that the lipids are uniformly mixed. If this assumption is incorrect, then there is some negative curvature in the function of the free energy vs. composition.

Since the highly polar water molecules play a dominant role in the formation and properties of bilayers, we concentrate on systems with solvent of pure water. We further model the solvent molecules as structureless hard spheres. Since our interests are mainly in the bilayer interior instead of solvent molecules, such simplification is defensible. We label solvent molecules as s. There are two kinds of lipids. We denote the lipids with longer chains as 1, and the lipids with shorter chains as 2. The chains are made up of a

series of CH_2 units, and a terminal CH_3 unit. Similar to what we have done for solvent molecules, we model these units as identical hard spheres labeled *c*, which are the same size as the units of solvent molecules. Similarly, each headgroup consists of identical hard sphere units denoted as *h* and having the same size as the other two kinds of units. In our model, the headgroups do not change their size and shape, whereas the internal conformations of each chain, which can be described by the position of each *c* unit, or by the bond sequence, are in constant change. The sequences of trans and gauche isomers can also be calculated by the above descriptions. This model does not take into account the effects due to the orientation and internal structure of solvent molecules, and the differences among the CH_2 units, the CH_3 units and the C = O complex which is at the beginning of each chain. When modeling the interactions of *c*, *h* and *s*, we also neglect their structures.

The lipid/solvent mixture occupies a volume *V*, and contains a fixed number of long lipid molecules, ${}_1N_l$, and short lipid molecules, ${}_2N_l$. The total number of lipid molecules is $N_l={}_1N_l+{}_2N_l$. Because of the existence of the reservoir of excess solvent molecules, the number of solvent molecules in the mixture can vary. Its equilibrium value is determined by its chemical potential, μ_s, which is a function of temperature and pressure. We will see that we can calculate the equilibrium density and pressure effects by fixing *V*, ${}_1N_l$ and ${}_2N_l$.

The partition function of this system is given by

$$Z(T,{}_1N_l,{}_2N_l,\mu_s,V)=\sum_{\Lambda}\frac{{}_1z_l^{{}_1N_l}}{{}_1N_l!}\frac{{}_2z_l^{{}_2N_l}}{{}_2N_l!}\frac{z_s^{N_s^{\Lambda}}}{N_s^{\Lambda}!}e^{-\beta[(U^{\Lambda}+W^{\Lambda})-\mu_s N_s^{\Lambda}]} \tag{2.1}$$

In this expression, Λ labels a particular configuration of the entire mixture, N_s^{Λ} is the number of solvent molecules present in configuration Λ, ${}_1z_l$ and ${}_2z_l$ are, respectively, the factors due to the kinetic energy of a long lipid and a short lipid, z_s is the kinetic energy factor of a solvent molecule, U^{Λ} and W^{Λ} together represent the potential energy of configuration Λ, and $\beta = 1/(k_B T)$, where k_B is the Boltzmann constant. The summation is over all possible configurations. The obvious difference between this partition function and the one used by Whitmore et al. [1] is the replacement of $z_l^{N_l}/N_l!$ by two such factors, which is due to the presence of two kinds of lipids.

According to the routine procedure to get some physical interpretation of Z, we differentiate Z with respect to β and obtain [1]

$$-\frac{1}{\beta}\ln Z = \mathrm{A} - \mu_s \langle N_s \rangle \equiv F \tag{2.2}$$

Here A is the Helmholtz free energy, and $\langle N_s \rangle$ is the average number of solvent molecules.

The first contribution to the potential energy, U^{Λ}, is the total energy due to the shapes, namely, the total energy of all the gauche isomers, of all the lipid molecules in configuration Λ. The calculation of U^{Λ} will involve four consecutive units in one lipid, and thus cannot be combined into W^{Λ}, which, in our present model, involves only the interactions between the nearest neighbors, as will be discussed afterwards. U^{Λ} can be calculated using the Rotational Isometric State approximation (RIS approximation) [23],

in which each C–C bond is in one of three discrete states. The entire system can be embedded in and described by a diamond lattice, and the shapes of a lipid can be enumerated by walks on the diamond lattice. Not all the lattice sites are occupied, which incorporates the finite compressibility of the system into the model.

The second contribution to the potential energy, W^{Λ}, arises from all the other interactions. Since U^{Λ} and W^{Λ} are all due to interactions between different units, the division of potential energy into U^{Λ} and W^{Λ} might appear to risk double counting. However, as mentioned above, since we will include only nearest neighbor interactions in W^{Λ} and since the gauche isomer energy is not a nearest neighbor interaction, U^{Λ} and W^{Λ} are different. It is convenient to separate W^{Λ} into hard-core repulsions and long-range interactions. The hard-core repulsions imply that no two units can occupy the same region of space, namely, the same lattice site, no matter whether they are from the same molecule or two different ones. It is imposed by including only those configurations Λ satisfying this constraint. So W^{Λ} can refer only to the longer-range parts of the interactions. It should depend on the density distribution of each component in configuration Λ. In our model, we consider only two-body forces, so W^{Λ} can be given by

$$W^{\Lambda} = \frac{1}{2}\sum_{k,k'}\sum_{\vec{r},\vec{r}'}\rho_k^{\Lambda}(\vec{r})W_{kk'}(\vec{r},\vec{r}')\rho_{k'}^{\Lambda}(\vec{r}') \tag{2.3}$$

where $k,k' = c,h$ and s, $\vec{r}$ denotes a lattice site, $\rho_k^{\Lambda}(\vec{r})$ is the number density of species k at point $\vec{r}$ in a configuration Λ, and $W_{kk'}(\vec{r},\vec{r}')$ is the interaction energy between a unit of

species k at point $\vec{r}$ and a unit of species k' at $\vec{r}'$. Since all the units in the model are abstracted as structureless points, the densities can be expressed as delta functions.

2.2 Self-Consistent Field Approximation

By introducing field variables $\omega_k(\vec{r})$, we can write the partition function as [1]

$$Z(T,{}_1N_l,{}_2N_l,\mu_s,V)=\mathcal{N}^{-1}\prod_{k,\vec{r}}\int_{-\infty}^{\infty}d\omega_k(\vec{r})e^{-\beta F[\{\omega_k(\vec{r})\}]} \tag{2.4}$$

Here $\omega_k(\vec{r})$ is a field variable of species k at position $\vec{r}$, $\mathcal{N}$ is a normalization constant, and F denotes a free-energy functional given by

$$\begin{aligned}\beta F=&-\frac{1}{2\beta}\sum_{k,k'}\sum_{\vec{r},\vec{r}'}\omega_k(\vec{r})W^{-1}_{kk'}(\vec{r},\vec{r}')\omega_{k'}(\vec{r}')\\&+\ln\left[\sum_{\Lambda}\frac{1}{{}_1N_l!{}_2N_l!N_s^{\Lambda}!}e^{\beta U^{\Lambda}+\sum_{k,\vec{r}}\rho_k^{\Lambda}(\vec{r})\omega_k(\vec{r})-N_s^{\Lambda}(\ln z_s+\beta\mu_s)-\sum_j N_l\ln{}_jz_l}\right]\end{aligned} \tag{2.5}$$

where $j = 1, 2$ refers to the long or short chains respectively.

The above functional integrations over $\omega_k(\vec{r})$ cannot be done exactly. We approximate the functional integrations by the maximum value of the integrand, which corresponds to finding the minimum of F with respect to the $\{\omega_k(\vec{r})\}$. We denote the various values obtained by the minimization with a superscript 0. The minimization yields a set of self-consistent equations

$$\omega_k^0(\vec{r})=\beta\sum_{k'\vec{r}'}W_{kk'}(\vec{r},\vec{r}')\rho_{k'}^0(\vec{r}') \tag{2.6}$$

and

$$\rho_k^0(\vec{r}) = \left(\sum_{\Lambda} \rho_k^{\Lambda}(\vec{r}) e^{-E_{\Lambda}^0}\right) \Big/ \left(\sum_{\Lambda} e^{-E_{\Lambda}^0}\right) \tag{2.7}$$

where

$$E_{\Lambda}^0 = \beta U^{\Lambda} + \sum_{k,\vec{r}} \rho_k^{\Lambda}(\vec{r}) \omega_k^0(\vec{r}) - N_s^{\Lambda}(\ln z_s + \beta\mu_s) + \ln N_s^{\Lambda}! \tag{2.8}$$

The last two formulas can also be written as

$$\rho_k^0(\vec{r}) = \left(\sum_{\Lambda} \frac{1}{N_s^{\Lambda}!} \rho_k^{\Lambda}(\vec{r}) e^{-E_{\Lambda}^{0'}}\right) \Big/ \left(\sum_{\Lambda} \frac{1}{N_s^{\Lambda}!} e^{-E_{\Lambda}^{0'}}\right) \tag{2.9}$$

where

$$E_{\Lambda}^{0'} = \beta U^{\Lambda} + \sum_{k,\vec{r}} \rho_k^{\Lambda}(\vec{r}) \omega_k^0(\vec{r}) - N_s^{\Lambda}(\ln Z_s + \beta\mu_s) = E_{\Lambda}^0 - \ln N_s^{\Lambda}! \tag{2.10}$$

where the $E_{\Lambda}^{0'}$ is the energy associated with configuration Λ, so it is obvious that $\rho_k^0(\vec{r})$ is the equilibrium density of component k at $\vec{r}$. Then $\omega_k^0(\vec{r})$ is the statistical mean (or effective) value of the longer range part of the interaction experienced by a unit of species k at point $\vec{r}$, i.e., it is a mean field. From equations (2.6) – (2.8), $\omega_k^0(\vec{r})$ and $\rho_k^0(\vec{r})$ can be calculated from each other, i.e., they are self-consistent. These are why equations (2.6) – (2.8) are regarded as a self-consistent, mean-field description of both the equilibrium densities and the effective potentials. Thus the partition function becomes

$$Z(T, {}_1N_l, {}_2N_l, \mu_s, V) \propto e^{-\beta F^0} \tag{2.11}$$

where $F^0 = F\left[\{\omega_k^0(\vec{r})\}\right]$.

Next, we should apply the above general results to what we are interested in, the layered structures. We require that the system be composed of a series of parallel planes within each of which the equilibrium density distribution is uniform, and the equilibrium density distributions are periodic in the direction normal to these planes. We label this period by R, and the area of the planes by A. The system is composed of a series of identical unit cells of dimensions $A \times R$. We further require that each unit cell contain one bilayer and surrounding solvent. There are a total of L/R of such unit cells, where $L = V/A$ is the total length of the mixture. Our calculation should determine the number of lipids per bilayer, bilayer thickness and shapes of lipids. Choosing the x-axis to be normal to the layer planes, we have $\rho_k^0(\vec{r}) \to \rho_k^0(x)$, and $\omega_k^0(\vec{r}) \to \omega_k^0(x)$ in equations (2.6) — (2.8). Their periods are all R. The equilibrium density on layer x is given by

$$\rho_k^0(x) = \frac{1}{A}\left(\sum_{\Lambda} N_k^{\Lambda}(x) e^{-E_{\Lambda}^0}\right) \Big/ \left(\sum_{\Lambda} e^{-E_{\Lambda}^0}\right) \tag{2.12}$$

where

$$E_{\Lambda}^0 = \beta U^{\Lambda} + \sum_{k,x} N_k^{\Lambda}(x)\omega_k^0(x) - N_s^{\Lambda}(\ln z_s + \beta\mu_s) + \ln N_s^{\Lambda}! \tag{2.13}$$

and

$$N_k^{\Lambda}(x) = \sum_{y,z} \rho_k^{\Lambda}(\vec{r}) \tag{2.14}$$

which is the total number of units k on layer x when the mixture is in configuration Λ.

For the layered system, the minimized free energy can be written as

$$\beta F^0 = -\left(I^0 + \ln Q^0\right) \tag{2.15}$$

where

$$I^0 = \frac{A}{2}\sum_{k,x} \rho_k^0(x)\omega_k^0(x) \tag{2.16}$$

and

$$Q^0 = \sum_{\Lambda} \exp\left\{-E_\Lambda^0 + {}_1N_l \ln({}_1z_l) - \ln({}_1N_l!) + {}_2N_l \ln({}_2z_l) - \ln({}_2N_l!)\right\} \tag{2.17}$$

Up to this point, we have used the states of the entire system, Λ, to label the configurations of the system. They can also be expressed by the states of individual molecules and associated occupation numbers. We now use this idea to reformulate the summations over configurations. The state of a single solvent molecule can be fully specified by the layer it resides on. The states of a single lipid of type *j* can be specified by (x, λ, j). Here x is the layer occupied by its headgroup unit bonded to either one of the hydrocarbon chains, and λ specifies the sequence of all the bond vectors. It is worth noticing that at this point, the defining layer "x" can be in any layer in the system. The states of the entire system can then be specified by sets of occupation numbers $\{{}_1N_\lambda(x)\}$, $\{{}_2N_\lambda(x)\}$ and $\{N_s(x)\}$. Here ${}_1N_\lambda(x)$ and ${}_2N_\lambda(x)$ denote, respectively, the number of lipids in state (x, λ, j), and $N_s(x)$ denotes the number of solvent molecules on layer x. Since these states are independent of where the molecules are within the layer x, a given set of occupation numbers generally corresponds to many distinct configurations, Λ.

The sums over configurations Λ can be re-expressed in terms of summations over sets of these occupation numbers as

$$\sum_{\Lambda} \cdots \rightarrow \sum_{\{{}_1N_\lambda(x),{}_2N_\lambda(x),N_s(x)\}} {}_1N_l!\ {}_2N_l!\ N_s! \left[\frac{1}{\prod_{x,\lambda} {}_1N_\lambda(x)!\ \prod_{x,\lambda} {}_2N_\lambda(x)!\ \prod_x N_s(x)!}\, g\right] \cdots$$

(2.18)

where the quantity in the square bracket is the number of allowed configurations of the system that can be characterized by the sets $\{_1N_\lambda(x)\}$, $\{_2N_\lambda(x)\}$ and $\{N_s(x)\}$.

Since the numbers of long and short lipids are all fixed, the sum should be over all possible sets satisfying the constraint that

$$\sum_{x,\lambda} {}_jN_\lambda(x) = {}_jN_l \tag{2.19}$$

There is no corresponding constraint on the solvent because of the existence of the solvent reservoir. For each configuration, N_s is simply the sum of the $N_s(x)$.

The hard core repulsions should be incorporated into the model through the function g in equation (2.18). It is just the number of ways to add sequentially all the bonds of all the lipids as well as all the solvent molecules to the system. It should not include configurations having doubly occupied sites. For most cases, it is impossible to evaluate g exactly, so g has to be approximated. The function of g given by Whitmore et al. [1], which is based on the generalization by Leermakers and Scheutjens [11] of earlier work by Dimarzio [24], can be used in our case without any revision. In this method, the probability that a bond can be added to a layer in an existing collection of molecules depends not only on the number of vacancies on that layer, but also on the number of each type of bonds associated with that layer. This contributes to the anisotropy of the effective field, self-organization of the bilayer, and the phase transition.

In a diamond lattice, there are four distinct possible C–C bond vectors (or eight counting antiparallel vectors). However, for approximating g, it is convenient to combine

them into two types of bonds, labeled *V* and *H*. Bonds of type *V* join monomers on two adjacent layers, and bonds of type *H* joins two monomers within the same layer. The form of *g* is

$$g = \prod_x \frac{(A-\Psi_V(x))!(A-\Psi_H(x))!}{A!(A-N(x))!} \tag{2.20}$$

where *N(x)* is the total number of units, due to long and short chains and solvent molecules, on layer x, $\Psi_V(x)$ is the total (including long and short chains) number of bonds joining units on layer x and layer x+1, and $\Psi_H(x)$ is the total number of bonds within layer x. In order to express them with $\{{}_jN_\lambda(x)\}$ and $\{N_s(x)\}$, we define ${}_jn_\lambda^c(x'\mid x)$ and ${}_jn_\lambda^h(x'\mid x)$, respectively, as the number of hydrocarbon and headgroup units on layer x and belonging to one lipid of type j in state (x',λ,j). The number of units of type k on layer x, for $k = c$ or h, can now be expressed as

$$N_k(x) = \sum_{x',\lambda} {}_1N_\lambda(x')_1n_\lambda^k(x'\mid x) + \sum_{x',\lambda} {}_2N_\lambda(x')_2n_\lambda^k(x'\mid x) \tag{2.21}$$

We can express the total number of units of all types on layer x as

$$N(x) = \sum_{x',\lambda,k} \{{}_1N_\lambda(x')_1n_\lambda^k(x'\mid x) + {}_2N_\lambda(x')_2n_\lambda^k(x'\mid x)\} + N_s(x) \tag{2.22}$$

We then define ${}_jm_V^\lambda(x'\mid x)$ and ${}_jm_H^\lambda(x'\mid x)$ respectively as the number of bonds connecting units on layers x and x+1, and the number of bonds within layer x, associated with one lipid molecule of type j in state (x',λ,j). Note that ${}_jm_V^\lambda(x'\mid x)$ includes both bonds beginning on x and ones beginning on x+1. Then

$$\Psi_b(x) = \sum_{x',\lambda} \{{}_1N_\lambda(x')_1m_b^\lambda(x'\mid x) + {}_2N_\lambda(x')_2m_b^\lambda(x'\mid x)\} \tag{2.23}$$

where $b = V, H$.

Equation (2.12) and (2.17) can be rewritten with (2.18) and (2.20) – (2.23) as

$$\rho_k^0(x) = \frac{1}{Q^0 A} \sum_{\{{}_1N_\lambda(x')\},\{{}_2N_\lambda(x')\},\{N_s\}} \sum_{x',\lambda,j} {}_jN_\lambda(x')\, {}_jn_\lambda^k(x' \mid x) \exp\{\mathcal{W}[\{{}_1N_\lambda(x')\},\{{}_2N_\lambda(x')\},\{N_s\}]\} \quad (2.24)$$

where $k = c$ and h, and

$$Q^0 = \sum_{\{{}_1N_\lambda(x')\},\{{}_2N_\lambda(x')\},\{N_s\}} \exp\{\mathcal{W}[\{{}_1N_\lambda(x')\},\{{}_2N_\lambda(x')\},\{N_s\}]\} \quad (2.25)$$

The solvent density can be expressed similar to (2.24). Here $\mathcal{W}$ is given by

$$\begin{aligned}
\mathcal{W} = & -\sum_{x,\lambda} {}_1N_\lambda(x)\left[\beta E_g\, {}_1\eta_\lambda + \ln({}_1N_\lambda(x)) + \sum_{x',k} {}_1n_\lambda^k(x \mid x')\omega_k^0(x') - \ln({}_1z_l)\right] \\
& -\sum_{x,\lambda} {}_2N_\lambda(x)\left[\beta E_g\, {}_2\eta_\lambda + \ln({}_2N_\lambda(x)) + \sum_{x',k} {}_2n_\lambda^k(x \mid x')\omega_k^0(x') - \ln({}_2z_l)\right] \\
& -\sum_x N_s(x)\left[\ln(N_s(x)) + \omega_s^0(x) - \beta\mu_s - \ln z_s\right] \\
& +\sum_{x,b}[A - \Psi_b(x)]\ln[A - \Psi_b(x)] \\
& -\sum_x [A - N(x)]\ln[A - N(x)] - \sum_x A \ln A
\end{aligned} \quad (2.26)$$

Here E_g is the energy of a gauche bond relative to a trans bond for long or short chains, and ${}_j\eta_\lambda$ is the total number of gauche isomers in a particular sequence λ of long or short chains depending on j. Stirling's approximation has also been used where appropriate.

Next we use the most probable set of occupation numbers for each component to approximate the above summations over sets of occupation umbers because the latter cannot be done exactly. These most probable sets of occupation numbers, which we denote by $\{{}_1\overline{N}_\lambda(x)\}$, $\{{}_2\overline{N}_\lambda(x)\}$ and $\{\overline{N}_s(x)\}$, can be found by minimizing W with respect

to them, subject to the constraint of constant numbers of each kind of lipid. This minimization gives

$$ {}_j\overline{N}_\lambda(x) = \frac{{}_jN_l}{{}_j\overline{Q}_l} e^{-{}_j\varepsilon_\lambda(x)} \tag{2.27} $$

and

$$ \overline{N}_s(x) = Ae^{-[\varepsilon_s(x)-\beta\mu_s-\ln z_s]} \tag{2.28} $$

where

$$ \begin{aligned} {}_j\varepsilon_\lambda(x) = {} & \beta E_g\, {}_j\eta_\lambda + \sum_{x'}\left[{}_jn_\lambda^c(x\mid x')\overline{\omega}_c(x') + {}_jn_\lambda^h(x\mid x')\overline{\omega}_h(x')\right] \\ & + \sum_{x',b} {}_jm_b^\lambda(x\mid x')\ln(1-\psi_b(x')) - \sum_{x'} {}_jn^\lambda(x\mid x')\ln(1-\overline{\rho}(x')) \end{aligned} \tag{2.29} $$

where ${}_jn^\lambda(x\mid x') = {}_jn_\lambda^c(x\mid x') + {}_jn_\lambda^h(x\mid x')$,

$$ \varepsilon_s(x) = \overline{\omega}_s(x) - \ln(1-\overline{\rho}(x)) \tag{2.30} $$

and

$$ {}_j\overline{Q}_l = \sum_{x,\lambda} e^{-{}_j\varepsilon_\lambda(x)} \tag{2.31} $$

For the above equations we have used

$$ \overline{\rho}(x) = \frac{\overline{N}(x)}{A} \tag{2.32} $$

and

$$ \overline{\psi}_b = \frac{\overline{\Psi}_b(x)}{A} \tag{2.33} $$

With (2.22) and (2.23), we use $\{{}_j\overline{N}_\lambda(x)\}$ and $\{\overline{N}_s(x)\}$ to calculate $\overline{N}(x)$ and $\overline{\Psi}_b(x)$. From now on, the "bar" over a quantity means that the quantity is calculated from the set of

most probable occupation numbers. The quantities calculated from these barred quantities are obtained in the self-consistent field, or SCF, approximation.

Using these most probable sets of occupation numbers for all the components, we can approximate the summations in (2.24) and (2.25) as

$$\overline{Q} = \exp\{\mathcal{W}[\{_1\overline{N}_\lambda(x')\},\{_2\overline{N}_\lambda(x')\},\{N_s\}]\} \tag{2.34}$$

and

$$\overline{\rho}_k(x) = \frac{1}{A}\sum_{x',\lambda,j} {}_j\overline{N}_\lambda(x')\, n_\lambda^k(x' \mid x) \tag{2.35}$$

where k = c and h, and

$$\overline{\rho}_s(x) = \frac{1}{A}\overline{N}_s(x) \tag{2.36}$$

for the solvent. Then the total average density on layer x is

$$\overline{\rho}(x) = \sum_k \overline{\rho}_k(x) \tag{2.37}$$

where k = c, h and s. The definition of potential $\omega_k(x)$ in (2.29) and (2.30) should still be (2.6), except using $\overline{\rho}_k(x)$ instead of $\rho_k^0(\vec{r}')$.

The equilibrium value of the total number of solvent molecules in the mixed phase, $\overline{N}_s$, is a function of the solvent chemical potential, which is

$$\mu_s = -\frac{1}{\beta}\ln\left(\frac{\overline{Q}_s A z_s}{\overline{N}_s}\right) \tag{2.38}$$

with

$$\overline{Q}_s = \sum_x e^{-\varepsilon_s(x)} \tag{2.39}$$

By substituting (2.27) and (2.28) into (2.34) for $\overline{Q}$, and approximating I^0 defined in (2.16) as $\bar{I}$ with $\overline{\rho}_k(x)$, we can obtain the SCF approximation for the free energy, which is

$$\begin{aligned}\overline{F} = &\frac{-A}{2\beta}\sum_{x,k}\overline{\rho}_k(x)\overline{\omega}_k(x) - \frac{1}{\beta}\sum_j {}_jN_l \ln\left(\frac{{}_jQ_l A_j z_l}{{}_jN_l}\right) \\ &+\frac{A}{\beta}\sum_x\left\{\ln[1-\overline{\rho}(x)]+\ln[1-\overline{\Psi}_H(x)]+\ln[1-\overline{\Psi}_V(x)]\right\}\end{aligned} \tag{2.40}$$

From the properties of individual molecules immersed in effective fields determined by bond and density, we can calculate the SCF approximation of $\overline{\rho}_k(x)$, $\overline{\psi}_b(x)$ and $\overline{\omega}_k(x)$, and then obtain $\overline{F}$ by the above equation. We can first fix the repeat distance R as any reasonable value, and then make SCF calculations until we get $\overline{F}$. In principle, we then vary R and repeat the calculations, searching for the value of R which minimizes $\overline{F}$. The results give the equilibrium values of R and $\overline{F}$, whose physical meaning is the minimum free energy at repeat distance R.

Chapter 3

Simplified Model Bilayers

3.1 Physical Description

The above self-consistent mean-field theory is applicable to any fully hydrated lipid/solvent mixture that is periodic and planar. Now we will apply it to a simplified model of the mixture whose one unit cell and bilayer is shown in Figure 3.1, and which can be defined by the following six assumptions and related approximations.

First, each unit cell of the periodic mixture structure exhibits mirror symmetry about the central plane of its bilayer.

Second, in this model the headgroup complex of each lipid is composed of two series of h units all perpendicular to the bilayer plane. We assume this headgroup orientation does not change throughout the temperature and pressure ranges of interest.

At either side of each bilayer, all the bonds linking headgroups to hydrocarbon chains should undergo thermal fluctuations about a plane defining the average position of these bonds, leading to a finite width for the headgroup/hydrocarbon interface. However, the fluctuations will produce large enthalpic penalties which will in turn limit this width. Our third assumption is to neglect such fluctuations and suppose that these headgroup/hydrocarbon bonds are restricted to a single layer on each side of the bilayer.

Fourthly, we assume that the hydrocarbon chains of any lipid cannot penetrate into or beyond the headgroup regions, i.e., we neglect the conformations with such penetration, which will result in large enthalpic penalties.

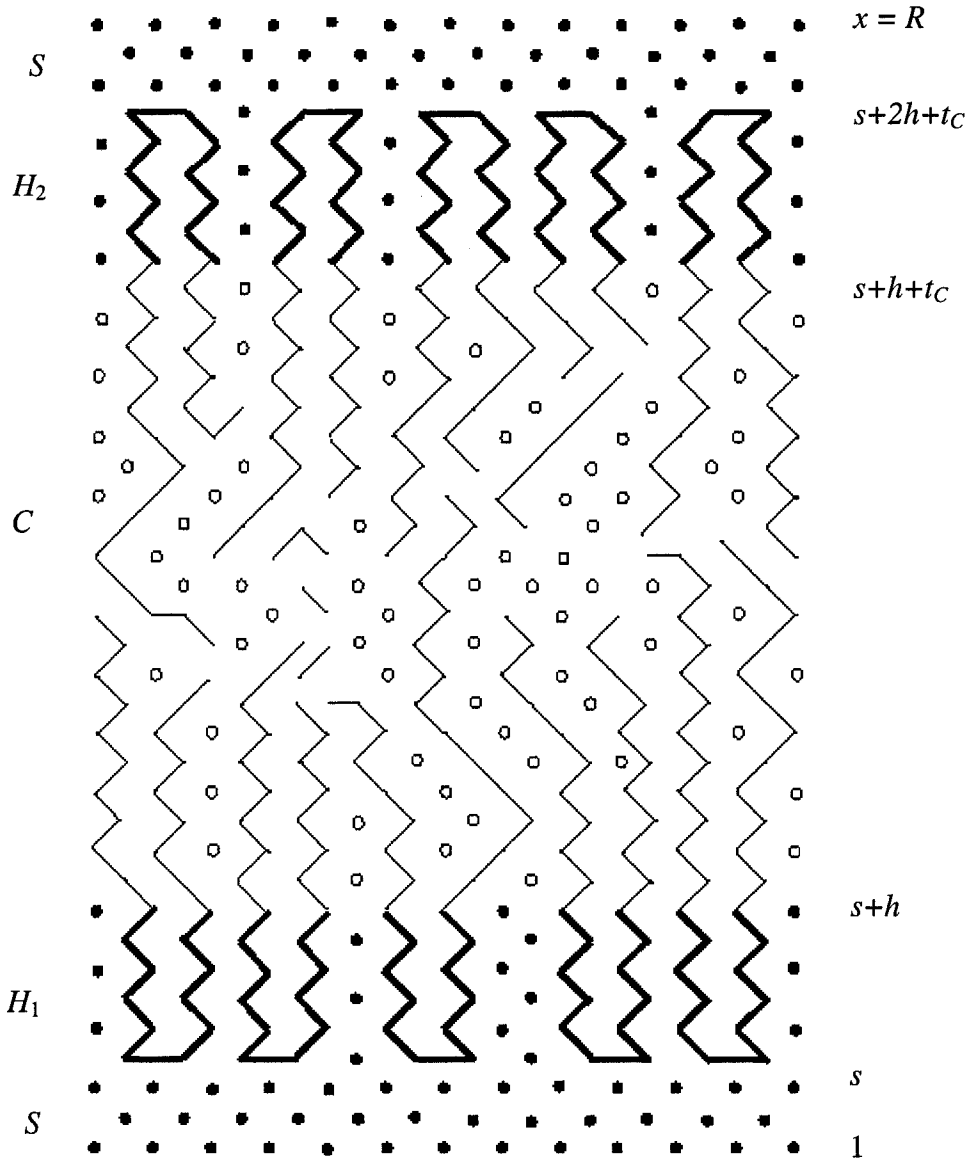

Figure 3.1 Diagram of one unit cell of fully hydrated model bilayer. The acyl chains are represented by light lines, the headgroups by darker lines, the vacancies by open circles, and the solvent molecules by solid circles. The broken lines in the *C* region represent the parts of the acyl chains whose other parts are not in the plane. The figure is for a bilayer of $h = 6$, $l_1 = 14$ and $l_2 = 10$. The thicknesses of bilayer interior and the full bilayer are $t_C = 21$ and $t_B = 33$.

We also assume that the long and short chain lipids are randomly mixed.

In this model, we assume that the cross-sectional area of each headgroup is equal to that of two fully extended hydrocarbon chains. For some lipids such as PE's, this assumption is reasonable, but for some others such as PC's, the headgroup is broader. As well, in this model, the headgroups are not allowed to tilt and the surfaces are not allowed to fluctuate. All these assumptions mean that this model is most suitable for the liquid crystal phase of PE's and PC's, as well as the gel phase and main transition of PE's.

The structure of each unit cell is shown in Figure 3.1. The two S regions are composed of pure solvent. The H_1 and H_2 are headgroup regions composed of all the headgroup units of a bilayer and solvent. The C region contains all the hydrocarbon units and some solvent. Because of the hydrophobic effect, the amount of solvent in this region is very small, which is also experimentally true, so we neglect solvent in this region.

Associating a volume v_0 with each site, we can calculate the volume of each region. The S region has $2s$ lattice planes, so its volume is $\Omega_S = 2sAv_0$. The total headgroup region, $H = H_1 \cup H_2$, has $2h$ layers, so its volume is $\Omega_H = 2hAv_0$. The C region contains t_C layers and has a volume $\Omega_C = t_C Av_0$. The whole bilayer is composed of both the hydrocarbon chains and the headgroups, so its thickness is $t_B = t_C + 2h$. The overall repeat distance is $R = t_B + 2s$.

Since the headgroups are perpendicular to the layer planes, h is determined by the number of headgroup units per lipid molecule. However, the flexibility of hydrocarbon chains makes t_B and t_C variable. Let l_1 be the number of hydrocarbon units in each long chain, so that their maximum values are $t_C^0 = 2l_1$ and $t_B^0 = 2(l_1 + h)$. The bilayer can

assume such maximum value when every long chain of it is fully extended, i.e., has no gauche isomers, and the chains from opposite sides of the bilayer do not penetrate into each other.

3.2 Interactions

We need six two-body potentials, $W_{kk'}(\vec{r})$, to fully specify the longer range interactions of all the three distinct species of the system. In this work, we approximate them with effective, nearest-neighbor interactions, which reduce the expression for the self-consistent fields to

$$\overline{\omega}_k(x) = \beta \sum_{k'} 4W_{kk'} \langle \overline{\rho}_{k'}(x) \rangle \tag{3.1}$$

where each of the $W_{kk'}$ is only the effective, nearest-neighbor part of the interaction, and

$$\langle \overline{\rho}_k(x) \rangle = \frac{1}{4}[\overline{\rho}_k(x-1) + 2\overline{\rho}_k(x) + \overline{\rho}_k(x+1)] \tag{3.2}$$

which is a local density average.

We define $\chi_{kk'}$ as

$$\chi_{kk'} = W_{kk'} - \frac{1}{2}[W_{kk} + W_{k'k'}] \tag{3.3}$$

which is proportional to the usual Flory parameters [25], and the proportionality constant depends on the lattice constant and coordination number.

For non-polar polymer systems whose change in the density of each component is small within the range of the interactions, the above nearest-neighbor approximation is generally considered to be appropriate in mean field treatments. However, because of the

complexity of the interactions, the interaction parameters cannot be calculated from first principles. Instead, they are usually determined by fitting to various experiments. However, for different temperature, molecular weights and overall blend composition, the fitted results are often different, which means that the mean-field theory neglects some other effects.

In this work, we apply the above nearest-neighbor simplification to all interactions, including those involving polar constituents. This is questionable. Its advantage is to make it possible for us to treat all the interactions in a consistent and relatively simple way. The $W_{kk'}$ are obtained by fitting this model to experiments, as in most polymer theories, instead of calculating from first principles.

In addition, treating the compressibility of bilayers requires including all six interaction parameters, $W_{kk'}$, not just the $\chi_{kk'}$ parameters.

3.3 Density and Bond Distributions

In Chapter 2, we showed SCF equations from which the density distribution of each component could, in principle, be calculated. We now apply them to the simplified model to acquire explicit SCF equations for the bond and density distributions within the *C* region and will find that such application will lead to considerable simplification.

First we should note that the headgroup units are confined to the *H* regions where their density is uniform, so we have

$$\overline{\rho}_h(x)=\begin{cases}0 & \text{if } x\in S\\ \rho_h & \text{if } x\in H\\ 0 & \text{if } x\in C\end{cases} \tag{3.4}$$

Here $\rho_h = 2_1\rho_l + 2_2\rho_l$, where ${}_1\rho_l$ and ${}_2\rho_l$ are given by

$${}_1\rho_l = \frac{{}_1N_lR}{2LA} \tag{3.5}$$

and

$${}_2\rho_l = \frac{{}_2N_lR}{2LA} \tag{3.6}$$

which are, respectively, the number of longer chain length lipid molecules per unit area at each interface, and the number of shorter chain length lipid molecules per unit area at each interface.

For solvent, with the same method as that of Whitmore et al. [1], we can show that the solvent (water) density is exponentially smaller than the vacancy concentration, which is itself small in the C region, and is equal to $1-\rho_h$ to within exponentially small corrections in H region. So for most cases, with negligible error, we can use

$$\overline{\rho}_s(x)=\begin{cases}\rho_0 & \text{if } x\in S\\ 1-\rho_h & \text{if } x\in H\\ 0 & \text{if } x\in C\end{cases} \tag{3.7}$$

where ρ_0 is the solvent density in the reservoir. However, in the expressions for the entropy, pressure and free energy, there are terms of the form $\ln(1-\overline{\rho}(x))$, which will cause divergence if equation (3.7) is used. This divergence is because equation (3.7)

neglects the tiny vacancy density in water. Whitmore et al. [1] calculated this vacancy density. Their results are adopted in this thesis to solve this divergence problem.

In the model, the hydrocarbon units are confined to the region *C*, so we have

$$\overline{\rho}_c(x) = \begin{cases} 0 & \text{if } x \in S \\ 0 & \text{if } x \in H \\ \overline{\rho}_c(x) & \text{if } x \in C \end{cases} \tag{3.8}$$

The calculation of $\overline{\rho}_c(x)$ is far more complicated than $\overline{\rho}_s(x)$ and $\overline{\rho}_h(x)$, although their above expressions are similar. We calculate $\overline{\rho}_c(x)$ by the SCF method.

Since in the model there is mirror symmetry about the bilayer mid-plane, we can use it through the following new notation. First of all, we note that there are only two states for headgroup complexes in one unit cell, namely, the headgroup being on either side of the bilayer in each unit cell. We label these two headgroup states by $\sigma = \uparrow$ and $\sigma = \downarrow$, which are mirror images of each other. Then it is straightforward to change the label of lipid states from (x, λ, j) to $(i, \sigma, \lambda_c, j)$, where i specifies the unit cell holding the lipid, σ denotes the headgroup state we have just defined, and λ_c specifies the state of the hydrocarbon chains.

We now consider lipids in a particular unit cell, *i*. For lipids in each state $(i, \sigma, \lambda_c, j)$, we introduce two new symbols: ${}_j n^{\sigma}_{\lambda_c}(x)$ is the number of hydrocarbon units on layer *x*, and ${}_j m^{\sigma}_{b\lambda_c}(x)$ is the number of bonds of type *b*, *b* = 1,2, associated with layer *x* and belonging to hydrocarbon chains of type *j*. For headgroups, we also introduce two similar symbols: ${}_j n^{\sigma}_h(x)$ is the number of headgroup units on layer *x* and ${}_j m^{\sigma}_{bh}(x)$ is the number

of bonds of type b, associated with layer x and belonging to headgroups. For both units c and h, the bond of type 2, which connects units on layer x and $x + 1$, is associated with the unit on layer x.

The form of ${}_j\varepsilon_\lambda(x)$ given by (2.28) can also be simplified by the assumption that the lipids are confined to the bilayer and thus do not penetrate into other unit cells. Furthermore, since all the headgroup/hydrocarbon junctions are confined to two planes per bilayer, ${}_j\varepsilon_\lambda(x)\to\infty$ if x is not one of these planes. We can also denote the mirror image of lipid state $(i,\uparrow,\lambda_c,j)$ by $(i,\downarrow,\lambda_c^*,j)$, where λ_c^* is the mirror image of state λ_c. These two states should have the same energy because of the reflection symmetry of the bilayer.

The self-consistent equations can be rewritten by the above analysis and notations. First of all, we can express the average hydrocarbon density on layer x within the bilayer i as

$$\overline{\rho}_c(x)=\sum_j \frac{{}_j\rho_l}{{}_j\overline{Q}_c}\sum_{\lambda_c}\left[{}_jn^{\uparrow}_{\lambda_c}(x)+{}_jn^{\downarrow}_{\lambda_c^*}(x)\right]e^{-{}_j\varepsilon_{\lambda_c}} \tag{3.9}$$

We should also notice that in this model, the headgroups cannot enter the C region, and the hydrocarbon chains cannot enter the headgroup regions. No matter whether the bonds are associated with headgroups or with hydrocarbon units, the bond density throughout the bilayer can be written as

$$\overline{\psi}_b(x)=\sum_j {}_j\rho_l\left\{{}_jm^{\uparrow}_{bh}(x)+{}_jm^{\downarrow}_{bh}(x)+\frac{1}{{}_j\overline{Q}_c}\sum_{\lambda_c}\left[{}_jm^{\uparrow}_{b\lambda_c}(x)+{}_jm^{\downarrow}_{b\lambda_c^*}(x)\right]e^{-{}_j\varepsilon_{\lambda_c}}\right\} \tag{3.10}$$

where

$$ {}_j\overline{Q}_c = \sum_{\lambda_c} e^{-{}_j\varepsilon_{\lambda_c}} \tag{3.11} $$

and

$$ {}_j\overline{Q}_l = \left(\frac{2L}{R}\right) e^{-{}_j\varepsilon_h}\, {}_j\overline{Q}_c \tag{3.12} $$

In addition, in state $(i, \uparrow, \lambda_c, j)$ (or its mirror image),

$$ {}_j\varepsilon_{\lambda_c} = \beta\, {}_jg_\lambda + \sum_x {}_jn^{\uparrow}_{\lambda_c}(x)[\overline{\omega}_c(x) - \ln(1-\overline{\rho}(x))] + \sum_{x,b} {}_jm^{\uparrow}_{b\lambda_c}(x)\ln(1-\overline{\psi}_b(x)) \tag{3.13} $$

and

$$ {}_j\varepsilon_h = \sum_x {}_jn^{\uparrow}_h(x)[\overline{\omega}_{hc}(x) - \ln(1-\overline{\rho}(x))] + \sum_{x,b} {}_jm^{\uparrow}_{bh}(x)\ln(1-\overline{\psi}_b(x)) \tag{3.14} $$

Equations (3.1), (3.2) and (3.9)—(3.14) are the self-consistent equations used in calculating $\overline{\rho}_c(x)$, $\overline{\psi}_b(x)$ and $\overline{\omega}_k(x)$. In the program, the hydrocarbon density and bond density are acquired from propagators, $G^{(m)}(\vec{r}_0, \vec{r} \mid \beta_2, \beta_1)$ and $Q^{(m)}(\vec{r} \mid \beta_2, \beta_1)$. Since many other quantities such as orientational order parameter, gauche isomer, and etc., can also be obtained from propagators, calculating propagators first in the program can bring great convenience to the subsequent calculations. Here we use the definition given by Whitmore et al. [1]:

Propagator $G^{(m)}(\vec{r}_0, \vec{r} \mid \beta_2, \beta_1)$ is proportional to the probability that a chain with $m + 1$ units has unit 0 at $\vec{r}_0$, terminates with its mth unit at $\vec{r}$, its last bond is of type β_1, and, if $m \geq 2$, its second last bond is type β_2.

Propagator $Q^{(m)}(\vec{r} \mid \beta_2, \beta_1)$ is proportional to the probability that a chain with m + 1 units has unit 0 at $\vec{r}$, its first bond is of type β_1, and, if $m \geq 2$, its second bond is type β_2, but its terminal point is unspecified.

The calculation of the propagators, the $\overline{\rho}_c(x)$, the $\overline{\psi}_b(x)$ and other related quantities, which is based on the RIS approximation, is described by Whitmore et al. [1]

Finally, in this model, the bond and unit densities associated with the headgroup units are very simple. We summarize them in Table 3.1.

Table 3.1

Bond and particle densities associated with the headgroup and solvent regions, corresponding to Figure 3.1. See text for definition of ρ_0 and $\overline{\rho}_s(x)$.

Layer, x	$\psi_V^h(x)$	$\psi_H^h(x)$	$\overline{\rho}(x)$
$x \leq s$	0	0	ρ_0
$x = s+1$	$\rho_h/2$	ρ_h	$\overline{\rho}_s(x)+\rho_h$
$s+2 \leq x \leq s+h-1$	0	ρ_h	$\overline{\rho}_s(x)+\rho_h$
$x = s+h$	0	0	$\overline{\rho}_s(x)+\rho_h$
$s+h+t_C+1 \leq x \leq s+2h+t_C-1$	0	ρ_h	$\overline{\rho}_s(x)+\rho_h$
$x = s+2h+t_C$	$\rho_h/2$	0	$\overline{\rho}_s(x)+\rho_h$
$x \geq s+2h+t_C+1$	0	0	ρ_0

In table 3.1, ρ_0 is the solvent density in the reservoir, and

$$\overline{\rho}_s(x) \approx [1-\rho_h]\,\left[1-z_s^{-1}e^{-[\overline{\omega}_s(x)-\beta\mu_s]}\right] \tag{3.15}$$

whose derivation is given in the paper of Whitmore et al. [1]. Except when calculating $\ln(1-\overline{\rho}(x))$, we use $\overline{\rho}_s(x) \approx 1-\rho_h$ in the headgroup regions, then $\overline{\rho}(x) \approx 1$.

Chapter 4

Equation of State, Partial Lipid Gibbs Free Energy and the Stability of Mixtures

4.1 Equation of State and the Partial Lipid Gibbs Free Energy

In our calculations, we need the internal pressure to be equal to the applied pressure, and we need to minimize the Gibbs free energy in order to find the equilibrium thickness. Hence, we need their expressions as well as the basic thermodynamic relations.

Within the saddle point approximation, the pressure, P, can be expressed as

$$P \to -\left(\frac{\partial F^0}{\partial V}\right)_{{}_1N_l,{}_2N_l,\mu_s} \tag{4.1}$$

Using equation (2.14) for F^0 and equation (2.24) for Q^0, and noticing that W is evaluated at its extremum, we can obtain from the above formula

$$\overline{P}L = \frac{1}{2\beta}\sum_{x,k}\overline{\rho}_k\overline{\omega}_k(x) - \frac{1}{\beta}\sum_x\left[\ln\left(1-\overline{\rho}(x)\right) - \sum_b \ln\left(1-\overline{\psi}_b(x)\right)\right] \tag{4.2}$$

Combining the results from the analysis of the simplified model, we can rewrite it as

$$\begin{aligned}\overline{P}t_B - 2hP_0 + 2s\left(\overline{P}-P_0\right) = {} & W_{ss} + 2\left(W_{ch}-W_{cs}\right)\rho_c^{(1)}\rho_h + (4-8h)\chi_{hs}\rho_h^2 \\ & + \frac{2}{\beta}\left[\ln\left(1-\rho_h/2\right) - \ln\left(1-\rho_h\right)\right] \\ & + \frac{1}{2}\sum_{x\in C} 4W_{cc}\overline{\rho}_c(x)\left\langle\overline{\rho}_c(x)\right\rangle \\ & - \frac{1}{\beta}\sum_{x\in C}\left[\ln\left(1-\overline{\rho}(x)\right) - \sum_b \ln\left(1-\overline{\psi}_b(x)\right)\right]\end{aligned} \tag{4.3}$$

where χ_{hs}, which is defined by (3.3), is proportional to the relevant Flory parameter and reflects effective headgroup-solvent interaction, $\rho_c^{(1)}$ is the carbon unit density on layers $x = s + h + 1$ and $x = s + h + t_C$, and P_0 is the ambient pressure, which comes from the summation over the $2s$ layers of pure solvent region.

Applying (2.39) to a system of pure solvent, we obtain the free energy appropriate to the reservoir. Differentiating it with respect to volume, as in (4.1), we get

$$P_0 = 2\rho_0^2 W_{ss} - \frac{1}{\beta}\ln(1-\rho_0) \tag{4.4}$$

This equation relates the environmental hydrostatic pressure, P_0, temperature, and solvent density, ρ_0, in the reservoir. It was used in deriving equation (4.3) from (4.2).

For an equilibrium system, $\overline{P}$, which is the pressure obtained from the SCF calculation, can be calculated from either (4.2) or (4.3), which is the equation of state.

The Gibbs free energy of the system is important in analyzing the system at constant pressure. For our system, the Gibbs free energy is the sum of the partial Gibbs free energy of the lipids and solvents. The contact of the mixture with the reservoir makes the chemical potential of the solvent molecules constant, regardless of the lipid structure. Consequently, we can consider only the partial Gibbs free energy of lipids of each kind, which is ${}_jN_{l\,j}\mu_l$, with the ${}_j\mu_l$ being the lipid chemical potential of the long or short chain length lipids. Given $F = A - \mu_s\langle N_s\rangle$ as in (2.2), we have

$$G_l = F + PV \tag{4.5}$$

Substituting (2.39) and (4.2) for $\overline{F}$ and $\overline{P}$, we can express the SCF approximation for G_l as

$$\begin{aligned}\overline{G}_l &= \overline{F} + \overline{P}V \\ &= -\left(\frac{{}_1N_l}{\beta}\right)\ln\left(\frac{{}_1\overline{Q}_l A_1 z_l}{{}_1N_l}\right) - \left(\frac{{}_2N_l}{\beta}\right)\ln\left(\frac{{}_2\overline{Q}_l A_2 z_l}{{}_2N_l}\right)\end{aligned} \tag{4.6}$$

which implies that

$${}_j\mu_l = -\frac{1}{\beta}\ln\left(\frac{{}_j\overline{Q}_l A_j z_l}{{}_jN_l}\right) \tag{4.7}$$

We can see that it has the same form as (2.37) for the solvent chemical potential.

Using equation (3.12), (3.14), (3.4), (3.1), (3.2), and (3.3) in this sequence, from equation (4.6), we get

$$\begin{aligned}\frac{\overline{G}_l}{N_l} = -\sum_j f_j\{\frac{1}{\beta}\big[&\ln {}_jz_l + \ln {}_j\overline{Q}_c - \ln\left({}_j\rho_h/2\right) + 2\ln\left(1-\rho_h\right) - \ln\left(1-\rho_h/2\right) + 2h\ln\rho_0\big] \\ &+ 2hP_0 + 2\big[W_{hs}\left(4h-1\right) - W_{ss}\left(2h-1\right) + \left(4-8h\right)\chi_{hs}\rho_h + \left(W_{ch}-W_{cs}\right)\rho_c^{(1)}\big]\}\end{aligned} \tag{4.8}$$

where f_j is the fraction of long or short length lipids.

Since only changes in $\overline{G}_l$, rather than its absolute value, are important, we have the freedom to subtract off the Gibbs free energy of a reference state. The reference state we choose is the state in which all the lipids are fully extended and closely packed, and in equilibrium with the bulk so $\overline{P} = P_0$, and the mixture separates into two phases, with one phase being composed of only long chains and having thickness $2l_1$, and the other being composed of only short chains and having thickness $2l_2$. The Gibbs free energy of this reference state can be obtained by considering each phase separately and by noticing that

in each phase there are no gauche isomers, all the bond densities are either equal to zero or equal to the carbon or headgroup density on each layer, and ${}_jQ_c$ depends only on interaction energies. By subtracting the Gibbs free energy of this reference state from (4.8), we obtain

$$\begin{aligned}\frac{\Delta\overline{G}_l}{N_l} &= 2h\left(P_0-\overline{P}\right)+\left(W_{hh}-W_{ss}\right)\rho_c^{(1)}+2\left(W_{ss}-W_{hs}\right)+2\chi_{sh}\left[4h-1+\left(4-8h\right)\rho_h\right]\\ &\quad+2\chi_{ch}\left[\rho_c^{(1)}-1\right]-2\chi_{sc}\rho_c^{(1)}\\ &\quad+\frac{1}{\beta}\left[\ln\left(1-\frac{\rho_h}{2}\right)+\ln\left(\frac{\rho_h}{2}\right)-2\ln\left(1-\rho_h\right)\right]\\ &\quad+\sum_{j=1}^{2}f_j\left[-2l_j\overline{P}-\frac{1}{\beta}\ln {}_jQ_c-4W_{cc}l_j+\frac{1}{\beta}\ln f_j\right]\end{aligned} \tag{4.9}$$

Equation (4.3) is the equation of state, for which the solvent between bilayers contributes only to $\overline{P}$ and only through the term $2s\left(\overline{P}-P_0\right)$, which will vanish in equilibrium. Consequently, the equilibrium state of our model bilayer is independent of the thickness of the solvent region, except that it should be large enough to screen the interactions between the headgroups of neighboring unit cells. The pressure can be calculated from equation (4.3). Equation (4.9) is used to calculate Gibbs free energy. In the actual calculation, we first fix the thickness of the bilayer, then do the SCF calculations to obtain a converged solution, with $\overline{P}=P_0$. We make such calculations for a series of bilayer thickness. The equilibrium bilayer thickness is found by minimizing the Gibbs free energy.

4.2 Stability of Mixtures

The calculations so far are to find the bilayer thickness minimizing the Gibbs fee energy, namely, the equilibrium thickness, for a certain composition, which we can describe simply by the fraction of the long chains, f_1, since the fraction of the short chains is $f_2 = 1 - f_1$. The resulting minimum of Gibbs free energy is for a homogeneous mixture with a composition of f_1 everywhere. We can find the equilibrium thickness for all the compositions and generate a composition dependence of Gibbs free energy, $\overline{G}_l(f_1)$. However, sometimes the system can further minimize its Gibbs free energy by phase separating into two phases, each having a different value of long-chain fraction f_1, but the composition of the whole system not changing.

Consider a mixture with long-chain fraction f_1. Since it is a mixture, $f_1 \neq 0 \text{ or } 1$. Now, suppose there is a tiny fluctuation of the system so that the system phase separates into two phases with long-chain fractions of $f_1' = f_1 - \delta_1$ and $f_1'' = f_1 + \delta_2$, respectively, where δ_1 and δ_2 are very small positive quantities. Let the fraction of all the lipids in the phase with long-chain fraction of f_1' be x, the fraction of all the lipids in the phase with long-chain fraction of f_1'' be (1 - x). To ensure that the average composition of the whole system is f_1, we must have

$$f_1 = xf_1' + (1-x)f_1'' \tag{4.10}$$

Equation (4.10) can be rewritten as

$$f_1'' = \frac{f_1 - xf_1'}{1-x} \tag{4.11}$$

According to equation (4.10)

$$\begin{aligned} f_1 &= xf_1' + (1-x)f_1'' \\ &= x(f_1 - \delta_1) + (1-x)(f_1 + \delta_2) \end{aligned} \tag{4.12}$$

Then the Gibbs free energy becomes

$$G_l(f_1', x) = x\overline{G}_l(f_1') + (1-x)\overline{G}_l(f_1'') \tag{4.13}$$

The change in Gibbs free energy due to this fluctuation is

$$\begin{aligned} \Delta\overline{G}_l &= x\overline{G}_l(f_1') + (1-x)\overline{G}_l(f_1'') - \overline{G}_l(f_1) \\ &= x\overline{G}_l(f_1 - \delta_1) + (1-x)\overline{G}_l(f_1 + \delta_2) - \overline{G}_l(x(f_1 - \delta_1) + (1-x)(f_1 + \delta_2)) \\ &= x\overline{G}_l(f_1 - \delta_1) + (1-x)\overline{G}_l(f_1 + \delta_2) - \overline{G}_l(f_1 - x\delta_1 + (1-x)\delta_2) \\ &= x\overline{G}_l(f_1) - x\overline{G}_l'(f_1)\delta_1 + \frac{\delta_1^2}{2}x\overline{G}_l''(f_1) + (1-x)\overline{G}_l(f_1) + (1-x)\overline{G}_l'(f_1)\delta_2 + \frac{\delta_2^2}{2}(1-x)\overline{G}_l''(f_1) \\ &\quad - \overline{G}_l(f_1) - [(1-x)\delta_2 - x\delta_1]\overline{G}_l'(f_1) - \frac{1}{2}\overline{G}_l''(f_1)[(1-x)\delta_2 - x\delta_1]^2 + O(\delta^3) \\ &= \frac{1}{2}\overline{G}_l''(f_1)[x(1-x)\delta_1^2 + x(1-x)\delta_2^2 + 2x(1-x)\delta_1\delta_2] + O(\delta^3) \\ &= \frac{x(1-x)}{2}(\delta_1 + \delta_2)^2\overline{G}_l''(f_1) + O(\delta^3) \end{aligned} \tag{4.14}$$

Since δ_1 and δ_2 are all very small, the term $O(\delta^3)$ can be omitted. Furthermore, since $0 < x < 1$, then

$$\Delta\overline{G}_l < 0 \tag{4.15}$$

if $\overline{G}_l''(f_1) < 0$. The physical meaning of this is that a tiny fluctuation will lower the Gibbs free energy if $\overline{G}_l''(f_1) < 0$. This means that such a system with $\overline{G}_l''(f_1) < 0$ is unstable with respect to phase separation. The points where $\overline{G}_l''(f_1) = 0$ are called spinodals.

If $\overline{G}_l''(f_1) > 0$, the system is either stable or metastable. To explore this further, we return to equation (4.13). It can be written as

$$G_l(f_1', x) = x\overline{G}_l(f_1') + (1-x)\overline{G}_l\left(\frac{f_1 - xf_1'}{1-x}\right) \tag{4.16}$$

Minimizing $G_l(f_1', x)$ with respect to x and f_1' gives, respectively, the following two equations

$$x\overline{G}_l'(f_1') - x\overline{G}_l'(f_1'') = 0 \tag{4.17}$$

$$\overline{G}_l'(f_1'') = \frac{\overline{G}_l(f_1') - \overline{G}_l(f_1'')}{f_1' - f_1''} \tag{4.18}$$

Equation (4.17) tells us that the slope of $\overline{G}_l$ at f_1' should be equal to that at f_1''. Equation (4.18) tells us the value of this slope. Equations (4.17) and (4.18) also mean that, if we draw a double tangent to the curve $\overline{G}_l(f_1)$, the touch points are just f_1' and f_1'', as shown in Figure 4.1. These points are called the binodals. If f_1 is between these binodals, the system can lower its Gibbs free energy by phase separation. The decrease in Gibbs free energy is the difference between $\overline{G}_l(f_1)$ and the value given by the tangent line at the same f_1. Systems with compositions between a binodal and its neighboring spinodal are metastable even though $\overline{G}_l''(f_1) > 0$

To summarize, if the long-chain fraction, f_1, is between the spinodals, a tiny fluctuation will lower the Gibbs free energy, and the system is unstable. If f_1 is between a binodal and the neighboring spinodal point, a tiny fluctuation will increase the Gibbs free energy of the system, so the system will return to f_1. However, since there are phase-separated states with lower Gibbs free energy, a big enough fluctuation will make the system jump into and then stay at such states. Hence, the single phase is metastable at

f_1. For f_1 outside these regions, there are no phase-separated states with lower Gibbs free energy. So after either small or big fluctuation, the system will return to f_1, and the system is stable. Finally, if $\partial^2 \overline{G}_l(f_1)/\partial f_1^2 \geq 0$ for all compositions, then there are no phase-separated states with lower Gibbs free energy, so the mixture is stable at all compositions, and there is no phase separation.

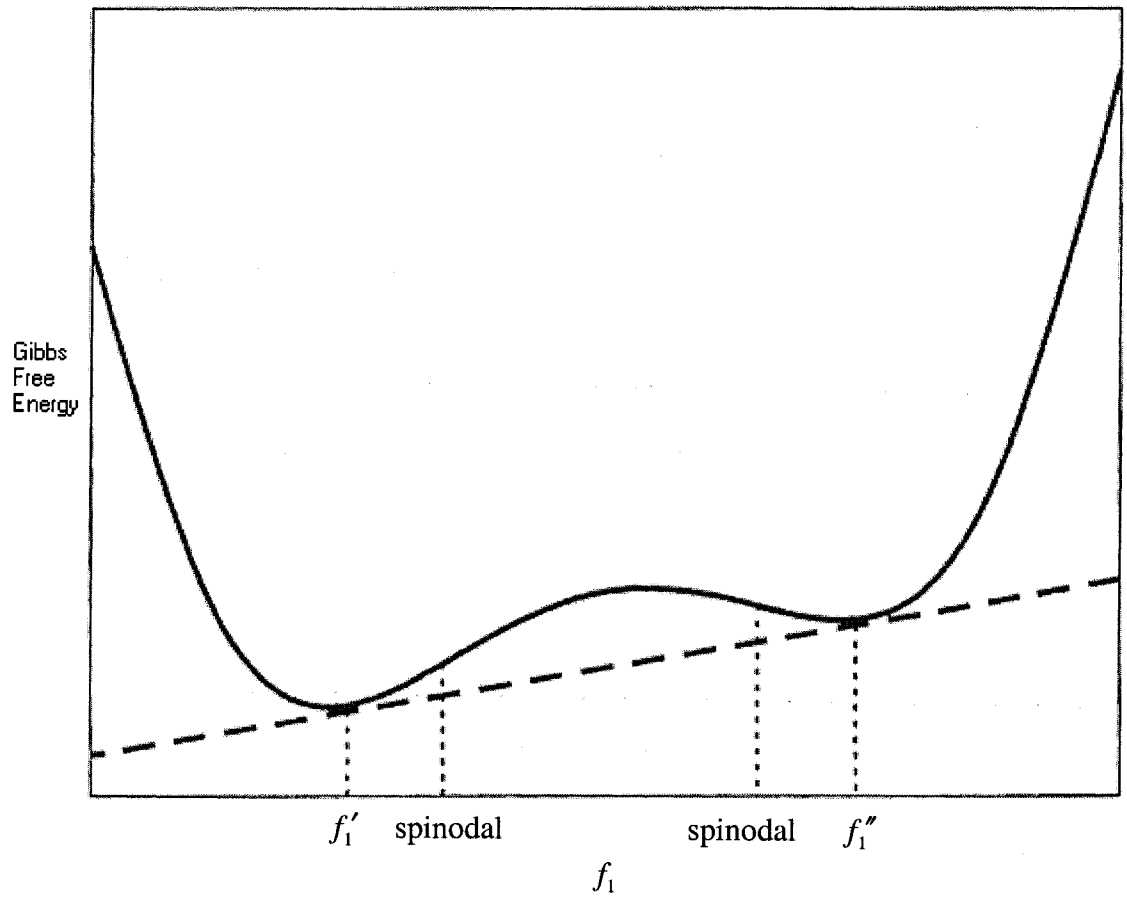

Figure 4.1

Composition dependence of the Gibbs free energy. There are two binodals f_1' and f_1'', and two spinodals.

We should notice that the Gibbs free energy of the reference state we chose is linear in f_1, i.e., its second derivative disappears, so we have

$$\partial^2 \overline{G}_l(f_1)/\partial f_1^2 = \partial^2 \Delta\overline{G}_l(f_1)/\partial f_1^2 \tag{4.19}$$

Combing this with the fact that N_l is a positive constant number, we have that if $\partial^2 \frac{\Delta\overline{G}_l}{N_l} \Big/ \partial f_1^2 \geq 0$ for all compositions, the mixture is stable, and there is no phase separation. The systems and temperatures in this thesis are all chosen so that $\partial^2 \frac{\Delta\overline{G}_l}{N_l} \Big/ \partial f_1^2 > 0$ at all compositions, so there is no phase separation.

Chapter 5

The Orientational Order Parameter, Gauche Isomer and Segment Distribution

5.1 Orientational Order Parameter Profile

The orientational order parameter can be measured by NMR experiments in which the hydrogen atoms of interests are replaced by deuterium atoms. It is also convenient to calculate it in our model. The orientational order parameter is an important comparing point to test our theoretical work. We calculate it for long chain lipids and short chain lipids separately.

We define the orientational order parameter associated with each carbon in the long chain or the short chain similarly as

$$ {}_jS_{CD}^m = \frac{1}{2}\left(3\left\langle \cos^2\left({}_j\theta_{CD}^m\right)\right\rangle - 1\right) \tag{5.1} $$

where ${}_j\theta_{CD}^m$ is the angle between the C–D bond and the reorientation axis, which is the bilayer normal in our model. The average is taken over the conformations of the long chains or the short chains depending on j. In our calculations, we take each $\cos^2\left({}_j\theta_{CD}^m\right)$ as the average over the two deuterium atoms bonded to the carbon m. We should notice that $0 \le {}_j\theta_{CD}^m < \pi$.

In our model, the orientational order parameter associated with carbon atom m is decided by the bond joining unit $m - 1$ and unit m as well as the bond joining unit m and unit $m + 1$. For example, for $m < n$, where n is the last hydrocarbon unit, if the bond

connecting atom $m-1$ and atom m is from layer $x-1$ to layer x, and the bond connecting atom m and atom $m+1$ is from layer x to layer $x+1$, the two C–D bonds all lie in the layer x, i.e., $\theta_{CD}^{m}=\frac{\pi}{2}$ for both the C–D bonds; so $S_{CD}^{m}=-\frac{1}{2}$. For a fully extended chain, for all carbon atom m, all its C–D bonds are parallel to the plane of bilayer, and thus $S_{CD}^{m}=-\frac{1}{2}$ and $\left|S_{CD}^{m}\right|=\frac{1}{2}$ for $m<n$, which is the largest value that $\left|S_{CD}^{m}\right|$ can assume. This is a highly ordered state, and there are no gauche isomers. The presence of gauche isomers increases the disorder of the system, and thus decreases the magnitude of the orientational order parameter.

In the actual calculation, we use one dimensional propagators $G^{(m)}\left(x_0,x|\beta_2,\beta_1\right)$ and $Q^{(m)}\left(x|\beta_2,\beta_1\right)$. The β_1 and β_2 are bond type. We have a total of four types of bonds, which are denoted as 1, 2, 3 and 4. Bonds of type 1 are from layer $x-1$ to x, bonds of type 4 are from layer $x+1$ to x, and bonds of types 2 and 3 are within layer x. The relationships of the one dimensional propagators with the three dimensional propagators defined in Section 3.3 are

$$G^{(m)}\left(x_0,x|\beta_2,\beta_1\right)=\frac{1}{A}\sum_{y_0,z_0}G^{(m)}\left(\vec{r}_0,\vec{r}\mid\beta_2,\beta_1\right) \tag{5.2}$$

where $\vec{r}=(x,y,z)$ and $\vec{r}_0=(x_0,y_0,z_0)$; and

$$Q^{(m)}\left(x|\beta_2,\beta_1\right)=Q^{(m)}\left(\vec{r}\mid\beta_2,\beta_1\right) \tag{5.3}$$

where $\vec{r} = (x, y, z)$. Expressions for all the one-dimensional propagators are given in the Appendix C of the paper of Whitmore et al. [1].Their physical interpretations are as follows.

Propagator $G^{(1)}(x_0, x|\beta_1)$ is proportional to the probability that a chain with 2 units has unit 0 on layer x_0, terminates with its first unit on layer x, its last bond is of type β_1 (in fact, it has only one bond);

Propagator $G^{(m)}(x_0, x|\beta_2, \beta_1), m \geq 2$, is proportional to the probability that a chain with $m + 1$ units has unit 0 on layer x_0, terminates with its unit m on layer x, its last bond is of type β_1, and its second last bond is type β_2;

Propagator $Q^{(1)}(x|\beta_1)$ is proportional to the probability that a chain with 2 units has unit 0 on layer x, its first bond is of type β_1 (in fact it has only one bond);

Propagator $Q^{(m)}(x|\beta_2, \beta_1)$, where $m \geq 2$, is proportional to the probability that a chain with $m + 1$ units has unit 0 on layer x, its first bond is of type β_1, and its second bond is type β_2, but its terminal point is unspecified.

The orientational order parameter can be calculated from these propagators. For example, for $2 \leq m \leq n-2$,

$$
\begin{aligned}
{}_jS_{CD}^{m} = \sum_{x}\sum_{x_0}\delta(x_0 - (s+h+1))\sum_{\beta_1\beta_2}\sum_{\beta_1'\beta_2'}\Big[G^{(m)}(x_0, x \mid \beta_2, \beta_1)\,{}_jP_{CD}^{m}(\beta_1, \beta_1') \\
\times e^{-[\varepsilon_2(\beta_1,\beta_1')+\varepsilon_3(\beta_2,\beta_1')+\varepsilon_3(\beta_1,\beta_2')]}Q^{(n-m)}(x \mid \beta_2', \beta_1')\Big]
\end{aligned}
\tag{5.4}
$$

where

$$e^{-\varepsilon_2(\beta_1,\beta_2)} = \begin{cases} 0 & \text{if } \beta_1 \text{ and } \beta_2 \text{ form backfolding} \\ 1 & \text{otherwise} \end{cases} \tag{5.5}$$

Here bond sequences 1 and 4, or 2 and 3 would form backfolding.

$$\varepsilon_3(\beta_1,\beta_2) = \begin{cases} 0 & \text{if } \beta_1 = \beta_2 \\ E_g/(k_B T) & \text{if } \beta_1 \neq \beta_2 \end{cases} \tag{5.6}$$

$${}_jP_{CD}^m(\beta_1,\beta_1') = \frac{1}{2}\left(3\cos^2\left({}_j\theta_{CD}^m\right)-1\right) \tag{5.7}$$

where β_1 and β_1' are respectively the bonds ending and starting at carbon atom m, $\cos^2\left({}_j\theta_{CD}^m\right)$ is the average value for the two C–D bonds associated with carbon atom m, and ε_3 is just the energy due to gauche isomer.

5.2 Order Parameter by Layer

We want to probe the bilayer environment as a function of depth within the bilayer. We do so by introducing the following two quantities, which are defined mathematically in what follows.

1. The average orientational order parameter on layer x, $\left\langle S_{CD}(x)\right\rangle$. For a given layer, it can have contributions from chains from either side of the bilayer, and many units on each chain. Both long and short chain lipids contribute.
2. The average order parameter due to all the units on layer x due to all the chains of a given type that start on one side of the bilayer. To calculate this, we choose

either long or a short chains, tethered at $x_0 = 0$. We denote this quantity by $\langle S_{CD}^{(1)}(x) \rangle$.

It is, in fact, non-trivial to relate these quantities directly to the measured average order parameters. In experiments, each deuteron visits many layers during the effective averaging time of the measurement. Thus, the experiment and the resulting definition of the order parameter both necessarily include multiple layers. With these quantities we are introducing here, we are taking a snapshot of the bilayer and averaging over all deuterons which are in one layer at a particular time.

Consider all the lipids of one kind (long or short) with headgroups on the left. They have a total of N chains. Each chain has n carbons. If we are considering lipids of type j, then $N = 2_j N_l$ and $n = l_j$. Let chain i be in configuration γ_i. The n carbons will be in layers $x_m^{\gamma_i}$, m = 1 to n, and the order parameter associated with carbon m is $S_{CD}^{\gamma_i}(m)$. The total number of carbons on layer x is

$$N_C(x) = \sum_{i=1}^{N} \sum_{m=1}^{n} \delta\left(x - x_m^{\gamma_i}\right) \tag{5.8}$$

The average order parameter associated with all the carbons on layer x is

$$\langle S_{CD}^{(1)}(x) \rangle = \frac{1}{N_C(x)} \sum_{i=1}^{N} \sum_{m=1}^{n} \delta\left(x - x_m^{\gamma_i}\right) S_{CD}^{\gamma_i}(m) \tag{5.9}$$

We can transform the sum over chains to a sum over the configurations of a single chain by

$$\sum_{i=1}^{N} \cdots \rightarrow \sum_{\gamma} N P_\gamma \cdots \tag{5.10}$$

where P_γ is the probability of a configuration γ. We then have

$$\begin{aligned} N_C(x) &= \sum_\gamma P_\gamma N \sum_{m=1}^{n} \delta\left(x - x_m^\gamma\right) \\ &= N \sum_\gamma P_\gamma C_\gamma(x) \end{aligned} \tag{5.11}$$

where $C_\gamma(x) = \sum_{m=1}^{n} \delta\left(x - x_m^\gamma\right)$, which is the number of carbons on layer x when a chain is in configuration γ. The average then becomes

$$\begin{aligned} \left\langle S_{CD}^{(1)}(x) \right\rangle &= \frac{1}{N \sum_\gamma P_\gamma C_\gamma(x)} \sum_\gamma N P_\gamma \sum_{m=1}^{n} \delta\left(x - x_m^\gamma\right) S_{CD}^\gamma(m) \\ &= \frac{1}{\sum_\gamma P_\gamma C_\gamma(x)} \sum_\gamma P_\gamma \sum_{m=1}^{n} S_{CD}^\gamma(m) \delta\left(x - x_m^\gamma\right) \end{aligned} \tag{5.12}$$

We next want to express $\left\langle S_{CD}^{(1)}(x) \right\rangle$ in terms of propagators.

We should notice that $S_{CD}^\gamma(m)$ depends only on the C–C bond ending at m, α_m^γ, and the C–C bond starting at m, α_{m+1}^γ. Here α_m^γ and α_{m+1}^γ can only be the integers from 1 to 4. Hence,

$$S_{CD}^\gamma(m) = P_{CD}^m\left(\alpha_m^\gamma, \alpha_{m+1}^\gamma\right) \qquad m = 1, 2, \ldots, n-1 \tag{5.13}$$

where P_{CD}^m is in fact the same as ${}_jP_{CD}^m$ defined in section 5.1.

For the last atom, there is no α_{n+1}^γ. We have $S_{CD}^\gamma(n) = P_{CD}^n\left(\alpha_n^\gamma\right)$, where $P_{CD}^n\left(\alpha_n^\gamma\right) = \frac{1}{2}\left(3\cos^2\theta_{CD}^{n,\gamma} - 1\right)$. In diamond lattice model, knowing only α_n^γ, we can decide

the angles of the three C–D bonds attached to the carbon atom n, then $\cos^2\theta_{CD}^{n,\gamma}$ means the value averaged over these three C–D bonds.

We should also notice that

$$\begin{aligned} P_\gamma\delta\left(x-x_m^\gamma\right)S_{CD}^\gamma(m) &= P_\gamma\delta\left(x-x_m^\gamma\right)P_{CD}^m\left(\alpha_m^\gamma,\alpha_{m+1}^\gamma\right) \\ &= \sum_{\beta_1\beta_1'} P_\gamma\delta\left(x-x_m^\gamma\right)P_{CD}^m(\beta_1,\beta_1')\delta_{\alpha_m^\gamma,\beta_1}\delta_{\alpha_{m+1}^\gamma,\beta_1'} \end{aligned} \tag{5.14}$$

for atom 1, 2, …, $n-1$, where β_1 and β_1' are all from 1 to 4.

For atom n,

$$\begin{aligned} P_\gamma\delta\left(x-x_n^\gamma\right)S_{CD}^\gamma(n) &= P_\gamma\delta\left(x-x_n^\gamma\right)P_{CD}^n\left(\alpha_n^\gamma\right) \\ &= \sum_{\beta_1} P_\gamma\delta\left(x-x_n^\gamma\right)P_{CD}^n(\beta_1)\delta_{\alpha_n^\gamma,\beta_1} \end{aligned} \tag{5.15}$$

So equation (5.12) can be expressed as

$$\left\langle S_{CD}^{(1)}(x)\right\rangle = \frac{\sum_\gamma\sum_{m=1}^{n-1}\sum_{\beta_1\beta_1'} P_\gamma\delta\left(x-x_m^\gamma\right)\delta_{\alpha_m^\gamma,\beta_1}\delta_{\alpha_{m+1}^\gamma,\beta_1'}P_{CD}^m(\beta_1,\beta_1') + \sum_\gamma\sum_{\beta_1} P_\gamma\delta\left(x-x_n^\gamma\right)\delta_{\alpha_n^\gamma,\beta_1}P_{CD}^n(\beta_1)}{\sum_\gamma\sum_{m=1}^{n-1}\sum_{\beta_1\beta_1'} P_\gamma\delta\left(x-x_m^\gamma\right)\delta_{\alpha_m^\gamma,\beta_1}\delta_{\alpha_{m+1}^\gamma,\beta_1'} + \sum_\gamma\sum_{\beta_1} P_\gamma\delta\left(x-x_n^\gamma\right)\delta_{\alpha_n^\gamma,\beta_1}} \tag{5.16}$$

Since $P_{CD}^m(\beta_1,\beta_1')$ and $P_{CD}^n(\beta_1)$ do not depend on γ, (5.16) can be further expressed as

$$\left\langle S_{CD}^{(1)}(x)\right\rangle = \frac{\sum_{m=1}^{n-1}\sum_{\beta_1,\beta_1'} P_{CD}^m(\beta_1,\beta_1')\left(\sum_\gamma P_\gamma\delta\left(x-x_m^\gamma\right)\delta_{\alpha_m^\gamma,\beta_1}\delta_{\alpha_{m+1}^\gamma,\beta_1'}\right) + \sum_{\beta_1} P_{CD}^n(\beta_1)\left(\sum_\gamma P_\gamma\delta\left(x-x_n^\gamma\right)\delta_{\alpha_n^\gamma,\beta_1}\right)}{\sum_{m=1}^{n-1}\sum_{\beta_1,\beta_1'}\left(\sum_\gamma P_\gamma\delta\left(x-x_m^\gamma\right)\delta_{\alpha_m^\gamma,\beta_1}\delta_{\alpha_{m+1}^\gamma,\beta_1'}\right) + \sum_{\beta_1}\left(\sum_\gamma P_\gamma\delta\left(x-x_n^\gamma\right)\delta_{\alpha_n^\gamma,\beta_1}\right)} \tag{5.17}$$

Here $\sum_{\gamma} P_\gamma \delta\left(x - x_m^\gamma\right)\delta_{\alpha_m^\gamma,\beta_1}\delta_{\alpha_{m+1}^\gamma,\beta_1'}$ is proportional to the total probability that the atom m of a chain is on the layer x, with C–C bond β_1 ending at atom m and C–C bond β_1' starting at atom m. Thus, if $m = 1$,

$$\sum_{\gamma} P_\gamma \delta\left(x - x_m^\gamma\right)\delta_{\alpha_m^\gamma,\beta_1}\delta_{\alpha_{m+1}^\gamma,\beta_1'} \propto \sum_{\beta_2'} G^{(1)}\left(x_0, x|\beta_1\right)e^{-[\varepsilon_2(\beta_1,\beta_1')+\varepsilon_3(\beta_1,\beta_2')]}Q^{(n-1)}\left(x|\beta_2', \beta_1'\right) \tag{5.18}$$

where $G^{(1)}\left(x_0, x|\beta_1\right)$, $Q^{(m)}\left(x|\beta_2', \beta_1'\right)$, ε_2 and ε_3 are defined in Section 5.1.

For $m = n - 1$

$$\sum_{\gamma} P_\gamma \delta\left(x - x_{n-1}^\gamma\right)\delta_{\alpha_{n-1}^\gamma,\beta_1}\delta_{\alpha_n^\gamma,\beta_1'} \propto \sum_{\beta_2} G^{(n-1)}\left(x_0, x|\beta_2, \beta_1\right)e^{-[\varepsilon_2(\beta_1,\beta_1')+\varepsilon_3(\beta_2,\beta_1')]}Q^{(1)}\left(x|\beta_1'\right) \tag{5.19}$$

where $G^{(m)}\left(x_0, x|\beta_2, \beta_1\right)$ and $Q^{(1)}\left(x|\beta_1'\right)$ are defined in Section 5.1.

For $m = 2, 3, \ldots, n - 2$

$$\sum_{\gamma} P_\gamma \delta\left(x - x_m^\gamma\right)\delta_{\alpha_m^\gamma,\beta_1}\delta_{\alpha_{m+1}^\gamma,\beta_1'} \propto \sum_{\beta_2\beta_2'} G^{(m)}\left(x_0, x|\beta_2, \beta_1\right)e^{-[\varepsilon_2(\beta_1,\beta_1')+\varepsilon_3(\beta_2,\beta_1')+\varepsilon_3(\beta_1,\beta_2')]}Q^{(n-m)}\left(x|\beta_2', \beta_1'\right) \tag{5.20}$$

Since $\sum_{\gamma} P_\gamma \delta\left(x - x_n^\gamma\right)\delta_{\alpha_n^\gamma,\beta_1}$ is proportional to the probability that the nth atom of a chain is on the layer x, with the C–C bond β_1 ending at atom n, we have

$$\sum_{\gamma} P_\gamma \delta\left(x - x_n^\gamma\right)\delta_{\alpha_n^\gamma,\beta_1} \propto \sum_{\beta_2} G^{(n)}\left(x_0, x|\beta_2, \beta_1\right) \tag{5.21}$$

On the whole,

$$\left\langle S_{CD}^{(1)}(x)\right\rangle = \frac{\left[\begin{array}{l}\sum_{\beta_1}\sum_{\beta_1'\beta_2'} G^{(1)}(x_0,x|\beta_1)e^{-[\varepsilon_2(\beta_1,\beta_1')+\varepsilon_3(\beta_1,\beta_2')]}S_{CD}(\beta_1,\beta_1')Q^{(n-1)}(x|\beta_2',\beta_1') \\ +\sum_{m=2}^{n-2}\sum_{\beta_1\beta_2}\sum_{\beta_1'\beta_2'} G^{(m)}(x_0,x|\beta_2,\beta_1)e^{-[\varepsilon_2(\beta_1,\beta_1')+\varepsilon_3(\beta_2,\beta_1')+\varepsilon_3(\beta_1,\beta_2')]}S_{CD}(\beta_1,\beta_1')Q^{(n-m)}(x|\beta_2',\beta_1') \\ +\sum_{\beta_1\beta_2}\sum_{\beta_1'} G^{(n-1)}(x_0,x|\beta_2,\beta_1)e^{-[\varepsilon_2(\beta_1,\beta_1')+\varepsilon_3(\beta_2,\beta_1')]}S_{CD}(\beta_1,\beta_1')Q^{(1)}(x|\beta_1') \\ +\sum_{\beta_1\beta_2} G^{(n)}(x_0,x|\beta_2,\beta_1)S_{CD}(\beta_1,-1)\end{array}\right]}{\left[\begin{array}{l}\sum_{\beta_1}\sum_{\beta_1'\beta_2'} G^{(1)}(x_0,x|\beta_1)e^{-[\varepsilon_2(\beta_1,\beta_1')+\varepsilon_3(\beta_1,\beta_2')]}Q^{(n-1)}(x|\beta_2',\beta_1') \\ +\sum_{m=2}^{n-2}\sum_{\beta_1\beta_2}\sum_{\beta_1'\beta_2'} G^{(m)}(x_0,x|\beta_2,\beta_1)e^{-[\varepsilon_2(\beta_1,\beta_1')+\varepsilon_3(\beta_2,\beta_1')+\varepsilon_3(\beta_1,\beta_2')]}Q^{(n-m)}(x|\beta_2',\beta_1') \\ +\sum_{\beta_1\beta_2}\sum_{\beta_1'} G^{(n-1)}(x_0,x|\beta_2,\beta_1)e^{-[\varepsilon_2(\beta_1,\beta_1')+\varepsilon_3(\beta_2,\beta_1')]}Q^{(1)}(x|\beta_1')+\sum_{\beta_1\beta_2} G^{(n)}(x_0,x|\beta_2,\beta_1)\end{array}\right]} \tag{5.22}$$

where $S_{CD}(\beta_1,\beta_1')$ gives the corresponding order parameter for an atom with bond β_1 ending at it and bond β_1' starting at it. The last carbon atom attaches three hydrogens. In the diamond lattice model, depending wholly on the bond ending at it, the associated orientational order parameter can only be $1/6$ or $-1/6$, which is the value averaged over all the three C–D bonds attached to the last carbon atom. This is different from all the other carbon atoms in a chain. For the last atom, the program sets $\beta_1'=-1$ so that $S_{CD}(\beta_1,\beta_1')$ can distinguish it as the last atom and give an order parameter of $\pm 1/6$ according to β_1. In fact, the $S_{CD}(\beta_1,\beta_1')$ is equivalent to $P_{CD}^{m}(\beta_1,\beta_1')$ and $P_{CD}^{n}(\beta_1)$.

Equation (5.22) is similar to the expression for S_{CD}^{m} in the paper of Whitmore et al. [1]. They have the same ingredients, but here we replace $\sum_{m}$ for $\sum_{x}$.

With $\langle S_{CD}^{(1)}(x)\rangle$, we want to further acquire the average orientational order parameter by layer for both the long and short chains from both sides of the bilayer, $\langle S_{CD}(x)\rangle$.

Now consider a chain of type *j*. Let ${}_j\gamma_i$ denote the configuration of chain *i* of length l_j, including the layer it starts on. Let there be ${}_jN$ of these chains. ${}_jN^l$ and ${}_jN^r$ denote respectively the number of chains of type *j* anchored to the left and right sides.

The total number of carbons in layer *x* is

$$N_C(x) = \sum_j \sum_{i=1}^{{}_jN} \sum_{m=1}^{l_j} \delta\left(x - x_m^{{}_j\gamma_i}\right) \tag{5.23}$$

The average order parameter associated with all the carbons on layer *x* is

$$\langle S_{CD}(x)\rangle = \frac{1}{N_C(x)} \sum_j \sum_{i=1}^{{}_jN} \sum_{m=1}^{l_j} \delta\left(x - x_m^{{}_j\gamma_i}\right) S_{CD}^{{}_j\gamma_i}(m) \tag{5.24}$$

We can transform the sum over chains to a sum over the configurations of a single chain by

$$\sum_{i=1}^{{}_jN} \cdots \rightarrow \sum_\sigma \sum_{{}_j\gamma^\sigma} {}_jN^\sigma P_{{}_j\gamma^\sigma} \cdots \tag{5.25}$$

where $\sigma = l$ or r, depending on whether the chain is attached to the left side or right side of the bilayer, and $P_{{}_j\gamma^\sigma}$ is the probability that a chain of type *j* anchored to the side σ is in configuration ${}_j\gamma^\sigma$. We then have

$$\begin{aligned} N_C(x) &= \sum_j \sum_\sigma \sum_{{}_j\gamma^\sigma} {}_jN^\sigma P_{{}_j\gamma^\sigma} \sum_{m=1}^{l_j} \delta\left(x - x_m^{{}_j\gamma^\sigma}\right) \\ &= \sum_j \sum_\sigma {}_jN^\sigma \sum_{{}_j\gamma^\sigma} P_{{}_j\gamma^\sigma} C_{{}_j\gamma^\sigma}(x) \end{aligned} \tag{5.26}$$

where $C_{{}_j\gamma^\sigma}(x)=\sum_{m=1}^{l_j}\delta\left(x-x_m^{{}_j\gamma^\sigma}\right)$, which is the number of carbons on layer x when a chain of type j anchored to the side σ is in configuration ${}_j\gamma^\sigma$. The average then becomes

$$\left\langle S_{CD}(x)\right\rangle=\frac{1}{\sum_j\sum_\sigma {}_jN^\sigma\sum_{{}_j\gamma^\sigma}P_{{}_j\gamma^\sigma}C_{{}_j\gamma^\sigma}(x)}\sum_j\sum_\sigma {}_jN^\sigma\sum_{{}_j\gamma^\sigma}P_{{}_j\gamma^\sigma}\sum_{m=1}^{l_j}\delta\left(x-x_m^{{}_j\gamma^\sigma}\right)S_{CD}^{{}_j\gamma^\sigma}(m) \tag{5.27}$$

Now let $f_j^\sigma=\frac{{}_jN^\sigma}{N}$, where N is the total number of chains.

$$\left\langle S_{CD}(x)\right\rangle=\frac{1}{\sum_j\sum_\sigma f_j^\sigma\sum_{{}_j\gamma^\sigma}P_{{}_j\gamma^\sigma}C_{{}_j\gamma^\sigma}(x)}\sum_j\sum_\sigma f_j^\sigma\sum_{{}_j\gamma^\sigma}P_{{}_j\gamma^\sigma}\sum_{m=1}^{l_j}\delta\left(x-x_m^{{}_j\gamma^\sigma}\right)S_{CD}^{{}_j\gamma^\sigma}(m) \tag{5.28}$$

The denominator is equivalent to

$$\begin{aligned}&\sum_j\left[\left\langle {}_jN^l(x)\right\rangle+\left\langle {}_jN^r(x)\right\rangle\right]\frac{1}{N}\\&=\frac{1}{2\overline{\rho}}\sum_j\left[\left\langle {}_j\rho^l(x)\right\rangle+\left\langle {}_j\rho^r(x)\right\rangle\right]\\&=\frac{\left\langle\rho(x)\right\rangle}{2\overline{\rho}}\end{aligned} \tag{5.29}$$

where $\left\langle {}_jN^l(x)\right\rangle=$ average number of units on layer x due to chains of type j coming from the left, and so on, and $\overline{\rho}=\frac{N}{2A}$, which is the area density of chains on the headgroup/hydrocarbon-chain interface, and $\left\langle {}_j\rho^l(x)\right\rangle=\frac{\left\langle {}_jN^l(x)\right\rangle}{A}$, etc., and define $\sum_j\left[\left\langle {}_j\rho^l(x)\right\rangle+\left\langle {}_j\rho^r(x)\right\rangle\right]=\left\langle\rho(x)\right\rangle$. Then we have

$$\left\langle S_{CD}(x)\right\rangle = \frac{2\overline{\rho}}{\left\langle \rho(x)\right\rangle}\sum_{j}\sum_{\sigma} f_j^{\sigma}\sum_{j\gamma^{\sigma}} P_{j\gamma^{\sigma}}\sum_{m=1}^{l_j}\delta\left(x - x_m^{j\gamma^{\sigma}}\right)S_{CD}^{j\gamma^{\sigma}}(m) \tag{5.30}$$

The numerator has a sum over left and right anchored chains, and a sum over long and short chains. Consider one of these terms, e.g., chains of type 1 from the left.

$$T_1^l = 2\overline{\rho}f_1^l\sum_{\gamma} P_{\gamma}\sum_{m=1}^{l_j}\delta\left(x - x_m^{\gamma}\right)S_{CD}^{\gamma}(m) \tag{5.31}$$

where γ now refers to configurations of a chain of type 1 anchored to the left.

Comparing with equation (5.12), we can write this as

$$T_1^l = 2\overline{\rho}f_1^l\left\langle {}_1S_{CD}^{(1)}(x)\right\rangle\sum_{\gamma} P_{\gamma}C_{\gamma}(x) \tag{5.32}$$

where $\left\langle {}_1S_{CD}^{(1)}(x)\right\rangle$ is for chains of type 1 anchored at left.

We then finish with

$$\begin{aligned}
&2\overline{\rho}f_1^l\sum_{\gamma} P_{\gamma}C_{\gamma}(x)\\
&= 2\overline{\rho}\frac{{}_1N^l}{N}\sum_{\gamma} P_{\gamma}C_{\gamma}(x)\\
&= 2\overline{\rho}\frac{\left\langle {}_1N^l(x)\right\rangle}{N}\\
&= \frac{\left\langle {}_1N^l(x)\right\rangle}{A}\\
&= \left\langle {}_1\rho^l(x)\right\rangle
\end{aligned} \tag{5.33}$$

since $\frac{2\overline{\rho}}{N} = \frac{N}{A}\frac{1}{N} = \frac{1}{A}$. So

$$T_1^l = \left\langle {}_1\rho^l(x)\right\rangle\left\langle {}_1S_{CD}^{(1)}(x)\right\rangle \tag{5.34}$$

Adding all four contributions, all of which have same denominator

$$\langle S_{CD}(x)\rangle = \frac{1}{\langle \rho(x)\rangle}\left\{\sum_j \left[\langle {}_j\rho^l(x)\rangle\langle {}_jS_{CD}^{(1)}(x)\rangle + \langle {}_j\rho^r(x)\rangle\langle {}_jS_{CD}^{(1)}(t_C - x)\rangle\right]\right\} \tag{5.35}$$

5.3 Gauche Isomers by Layer

In this section, we define and derive the equations for the average number of gauche isomers of a given chain on layer x. To calculate this, we choose either a long or a short chain, tethered at $x_0 = 0$. We denote this quantity by $\langle \eta^{(1)}(x)\rangle$.

Consider a chain of one kind (long or short) with headgroup on the left and chain length of n. If it is in configuration γ, the n carbons will be in layers x_m^γ, m = 1 to n. We denote the gauche isomer number associated with carbon m as $\eta^\gamma(m)$, with $\eta^\gamma(m) = 1$ or 0 depending on whether or not there is a gauche isomer associated with m. Then we have

$$\langle \eta^{(1)}(x)\rangle = \frac{\sum_\gamma P_\gamma \sum_{m=1}^{n} \eta^\gamma(m)\delta(x - x_m^\gamma)}{\sum_\gamma P_\gamma} \tag{5.36}$$

where P_γ is the probability of a configuration γ. The denominator is equal to unity, but is included this way for purposes below.

We next want to express $\langle \eta^{(1)}(x)\rangle$ in terms of propagators. Although $\eta^\gamma(m)$ depends on the sequence of three bond vectors, starting at carbons m-1, m, and m+1, it can actually be specified using only the C–C bond ending at m, α_m^γ, and the C–C bond starting at m + 1, α_{m+2}^γ. So

$$\eta^{\gamma}(m)=\eta\left(\alpha_m^{\gamma},\alpha_{m+2}^{\gamma}\right) \qquad m=1,2,\ldots,n-2 \tag{5.37}$$

$$\eta^{\gamma}(m)=0 \qquad m=n-1,n \tag{5.38}$$

Here $\eta\left(\alpha_m^{\gamma},\alpha_{m+2}^{\gamma}\right)=1$ if α_m^{γ} and α_{m+2}^{γ} form a gauche isomer, otherwise $\eta\left(\alpha_m^{\gamma},\alpha_{m+2}^{\gamma}\right)=0$. There are no gauche isomers beyond carbon $n-2$.

We should also notice that, for the n - 2 atoms,

$$\begin{aligned} P_{\gamma}\delta\left(x-x_m^{\gamma}\right)\eta^{\gamma}(m) &= P_{\gamma}\delta\left(x-x_m^{\gamma}\right)\eta\left(\alpha_m^{\gamma},\alpha_{m+2}^{\gamma}\right) \\ &= \sum_{\beta_1\beta_2'} P_{\gamma}\delta\left(x-x_m^{\gamma}\right)\eta(\beta_1,\beta_2')\delta_{\alpha_m^{\gamma},\beta_1}\delta_{\alpha_{m+2}^{\gamma},\beta_2'} \end{aligned} \tag{5.39}$$

where β_1 and β_2' are all from 1 to 4.

Equation (5.36) can be expressed as

$$\left\langle \eta^{(1)}(x)\right\rangle = \frac{\sum_{\gamma}\sum_{m=1}^{n-2}\sum_{\beta_1\beta_2'} P_{\gamma}\delta\left(x-x_m^{\gamma}\right)\delta_{\alpha_m^{\gamma},\beta_1}\delta_{\alpha_{m+2}^{\gamma},\beta_2'}\eta(\beta_1,\beta_2')}{\sum_{\gamma} P_{\gamma}} \tag{5.40}$$

Since $\eta(\beta_1,\beta_2')$ does not depend on γ, (5.40) can be further expressed as

$$\left\langle \eta^{(1)}(x)\right\rangle = \frac{\sum_{m=1}^{n-2}\sum_{\beta_1,\beta_2'}\eta(\beta_1,\beta_2')\left(\sum_{\gamma} P_{\gamma}\delta\left(x-x_m^{\gamma}\right)\delta_{\alpha_m^{\gamma},\beta_1}\delta_{\alpha_{m+2}^{\gamma},\beta_2'}\right)}{\sum_{\gamma} P_{\gamma}} \tag{5.41}$$

Here $\sum_{\gamma} P_{\gamma}\delta\left(x-x_m^{\gamma}\right)\delta_{\alpha_m^{\gamma},\beta_1}\delta_{\alpha_{m+2}^{\gamma},\beta_2'}$ is proportional to the total probability that the atom m of a chain is on layer x, with C–C bond β_1 ending at atom m and C–C bond β_2' starting at atom $m+1$. Thus, if $m=1$,

$$\sum_{\gamma} P_{\gamma}\delta\left(x-x_m^{\gamma}\right)\delta_{\alpha_m^{\gamma},\beta_1}\delta_{\alpha_{m+2}^{\gamma},\beta_2'} \propto \sum_{\beta_1'} G^{(1)}\left(x_0,x\middle|\beta_1\right)e^{-[\varepsilon_2(\beta_1,\beta_1')+\varepsilon_3(\beta_1,\beta_2')]}Q^{(n-1)}\left(x\middle|\beta_2',\beta_1'\right) \tag{5.42}$$

where $G^{(1)}(x_0, x|\beta_1)$, $Q^{(m)}(x|\beta_2', \beta_1')$, ε_2 and ε_3 are defined in Section 5.1.

For $m = 2, 3, \ldots, n-2$

$$\sum_{\gamma} P_\gamma \delta(x - x_m^\gamma) \delta_{\alpha_m^\gamma, \beta_1} \delta_{\alpha_{m+2}^\gamma, \beta_2'} \propto \sum_{\beta_2 \beta_1'} G^{(m)}(x_0, x|\beta_2, \beta_1) e^{-[\varepsilon_2(\beta_1, \beta_1') + \varepsilon_3(\beta_2, \beta_1') + \varepsilon_3(\beta_1, \beta_2')]} Q^{(n-m)}(x|\beta_2', \beta_1') \tag{5.43}$$

It is also obvious that

$$\sum_{\gamma} P_\gamma \propto \sum_{\beta_1' \beta_2'} Q^{(n)}(x_0|\beta_2', \beta_1') \tag{5.44}$$

So (5.41) can be expressed as

$$\langle \eta^{(1)}(x) \rangle = \frac{\left[\sum_{\beta_1} \sum_{\beta_1' \beta_2'} G^{(1)}(x_0, x|\beta_1) e^{-[\varepsilon_2(\beta_1, \beta_1') + \varepsilon_3(\beta_1, \beta_2')]} \eta(\beta_1, \beta_2') Q^{(n-1)}(x|\beta_2', \beta_1') + \sum_{m=2}^{n-2} \sum_{\beta_1 \beta_2} \sum_{\beta_1' \beta_2'} \left(G^{(m)}(x_0, x|\beta_2, \beta_1) e^{-[\varepsilon_2(\beta_1, \beta_1') + \varepsilon_3(\beta_2, \beta_1') + \varepsilon_3(\beta_1, \beta_2')]} \times \eta(\beta_1, \beta_2') Q^{(n-m)}(x|\beta_2', \beta_1') \right) \right]}{\sum_{\beta_1' \beta_2'} Q^{(n)}(x_0|\beta_2', \beta_1')} \tag{5.45}$$

5.4 Segment Distributions

We define the segment distribution as the probability that a certain carbon of one chain is on layer x within the bilayer. We denote it as $P_c(m, x)$, where m is the carbon number, and x is the layer number. It is clear that $P_c(m,0)$ and $P_c(m,t_C)$ are equal to 0 since the carbon density is 0 on these two layers. For the others, we can use the propagators again.

For $2 \le m \le n-2$, where n is the chain length, the probability that carbon atom m is on layer x is proportional to

$$\sum_{\beta_1 \beta_2} \sum_{\beta_1' \beta_2'} G^{(m)}(x_0, x|\beta_2, \beta_1) e^{-[\varepsilon_2(\beta_1, \beta_1') + \varepsilon_3(\beta_2, \beta_1') + \varepsilon_3(\beta_1, \beta_2')]} Q^{(n-m)}(x|\beta_2', \beta_1') \tag{5.46}$$

Since this carbon atom must be somewhere between layer 1 and layer $t_C - 1$ inclusive, the normalization constant should be

$$\sum_{x=1}^{t_C-1} \sum_{\beta_1\beta_2} \sum_{\beta_1'\beta_2'} G^{(m)}(x_0, x|\beta_2, \beta_1) e^{-[\varepsilon_2(\beta_1,\beta_1')+\varepsilon_3(\beta_2,\beta_1')+\varepsilon_3(\beta_1,\beta_2')]} Q^{(n-m)}(x|\beta_2', \beta_1') \tag{5.47}$$

It should be proportional to the sum of the probabilities of all the configurations. Because all the propagators are calculated with the same proportionality constant, (5.47) is equal to $\sum_{\beta_1'\beta_2'} Q^{(n)}(x_0|\beta_2', \beta_1')$, which is also proportional to the sum of the probabilities of all the configurations.

Thus, for $2 \le m \le n-2$,

$$P_c(m,x) = \frac{\sum_{\beta_1\beta_2} \sum_{\beta_1'\beta_2'} G^{(m)}(x_0, x|\beta_2, \beta_1) e^{-[\varepsilon_2(\beta_1,\beta_1')+\varepsilon_3(\beta_2,\beta_1')+\varepsilon_3(\beta_1,\beta_2')]} Q^{(n-m)}(x|\beta_2', \beta_1')}{\sum_{\beta_1'\beta_2'} Q^{(n)}(x_0|\beta_2', \beta_1')} \tag{5.48}$$

Similarly we have

$$P_c(1,x) = \frac{\sum_{\beta_1} \sum_{\beta_1'\beta_2'} G^{(1)}(x_0, x|\beta_1) e^{-[\varepsilon_2(\beta_1,\beta_1')+\varepsilon_3(\beta_1,\beta_2')]} Q^{(n-1)}(x|\beta_2', \beta_1')}{\sum_{\beta_1'\beta_2'} Q^{(n)}(x_0|\beta_2', \beta_1')} \tag{5.49}$$

$$P_c(n-1,x) = \frac{\sum_{\beta_1\beta_2} \sum_{\beta_1'} G^{(n-1)}(x_0, x|\beta_2, \beta_1) e^{-[\varepsilon_2(\beta_1,\beta_1')+\varepsilon_3(\beta_2,\beta_1')]} Q^{(1)}(x|\beta_1')}{\sum_{\beta_1'\beta_2'} Q^{(n)}(x_0|\beta_2', \beta_1')} \tag{5.50}$$

$$P_c(n,x) = \frac{\sum_{\beta_1\beta_2} G^{(n)}(x_0, x|\beta_2, \beta_1)}{\sum_{\beta_1'\beta_2'} Q^{(n)}(x_0|\beta_2', \beta_1')} \tag{5.51}$$

Chapter 6

Results and Experimental Comparisons

6.1 Model Parameters

Our present work for mixtures uses the parameters adopted by Whitmore et al. [1]. They are summarized in Table 6.1.

Table 6.1

Material and interaction parameters used in the calculations. For convenience, the interaction parameters are expressed here in units of $k_B T_0$, with $T_0 = 300\,K$. The interaction parameters, $W_{kk'}$, and gauche isomer energy, E_g, are defined in Sections 2.2 and 3.2.

C–C bond	Layer thickness	v_0	h	l	$E_g/k_B(K)$
$1.5\,\mathring{A}$	$1.25\,\mathring{A}$	$16\,\mathring{A}^3$	6	14 – 24	250
W_{cc}	W_{cs}	W_{ch}	W_{ss}	W_{hs}	W_{hh}
-1	-0.5	-1	-5	-5.2095	-5
χ_{cs}	χ_{ch}	χ_{hs}			
2.5	2	-0.2095			

The C-C bond distance is $1.5\,\mathring{A}$. Its projection along the bilayer perpendicular is $1.25\,\mathring{A}$, which is the layer thickness in our model. v_0 is the volume associated with each unit, including one carbon and two hydrogen atoms.

Each hydrocarbon unit along a chain is modeled as a unit in our model, and we include the initial C=O complex, so the units per chain is l = 14, 16, 18 and 20 respectively for dimyristoyl phosphatidylcholine (DMPC), dipalmitoyl phosphatidylcholine (DPPC), distearoyl phosphatidylcholine (DSPC) and diarachinoyl phosphatidylcholine (DAPC).

From experimental results we can obtain the volume of headgroup. Dividing this value by v_0, we can get the units per headgroup, $2h$, which should be rounded to an integer in our model. For all the PC's the appropriate value is $h = 6$, while for all the PE's $h = 5$. The work in this thesis is all for $h = 6$.

6.2 The Calculation Procedure

Our goal is to find the equilibrium phase and structure of the bilayers. First, we assume that the lipids mix, and find the equilibrium thickness and areal density of the mixture at the given temperature T and external pressure P_0. We need to minimize the partial Gibbs free energy, $\Delta\overline{G}_l$, subject to the condition that $\overline{P} = P_0$, where $\overline{P}$ is the internal pressure, given by equation (4.3). For a specific composition, the procedure is to conduct self-consistent calculations at a series of thicknesses, with $\overline{P} = P_0$ satisfied at every thickness, thus obtaining a curve of $\Delta\overline{G}_l$ as a function of bilayer thickness, and then find the minimum $\Delta\overline{G}_l$. There may be more than one local minimum. The location and value of the global minimum give the equilibrium thickness and partial Gibbs free energy for that composition, T and P_0. The corresponding value of areal density $\rho_l = {}_1\rho_l + {}_2\rho_l$ is the equilibrium areal density. We then repeat the procedure for all the compositions to check

that the mixtures are stable (The calculations in this thesis are all done for high enough temperature so that the systems are in the liquid crystal phase). Once we have located the minimum $\Delta\overline{G_I}$ for a certain composition, and made sure that the system is in a stable liquid crystal phase, we calculate other properties and quantities such as gauche isomers, orientational order parameter, segment distribution, etc.

The core calculations are the SCF calculations at each thickness. Each calculation is carried out for a specific system at a particular T and P_0. The system is specified by the headgroup and tail lengths of the two lipids in the mixture, i.e. the values of h, l_1 and l_2, and the proportion of each one. The SCF calculation is restricted to the hydrocarbon core, so the thickness can be specified by t_C.

We also need a convenient way of specifying the average density. In the calculations, we use the average free volume, ϕ, in the interior. Simple geometric volume considerations give

$$\phi = 1 - 4\left(\frac{{}_1\rho_l l_1 + {}_2\rho_l l_2}{t_C}\right) \tag{6.1}$$

where l_1 and l_2 are, respectively, the chain lengths of the long and short chains, and ${}_1\rho_l$ and ${}_2\rho_l$ are, respectively, the number densities of the hydrocarbon units for long and short chains.

Because there are almost no vacancies in the headgroup regions, the overall proportion of unoccupied sites in the whole bilayer is

$$\Phi_l = \phi\left(\frac{t_C}{t_B}\right) \tag{6.2}$$

and the proportion of the occupied sites of the bilayer is $1-\Phi_l$.

To calculate $\Delta\overline{G}_l$ for a given thickness, we first choose a reasonable value for ϕ, carry out the SCF calculation, and then calculate $\overline{P}$. In general, $\overline{P} \neq P_0$ at this step. We then repeat for different values of ϕ, searching until we find the value of ϕ for which $\overline{P} = P_0$. We then calculate $\Delta\overline{G}_l$ for that thickness.

We then repeat this for different thicknesses, thus generating the function $\Delta\overline{G}_l$ vs. thickness. The detailed description of the self-consistent calculations for each thickness and density can be found in the paper of Whitmore et al. [1].

The pressure scale in the calculations is $k_B/v_0 = 8.62\times10^5\, Nm^{-2} = 8.62\, bar$, which derives from the energy scale and the unit cell volume. Under this scale, ambient pressure corresponds approximately to $P_0 \approx 0.1$. In experiments, pressures on the order of hundreds of atmospheres are needed to affect the bilayers. Accordingly, we can choose $P_0 = 0$ to model ambient pressure in our calculations. All the results presented in this thesis are for this pressure.

6.3 Free Energy and Free Volume of Mixtures

Figures 6.1 to 6.4 show results for a typical mixture, which is a 50:50 blend of DMPC and DPPC, with $l = 14$ and 16, respectively. The temperature is 338 K, which is above their main transition temperatures of 297 K for DMPC and 314 K for DPPC [37]. For this

system, the free volume at each thickness is shown in Figure 6.1. When the thickness is smaller than 29, the free-volume/thickness relation gives a smooth curve, which reaches maximum at about thickness 17, while in the results of Whitmore et al. [1] for single component DPPE bilayer, the free volume reaches its maximum at about thickness 18.

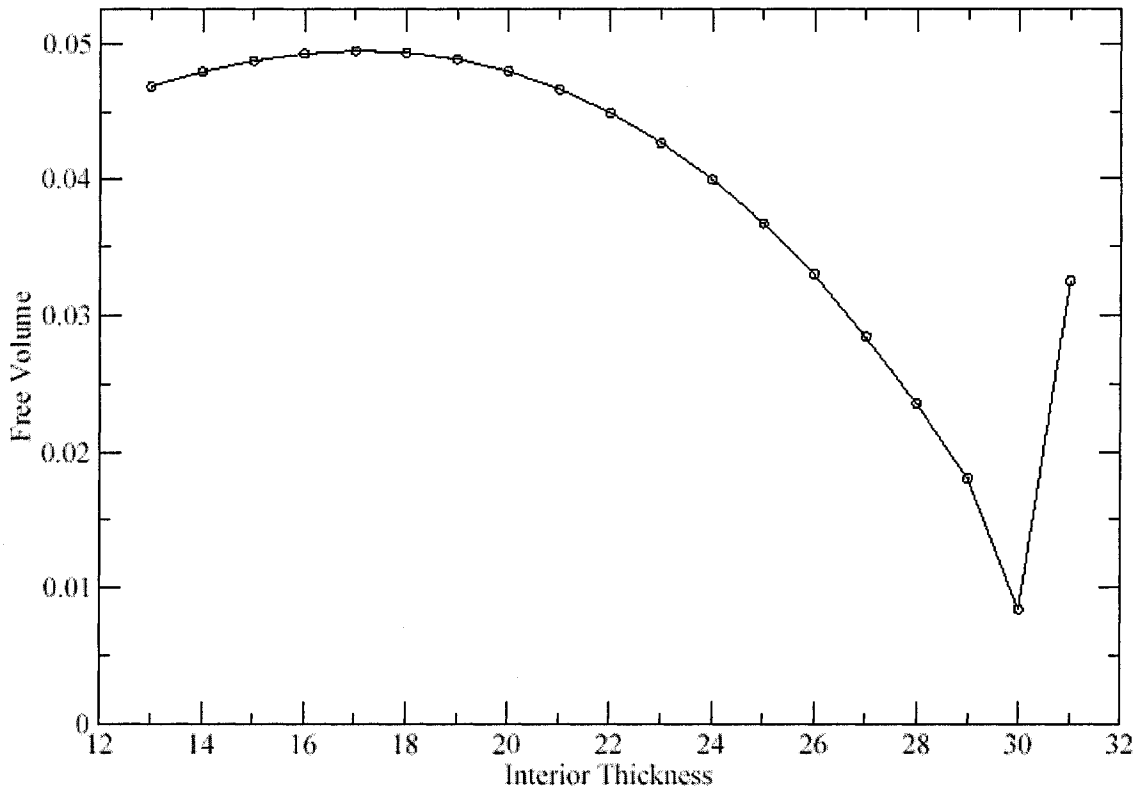

Figure 6.1

The relationship between the free volume and the interior thickness, for the binary mixture of equimolar DPPC and DMPC. The temperature is 338 K and the pressure is the ambient pressure.

For larger thicknesses up to 30, the free volume can be fitted to a power law function, with the result

$$\phi \propto \left(1 - t_C / t_C^0\right)^{0.54} \tag{6.3}$$

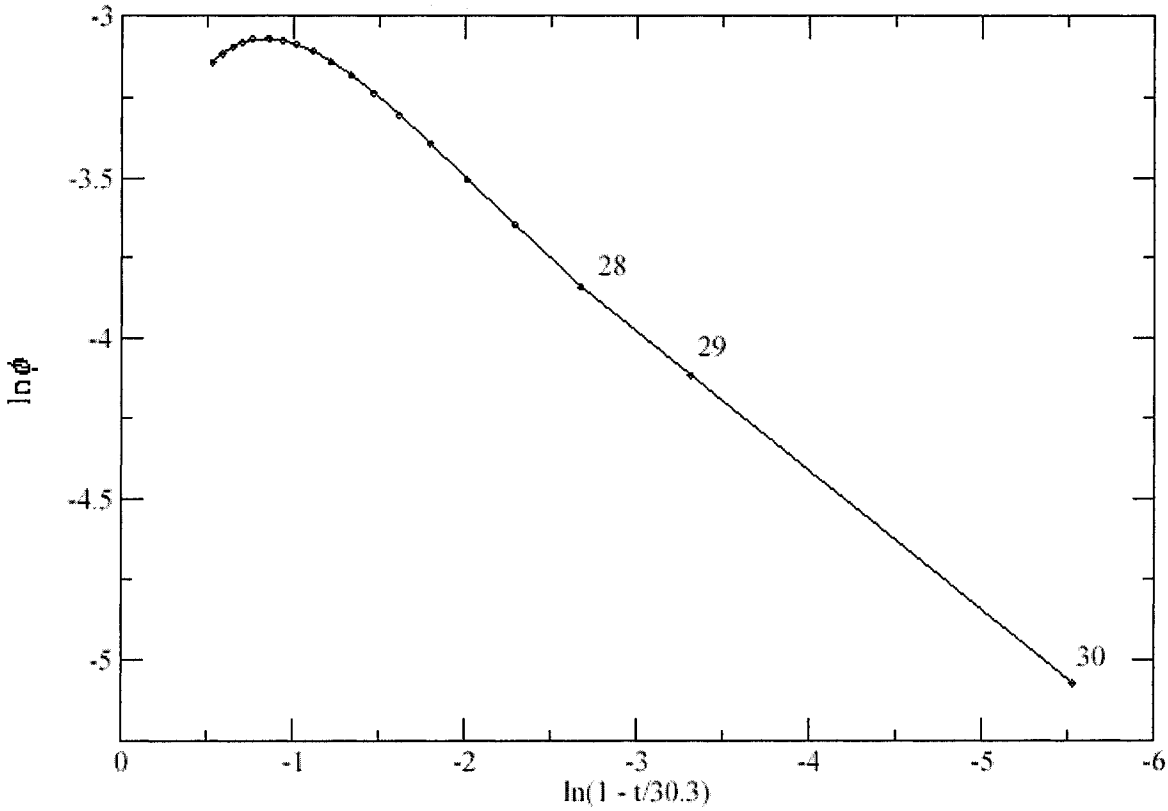

Figure 6.2

The relationship of $\ln\phi$ and $\ln(1-t_C/30.3)$, for the binary mixture of equimolar DPPC and DMPC. The temperature is 338K and the pressure is the ambient pressure.

where $t_C^0 = 30.3$. This fit is shown in Figure 6.2. It can be compared with the results of Whitmore et al. [1] for single component DPPE bilayer. They obtained the same form, but $t_C^0 = 32$, and power 0.55. So we can see that from single component bilayer to binary bilayer, the power remains essentially the same, while t_C^0 shifts. For our binary system, the linear relationship between $\ln\phi$ and $\ln(1-t_C/30.3)$ can be seen in Figure 6.2. The free volume decreases sharply at thickness 30 instead of at thickness 32 as in the results of Whitmore et al. [1] for pure DPPE bilayer. This is reasonable because the presence of

50% length-14 chains, which requires such a sharp decrease at thickness 28 in the case of pure length-14 chains, plays an important role.

We can also see that, at thickness 31, the free volume increases sharply to about 0.0325, while in the result of Whitmore et al. for single component DPPE bilayer, the free volume decreases smoothly at thickness 31, and then decreases to very near zero at thickness 32. The following calculation will help to explain the increase in free volume at larger thickness for binary bilayers:

Physically, the minimum possible value for ϕ, $\phi_{\min}$, will occur if the short chains are fully extended over their whole length l_2, the longer chains are fully extended up to l_2, and there are no vacancies in the region up to l_2. If $t_C > 2l_2$, for low enough fraction of long chains, there will be some free volume in the middle. We can calculate the minimum overall free volume as follows. If there are N_l lipids altogether, then the total volume of this bilayer is $N_l \cdot t_C$. If there are ${}_1N_l$ long lipids and ${}_2N_l$ short lipids, then the total volume occupied by the carbons is $2[{}_1N_l l_1 + {}_2N_l l_2]$ (Factor of 2 because of 2 chains per lipid). The fraction of sites occupied is thus

$$\begin{aligned} f_{occ} &= 2[{}_1N_l l_1 + {}_2N_l l_2]/[N_l \cdot t_C] \\ &= 2[f_1 l_1 + f_2 l_2]/t_C \end{aligned} \tag{6.4}$$

where f_i are the fractions of lipids. The overall free volume is $\phi = 1 - f_{occ}$. Using $f_2 = 1 - f_1$, we get

$$\phi_{\min} = 1 - 2[l_2 + f_1(l_1 - l_2)]/t_C \tag{6.5}$$

In our calculations, $l_1 = 16$, $l_2 = 14$ and $t_C = 31$. Substituting all these in gives

$$\phi_{\min} = 0.09677 - 0.129 f_1 \tag{6.6}$$

The free-volume/percentage-of-long-chain relationship is plotted in Figure 6.3 together with $\phi_{\min}$. We can see that when the percentage of long chains is lower than 65, the actual free volume is very near $\phi_{\min}$, which is a linear relationship. For example, for 50% of short chains, $\phi_{\min} = 0.0323$, while the SCF result is 0.0325. Their difference is only 0.02 percent.

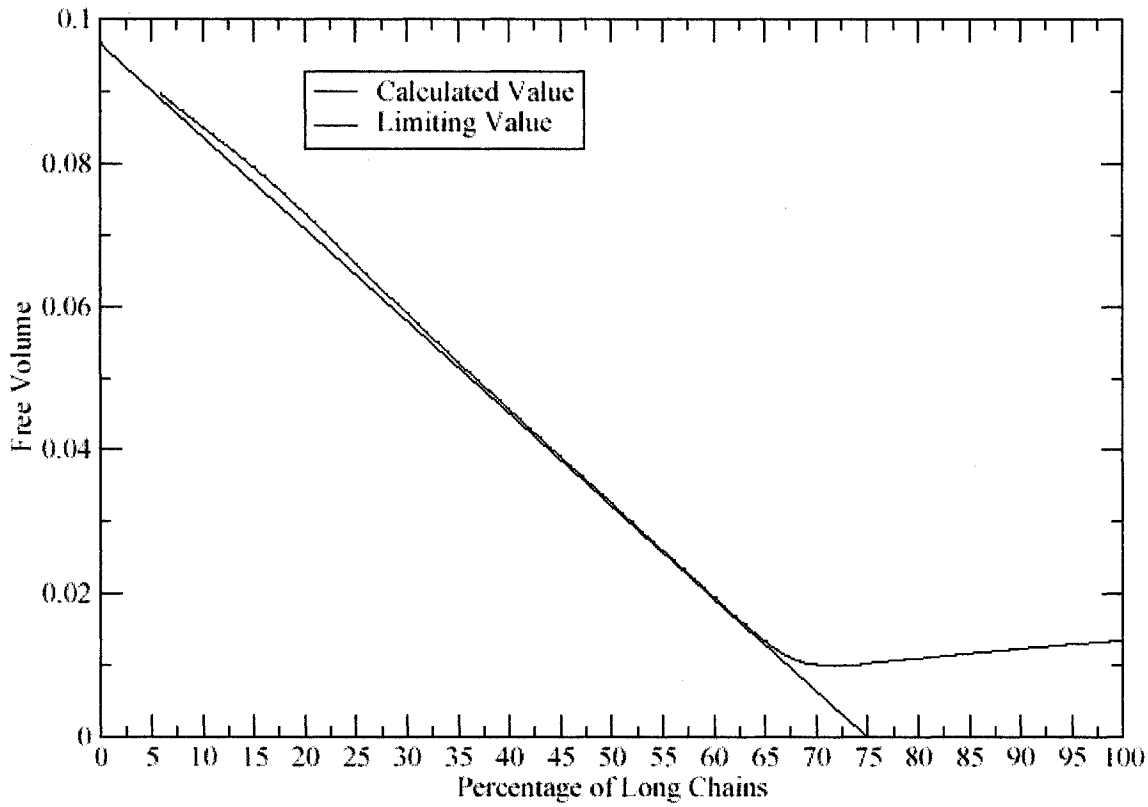

Figure 6.3

The relationship between the free volume and the long-chain percentage, for the binary mixture of DPPC and DMPC. The temperature is 338K, the pressure is the ambient pressure, and the thickness of the bilayer interior is 31. The black line is the predicted limiting value, $\phi_{\min}$, while the red line is the calculated value.

This observation is very useful for obtaining convergent results for a thickness near double the long chain length. For such thicknesses, we usually first calculate for 100% of long chains, then make further calculations by decreasing 5% or even 1% of long chains, and increasing the percentage of short chains correspondingly. Each time we use the converged mean field obtained by the last calculation. Under these circumstances, without the above analysis, it is very hard to make a good initial guess.

With the self-consistent solutions corresponding to each point on Figure 6.1, we can calculate the partial Gibbs free energy, $\Delta\overline{G}_l$, at each thickness. The results are shown in Figure 6.4. The global minimum of Figure 6.4 gives the equilibrium state. Its location is the equilibrium thickness. On Figure 6.4, the global minimum happens at $t_C \approx 19$, and the corresponding state is a liquid crystal phase. The actual minimum is found by interpolation.

For binary mixtures, we then make the above calculations for a series of compositions, and obtain the curve of partial Gibbs free energy vs. composition. Figure 6.5 shows this for binary mixtures of lipids of chain lengths 16 and 14, 18 and 14, as well as 20 and 14. The temperature is 338 K. It is obvious that the curvature, namely, the second derivative, of all three curves is always positive, which means that there is no phase separation in any of these three mixtures. The three curves all start at the same left point, which is the pure DMPC bilayer, but they have different right ending points, which correspond respectively to single-component bilayers of lipids with chain length 16, 18 and 20. The results show that under the same environment, the partial Gibbs free energy of single-

component bilayers increases with chain length, so the transition temperature also increases with chain length. Figure 6.5 also tells us that, at a given composition, mixing with lipids with longer chains will result in higher Gibbs free energy, and thus will lead to higher phase transition temperatures.

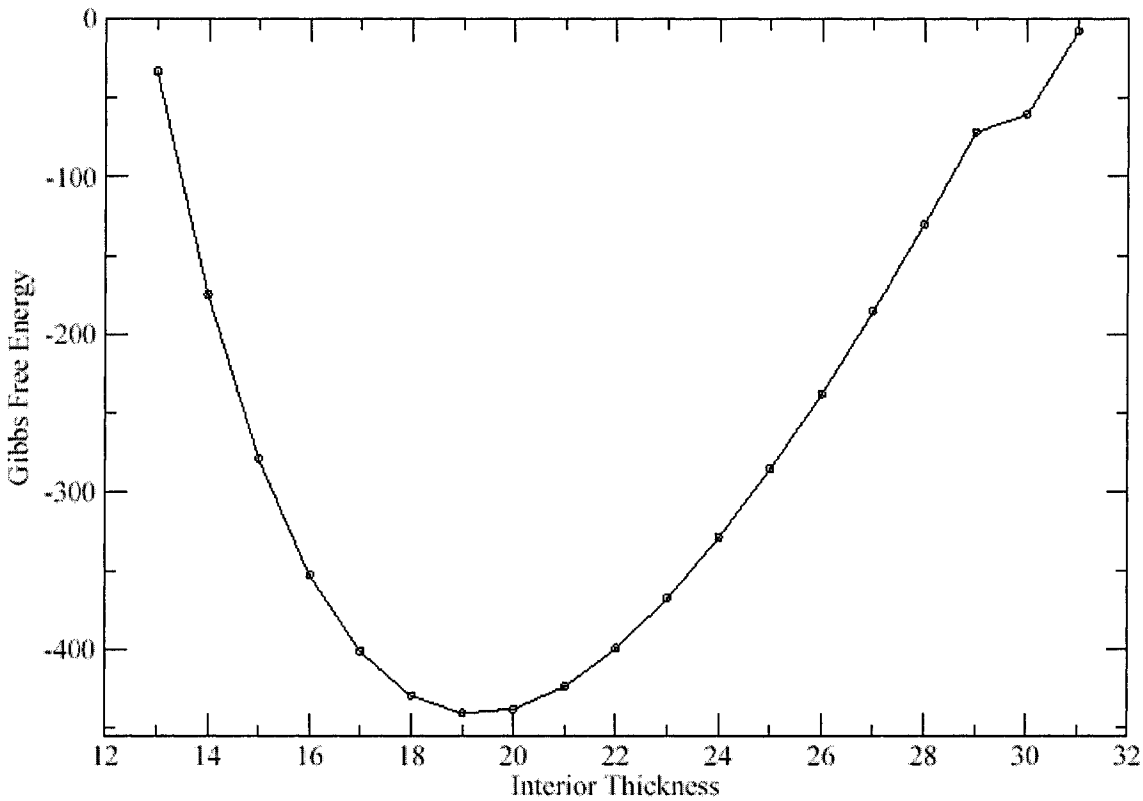

Figure 6.4

The dependence of Gibbs free energy on thickness, for the binary mixture of equimolar DPPC and DMPC. The temperature is 338K, and the pressure is the ambient pressure.

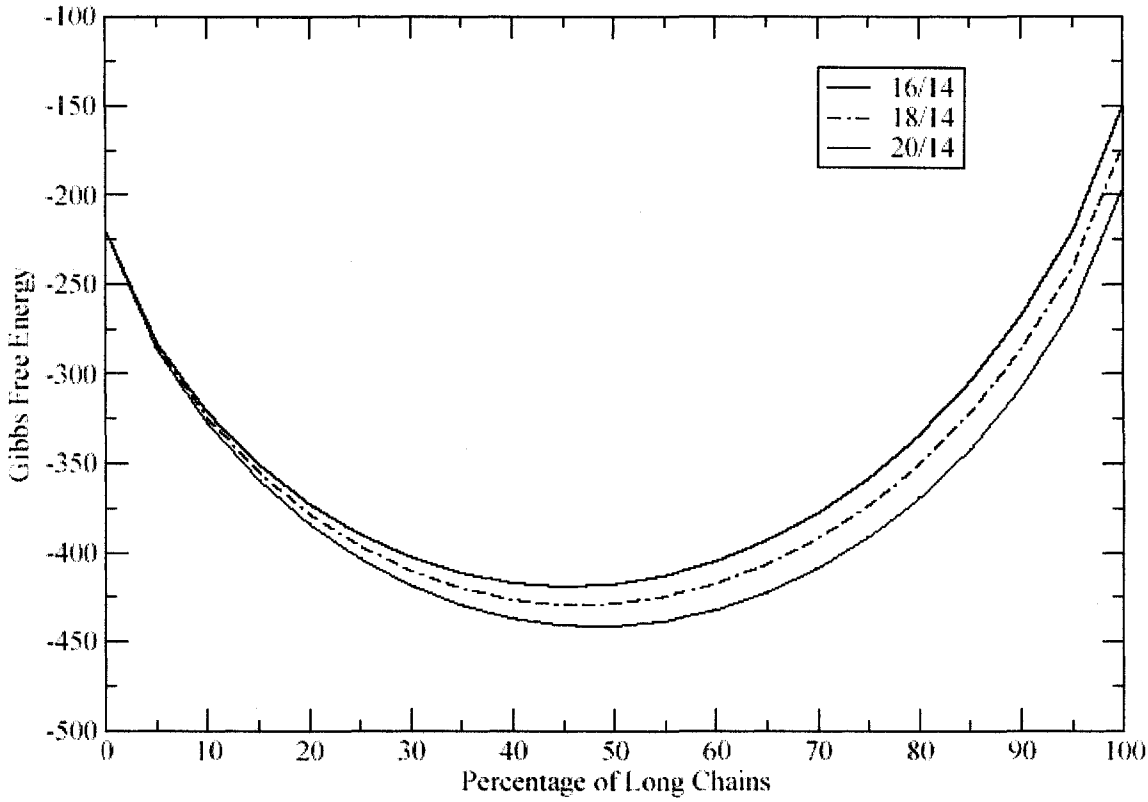

Figure 6.5

The relationship between the Gibbs free energy and the long-chain percentage, for the binary mixtures of DPPC/DMPC, DSPC/DMPC, and DAPC/DMPC. The temperature is 338K, and the pressure is the ambient pressure.

6.4 Order Parameters

6.4.1 Average Order Parameters

Figure 6.6 shows the dependence of the average orientational order parameter on composition for mixtures of DSPC and DMPC. The temperature is 338 K. The average orientational order parameter is the summation of the orientational order parameters corresponding to all the carbon atoms along a chain divided by the number of carbon

atoms along a chain. In this thesis we denote it as $\overline{S}_{CD}$. On Figure 6.6, the left hand side corresponds to pure DMPC (short chains) and the right hand side corresponds to pure DSPC (long chains). The upper and lower curves are the average order parameters of the short and long chains respectively. The left end of the upper curve corresponds to pure short chains, and the right end of this curve corresponds to a single short chain in a bilayer of long chains. Similarly, the right end of the lower curve corresponds to pure long chains, and the left end of this curve corresponds to a single long chain in a bilayer of short chains.

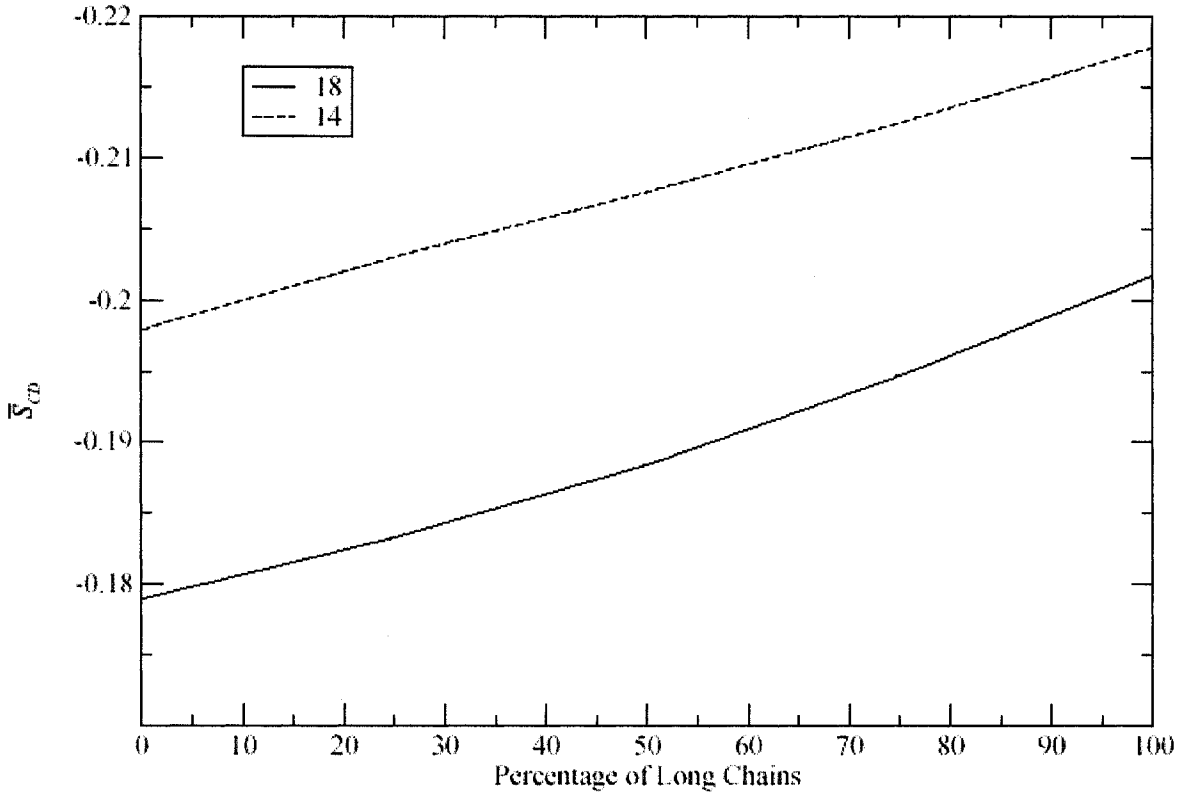

Figure 6.6

The relationship between the average orientational order parameter and the long-chain percentage, for the binary mixture of DSPC (chain length 18) and DMPC (chain length 14). The temperature is 338 K, and the pressure is the ambient pressure.

From this figure, we see that at any composition, the average orientational order parameter of the short chains is always larger in magnitude than that of the long chains. The magnitude of average orientational order parameter of single component bilayer of lipids of chain length 14, 0.198, lies below the average orientational order parameter of single component bilayer of lipids of chain length 18, 0.202. This observation can be generalized as that for single–component bilayer, under the same environment, the magnitude of the average orientational order parameter increases with increasing chain length. This is in agreement with the experimental results of Morrow et al. [26].

Figure 6.6 also shows that adding long chain lipids to a bilayer of short chain lipids increases the magnitude of average orientational order parameter of the short chains, while adding short chain lipids to a bilayer of long chain lipids reduces its value for long chain lipids. When there is only one lipid of chain length 18 in a single component bilayer of lipids of chain length 14, the magnitude of average orientational order parameter of the long chain is smaller than that of the host lipids. This is partly because the long chain is in a relatively thin bilayer, so it has to be more disordered to be accommodated. On the contrary, if a single lipid of chain length 14 is put in a single component bilayer of lipids of chain length 18, its average order is greater than that of the host lipids. Similarly, this is partly because the short chain is in a relatively thick bilayer, so its average extension, along with the magnitude of the average orientational order parameter, will increase.

6.4.2 Order Parameter Profiles

Figures 6.7, 6.8 and 6.9 show the orientational order parameter profiles of all components for mixtures of DPPC/DMPC, DSPC/DMPC, and DAPC/DMPC, respectively, at a temperature of 338 K. Each figure shows results for three compositions, which can be described as 0% DMPC, which means one DMPC molecule in a bilayer of the other component, 50% DMPC, which means equal mixture, and 100% DMPC, which means one DPPC, DSPC or DAPC molecule in a bilayer of DMPC. All results presented here are at the equilibrium thicknesses for the particular mixtures, determined through a full set of calculations as described in the Sections 6.2 and 6.3.

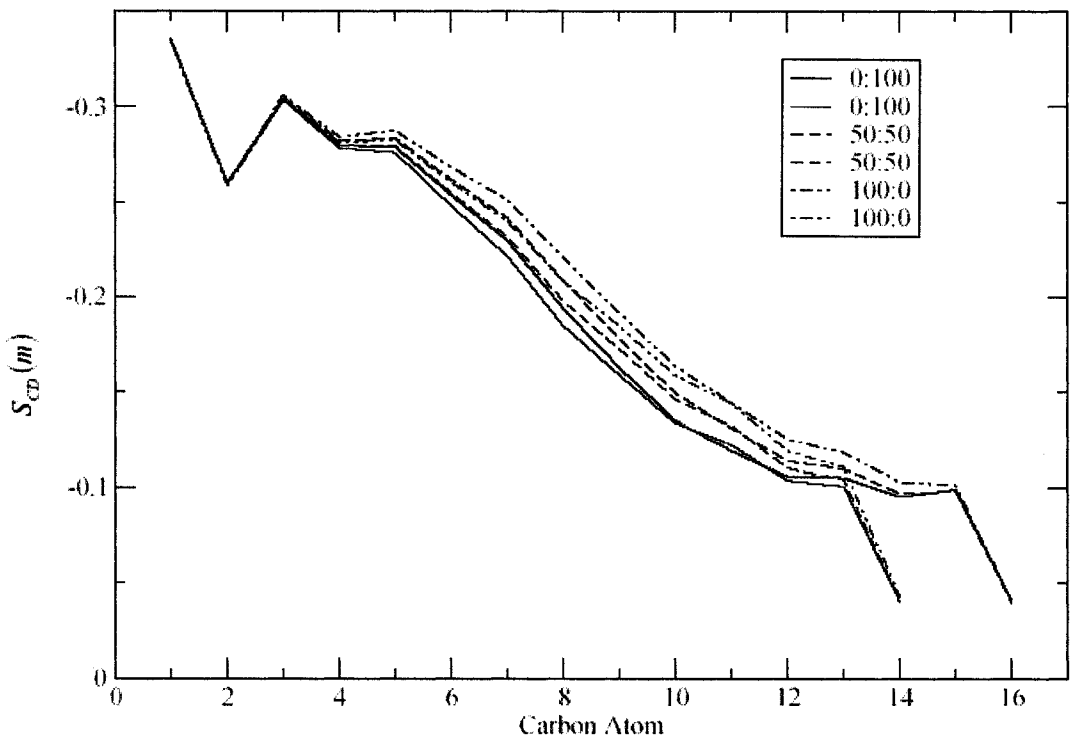

Figure 6.7

The orientational order parameter profiles for binary mixtures of DPPC and DMPC. The temperature is 338 K, and the pressure is the ambient pressure. Here 0:100 means one DPPC in a DMPC bilayer, 50:50 means 50% DPPC, and 100:0 means one DMPC in a DPPC bilayer.

We begin with Figure 6.7, DMPC and DPPC, which have a chain length difference of two units. The longer black dash-dotted curve is pure DPPC. The short red solid curve is pure DMPC. The curves are qualitatively the same. They start at the same value, $|S_{CD}| \approx 0.335$, initially oscillate, then decrease monotonically to a common final value of $|S_{CD}| \approx 0.041$. Throughout most of the chains, from $m \approx 3$ to $m \approx 13$, the individual values of $|S_{CD}(m)|$ for the longer chain are greater than for the shorter chain.

The shorter red dash-dotted curve is for one short-chain molecule in the long-chain bilayers. It starts and ends at the same values as the case of pure bilayers. However, in between, $|S_{CD}(m)|$ is increased above its values in pure DMPC, partly but not completely to the corresponding values of the long-chain hosts. Similarly, the long black solid curve describes a single long-chain molecule in a short-chain host. In this case, $|S_{CD}(m)|$ for the long chains is reduced, partly but not completely to the corresponding values for the hosts. One can see that mixing short and long chains generally reduces the order parameter of the long chains, and increases that of the short chains, except at the two ends of all the chains.

Perhaps the most interesting qualitative effect occurs near the free end of the long chain. For pure long chains, $|S_{CD}(m)|$ decreases monotonically in this region. However, as short chains are added, the values are nearly unchanged for the last two carbons, but decrease for the other ones. The result is the development of "plateau" in this region near the tail, which is called the "second plateau" by Lu et al. [3], to distinguish it from the first one that occurs at the other end of the chain.

Figure 6.8 and 6.9 show the effects of increasing differences in chain lengths. There are both quantitative and qualitative effects.

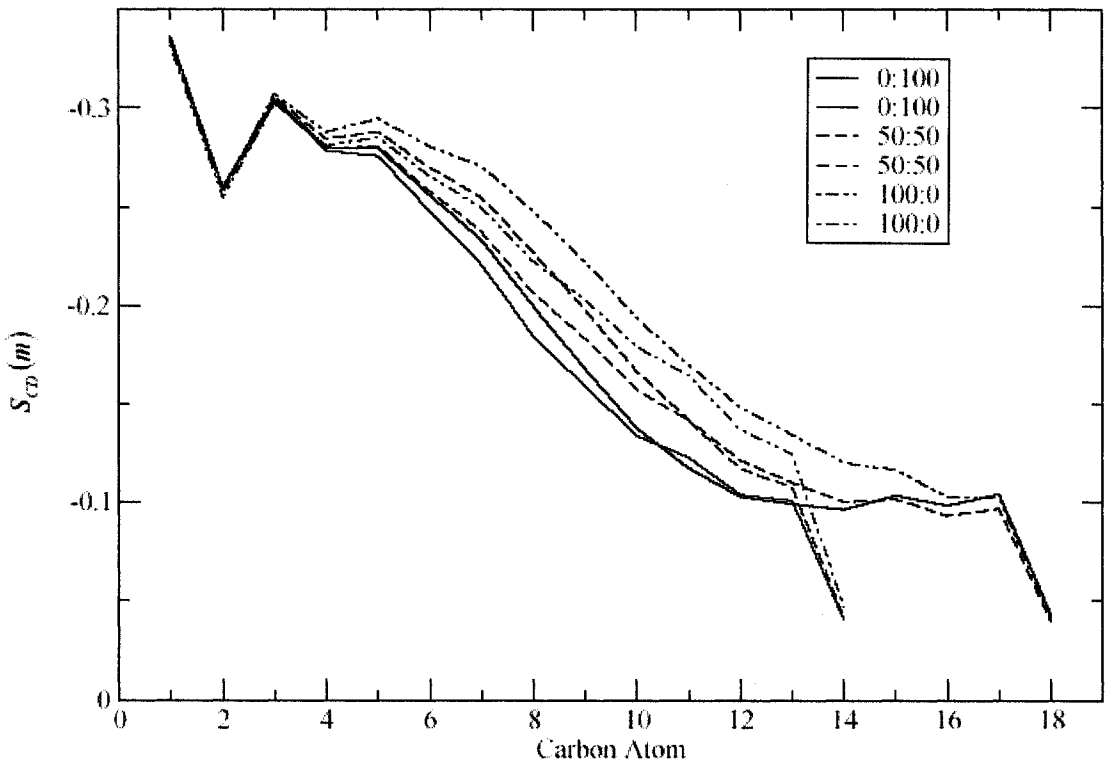

Figure 6.8

The orientational order parameter profiles for binary mixtures of DSPC and DMPC. The temperature is 338 K, and the pressure is the ambient pressure. Here 0:100 means one DSPC in a DMPC bilayer, 50:50 means 50% DSPC, and 100:0 means one DMPC in a DSPC bilayer.

First of all, one can see that the order parameter profile for each unit in a long chain in a bilayer of pure long chains (the longer dash-dotted curve) is always above that of the corresponding unit in a short chain (the shorter solid curve) in bilayer of pure short chains, except very near the headgroup. The difference increases with increasing chain length difference.

Secondly, $|S_{CD}(m)|$ for a long chain in pure short chain bilayer is reduced to about the same as that of the host short chains up to $m \approx 13$. They even cross, by a small amount. The $|S_{CD}(m)|$ for a short chain in pure long chain bilayer is increased, but not as close to that of the host long chains, and the larger the chain length difference, the greater their difference is.

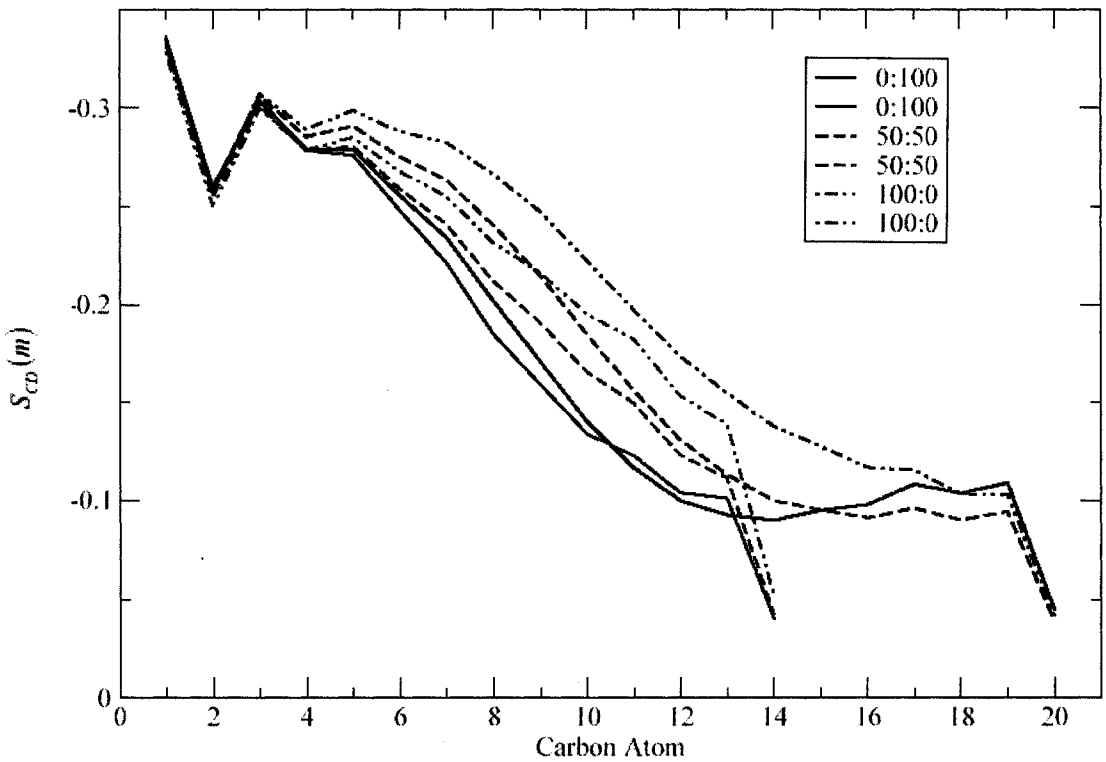

Figure 6.9

The orientational order parameter profiles for binary mixtures of DAPC and DMPC. The temperature is 338 K, and the pressure is the ambient pressure. Here 0:100 means one DAPC in a DMPC bilayer, 50:50 means 50% DAPC, and 100:0 means one DMPC in a DAPC bilayer.

Thirdly, for pure long chains, $|S_{CD}(m)|$ decreases monotonically in the region near the free end of the long chain. However, as short chains are added, all $|S_{CD}(m)|$ initially

decrease. For example, in the 50:50 mixture, they all are below the corresponding values in the pure long-chain bilayers. However, as further short-chain lipids are added, a new effect occurs. The $|S_{CD}(m)|$ near the chain end increase, while those in the middle of the chain continue to decrease. The values of the last two units for one DAPC molecule in DMPC are even slightly greater than those for pure long chain bilayer. The result is a very prominent second plateau in the region near the tail. Comparing the three figures, one can see that the larger the chain length difference, the clearer the second plateau becomes. In Figure 6.9, for one long chain in pure short chain bilayer, there is even a minimum near the free end of the long chain, at $m \approx 14$.

6.5 Interpretation of the Previous Results

We now want to probe in more details the reason for the changes in the order parameter profile, and the mutual effects of the long and short chains. We will argue, in particular, that the second plateau is due to the penetration of the longer chains beyond the middle of the bilayer.

We first need to show what the bilayer thickness is. This is shown in Figure 6.10 for the various systems at 338 K. The thickness increases smoothly and linearly with composition. The middle of the bilayer is, of course, always at one half of the thickness.

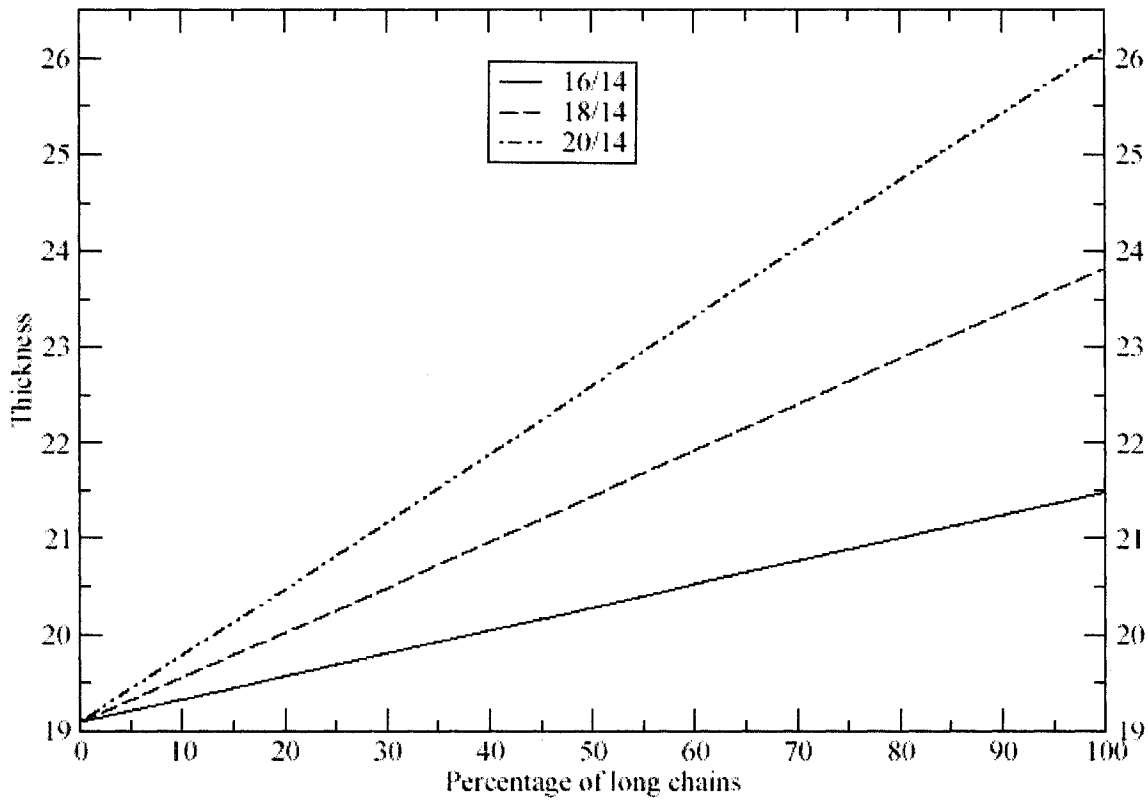

Figure 6.10

The relationship between the thickness and the long-chain percentage, for the binary mixtures of DPPC/DMPC, DSPC/DMPC, and DAPC/DMPC. The temperature is 338 K, and the pressure is the ambient pressure.

We next examine where the last units are, as a measure of how far the chains penetrate. Figure 6.11, 6.12 and 6.13 are the segment distributions of the last units of each chain for the various systems we considered. The maxima of the distribution profiles for the long chains always are approximately at the bilayer midplane. We see this by comparing Figure 6.10 and Figure 6.11 to 6.13.

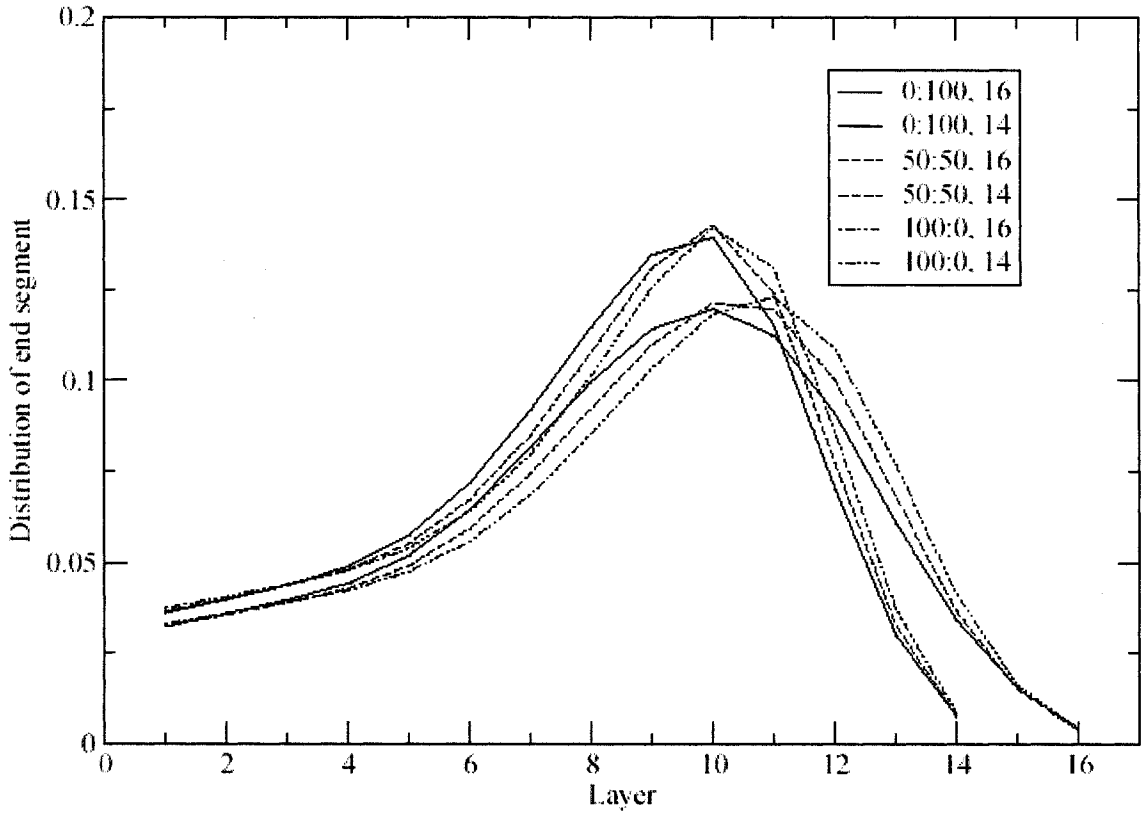

Figure 6.11

The distribution of the end segment for binary mixtures of DPPC and DMPC. The temperature is 338 K, and the pressure is the ambient pressure. Here 0:100 means one DPPC in a DMPC bilayer, 50:50 means 50% DPPC, and 100:0 means one DMPC in a DPPC bilayer.

We consider the 16/14 and 20/14 mixtures in detail. The results are similar for the 18/14 mixtures. From Figure 6.11, we see that the maximum in the distribution of the last segment of the long chain in the pure long-chain system is at about layer 11. As seen from Figure 6.10, the thickness of this bilayer is about 21.5, so the midplane is about layer 10.7, very near 11. As short chains are added, the maximum in the distribution shifts to about layer 10 for the single long chain in DMPC. In this case, Figure 6.11 shows that the midplane is about 9.5. So, again, the maximum in the distribution is about

the midplane. Similarly, for the 20/14 mixtures, the maximum in the distribution of the last segment of the long chain in the pure long-chain system is at about layer 13. As seen from Figure 6.10, the thickness of this bilayer is about 26, so midplane is about layer 13. As short chains are added, the maximum in the distribution shifts to about layer 10 for the single long chain in DMPC. In this case, Figure 6.10 shows that the midplane is about 9.5. So, again, the maximum in the distribution is about the midplane.

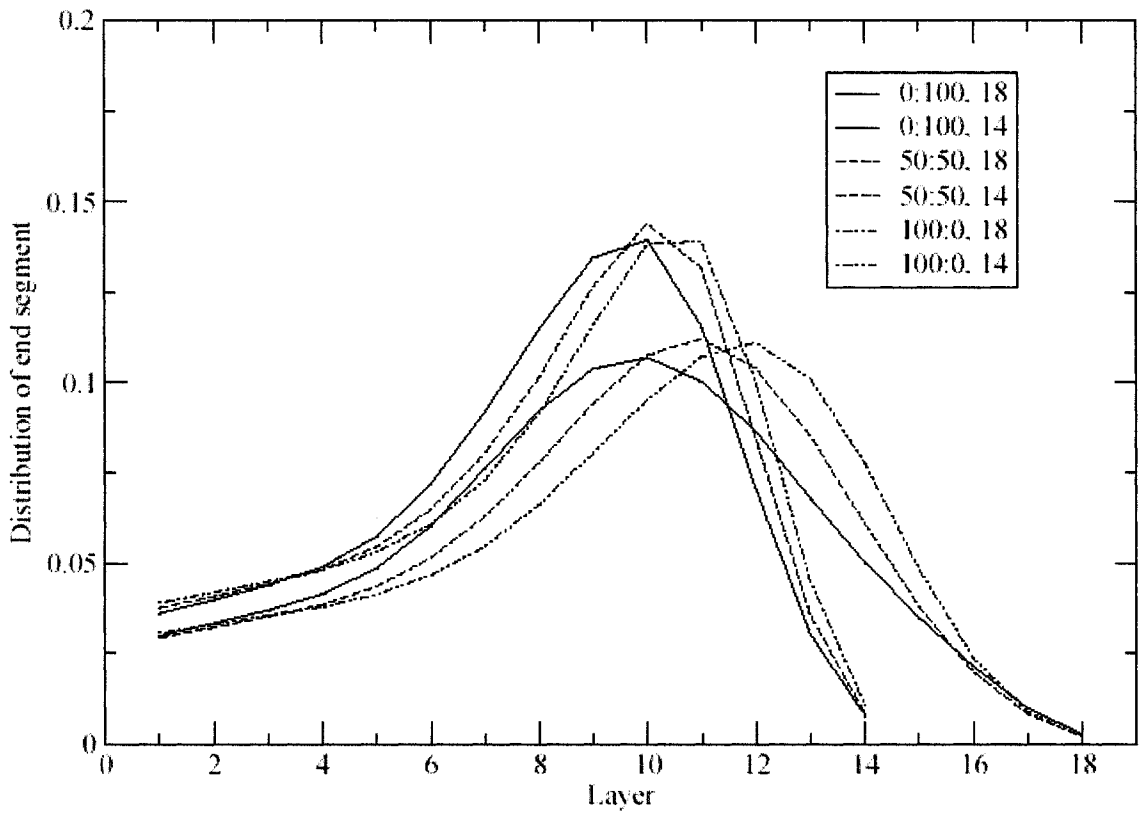

Figure 6.12

The distribution of the end segment for binary mixtures of DSPC and DMPC. The temperature is 338 K, and the pressure is the ambient pressure. Here 0:100 means one DSPC in a DMPC bilayer, 50:50 means 50% DSPC, and 100:0 means one DMPC in a DSPC bilayer.

For short chains, in pure short-chain bilayer, the maximum in the distribution of the last segment is, again, at about one half of the thickness. However, for one short chain in pure long-chain bilayer, the location of the maximum occurs before the midplane, especially when the chain length difference is large. For example, for one DMPC in pure DAPC bilayer, Figure 6.13, the maximum of the distribution of the last segment in the DMPC is at about layer 11, which is smaller than the one half of the thickness, 13.

It is also obvious that the long chains have considerable probability to pass across the bilayer midplanes and to reach low number layers.

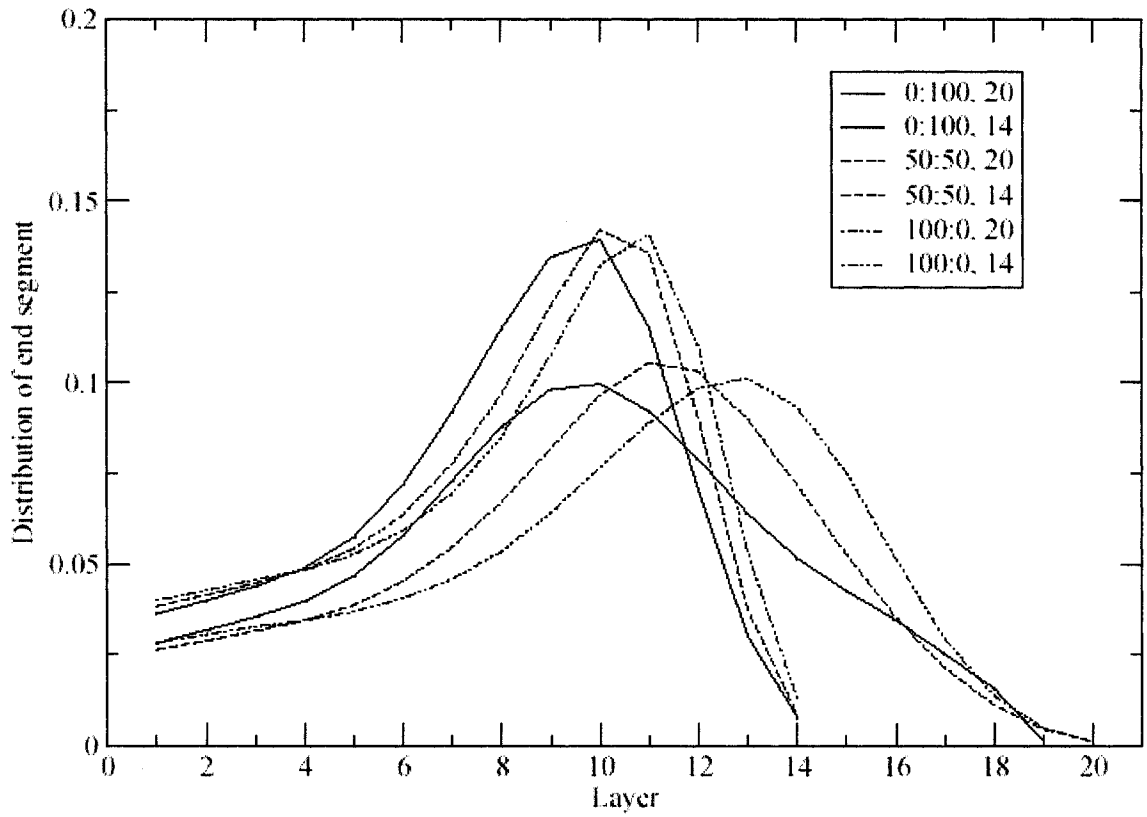

Figure 6.13

The distribution of the end segment for binary mixtures of DAPC and DMPC. The temperature is 338 K, and the pressure is the ambient pressure. Here 0:100 means one DAPC in a DMPC bilayer, 50:50 means 50% DAPC, and 100:0 means one DMPC in a DAPC bilayer.

We next turn to the average order parameter on each layer, $\langle S_{CD}(x) \rangle$. This is shown in Figure 6.14 to 6.16 for 18/14 at pure short, 50:50 and pure long. Because of the ambiguity inherent in the interpolation for $\langle S_{CD}(x) \rangle$ for non-integral thickness, these are shown at the integer thickness closest to the equilibrium thickness in each case. In all cases, $\langle S_{CD}(x) \rangle$ is symmetric about the midplane, has a maximum (in magnitude) a distance of about 1/6 thickness from each side, and a minimum at the center. There is little difference between these results for the three cases shown.

We next consider whether there is any difference in the environment sampled by the segments near the end of the long chains. Figures 6.14 to 6.16 also show the end-segment distribution functions for the corresponding integer thickness (These are the same as those shown in Figure 6.11 to 6.13). The maxima in the end-segment distributions are always at the middle of the bilayer, and the end-segment distribution always terminates at layer 18. In pure long-chain system, the thickness is about 24, but the end-segment distribution ends at layer 18, so the end segment cannot sample the five layers closest to the right side (here and below, layer 24 is not included, since it is the interface to the headgroup region and has no hydrocarbon units). In the 50:50 mixture, the end-segment distribution still ends at layer 18, but the thickness is reduced to 21, so only 2 layers to the right cannot be sampled. For one long chain in pure short-chains, the end-segment distribution still ends at 18, but the thickness is just 19, so all the layers can be sampled, which means that the chain in the mixture penetrates well into the opposite side.

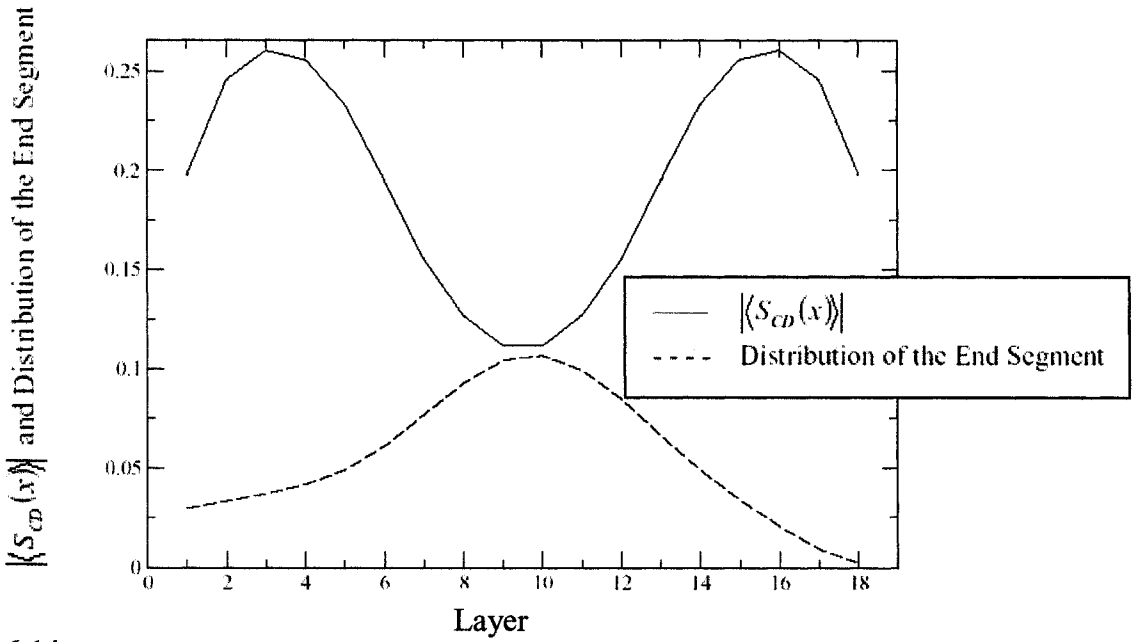

Figure 6.14

The average orientational order parameter on each layer and the distribution of the last segment of a DSPC in a bilayer of DMPC. The temperature is 338 K, and the pressure is the ambient pressure.

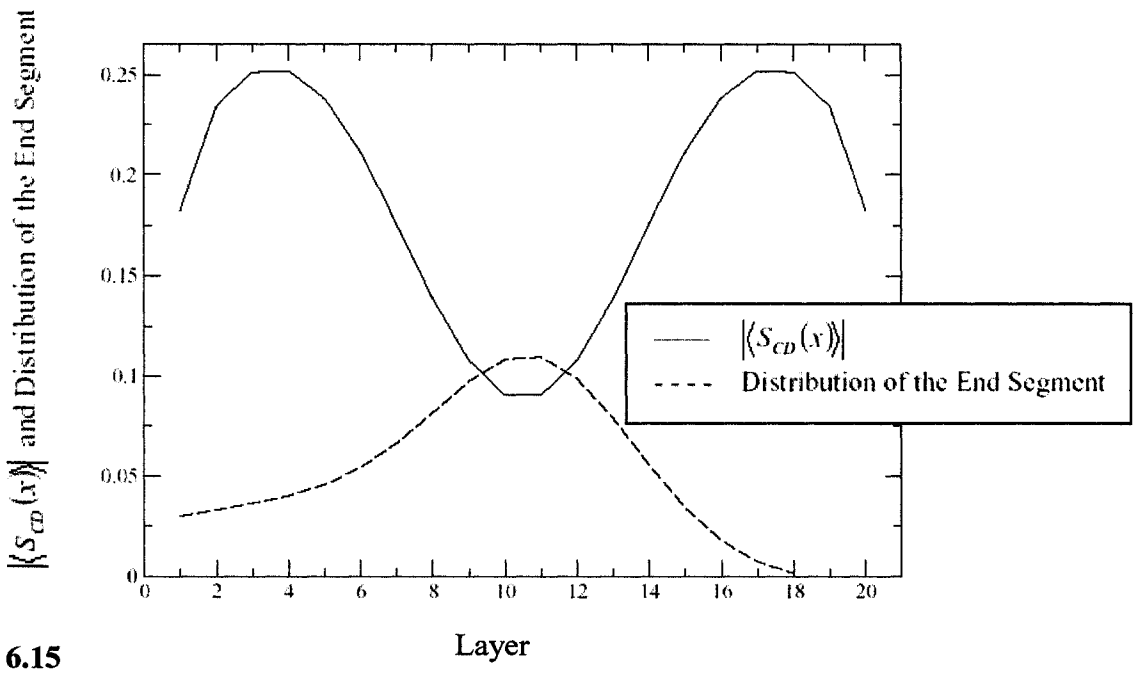

Figure 6.15

The average orientational order parameter on each layer and the distribution of the last segment of DSPC in a bilayer of equimolar DSPC and DMPC. The temperature is 338 K, and the pressure is the ambient pressure.

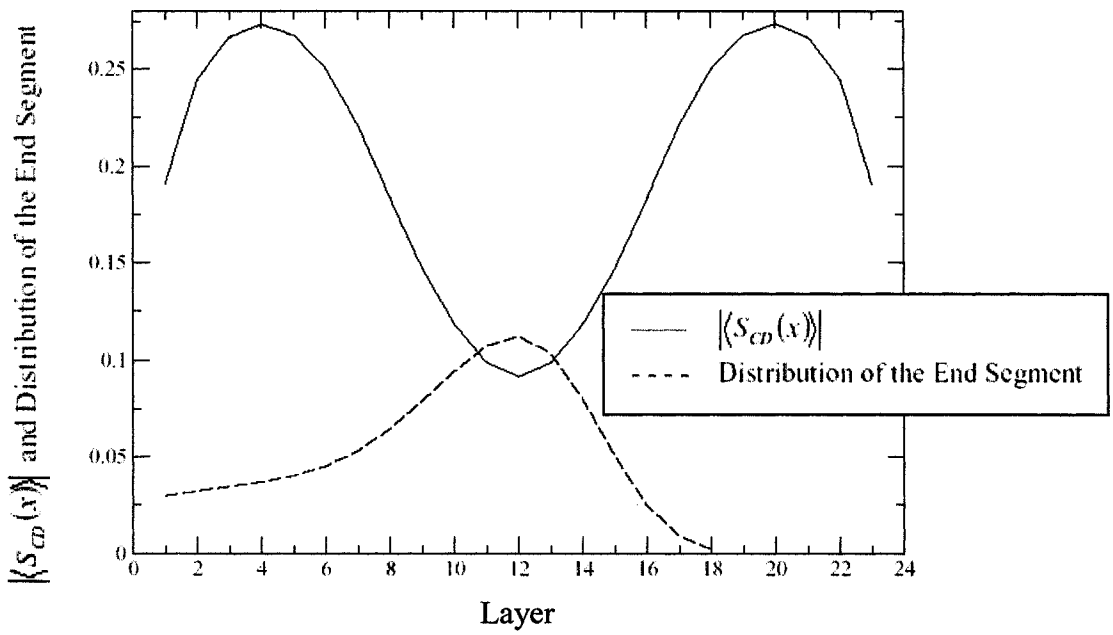

Figure 6.16

The average orientational order parameter on each layer and the distribution of the last segment of DSPC in a bilayer of pure DSPC. The temperature is 338 K, and the pressure is the ambient pressure.

One can notice that the maxima in the segment distributions are at about the same layers as the corresponding minima in $|\langle S_{CD}(x)\rangle|$; the distributions to the left of the bilayers are qualitatively the same in all cases; the important difference is in the right side of the bilayers. The end segment of a long chain in a pure short-chain bilayer has non-negligible probability of being in the region of higher $|\langle S_{CD}(x)\rangle|$ near the opposite side, even reaching the layers near and beyond the maximum in $|\langle S_{CD}(x)\rangle|$. This contrasts with the case of long chains in pure long-chain bilayer where the end-segment distribution decays relatively quickly beyond the minimum of $|\langle S_{CD}(x)\rangle|$ in the midplane, so does not experience layers of higher $|\langle S_{CD}(x)\rangle|$. This suggests that the increase in $|S_{CD}(m)|$ for

segments near the chain end is due to their penetration well beyond the midplane to layers of large $\left|\langle S_{CD}(x)\rangle\right|$.

To further probe these details, we consider $\langle S_{CD}^{(1)}(x)\rangle$. They are shown in Figures 6.17 and 6.18. As described in Chapter 5, this is the average order parameter of all the units on chains attached to the left side which are on layer x. On each layer x, it includes contributions from units x to l for each chain, where l is the length of the chain. The curves all end at the same value. This is because, when $x = l$, the only contribution to $\langle S_{CD}^{(1)}(x)\rangle$ is that of the terminal unit of a fully extended chain.

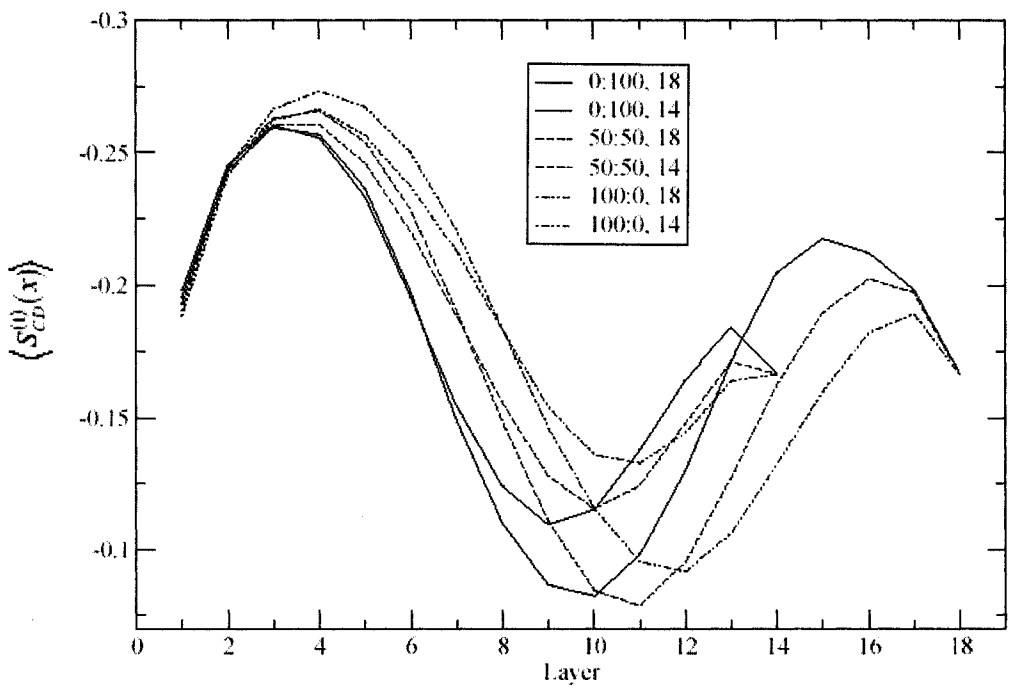

Figure 6.17

The average orientational order parameter on each layer for chains attached to the left side of binary bilayers of DSPC and DMPC. The temperature is 338 K, and the pressure is the ambient pressure. Here 0:100 means one DSPC in a bilayer of DMPC, 50:50 means equimolar mixture of DSPC and DMPC, and 100:0 means one DMPC in a bilayer of DSPC.

Layer $x = l$ has contributions only from unit $m = l$; layer $x = l - 1$ has contributions from units $m = l - 1$ and l, layer $x = l - 2$ has contributions from units $m = l - 2$, $l - 1$ and l, and so on. This implies that the layers most distant from the tethering point have contributions mainly from the far end of the chain, which are, on average, relatively disordered. One might have expected, therefore, that $\left|\left\langle S_{CD}^{(1)}(x)\right\rangle\right|$ would decrease monotonically with x, in a fashion qualitatively similar to the way $S_{CD}(m)$ normally decreases. This is, however, not the case. Instead, $\left|\left\langle S_{CD}^{(1)}(x)\right\rangle\right|$ behaves much like the other function $\left|\left\langle S_{CD}(x)\right\rangle\right|$, qualitatively following the average order parameter on each layer. Both $\left|\left\langle S_{CD}(x)\right\rangle\right|$ and $\left|\left\langle S_{CD}^{(1)}(x)\right\rangle\right|$ have an initial maximum at about the same point, and a minimum at about the same point. They both increase beyond that minimum, but the second maximum in $\left|\left\langle S_{CD}^{(1)}(x)\right\rangle\right|$ is lower than the first, and then this function terminates at layer $x = l$. For pure long chain bilayer, the left maximum of $\left|\left\langle S_{CD}^{(1)}(x)\right\rangle\right|$ of long chains is at layer 3, the minimum is at layer 12, and the right maximum is at layer 17. For one long chain in pure short-chain bilayer, the left maximum of $\left|\left\langle S_{CD}^{(1)}(x)\right\rangle\right|$ of the long chain shifts to layer 2 with decreased value, the minimum shifts to layer 10 with decreased value, and the second maximum shifts to layer 15 with increased value. The shifts are consistent with thinner bilayers, and the reduction in most values is also due to thinner bilayers. The increase in the value of the second maximum is consistent with the fact that the end segments sample regions near the second maximum in $\left|\left\langle S_{CD}(x)\right\rangle\right|$, which is due to the

chains from the right. This increase in $\left|\left\langle S_{CD}^{(1)}(x)\right\rangle\right|$ arises as chains from the left penetrate farther into the more ordered parts of the chains from the right. This observation supports the view that the second plateau is due to increased penetration of the longer chains into the region of the opposite chains which are more ordered.

Figure 6.18 shows $\left|\left\langle S_{CD}^{(1)}(x)\right\rangle\right|$ for the various binary bilayers composed of equimolar long and short chains. The temperature is 338 K.

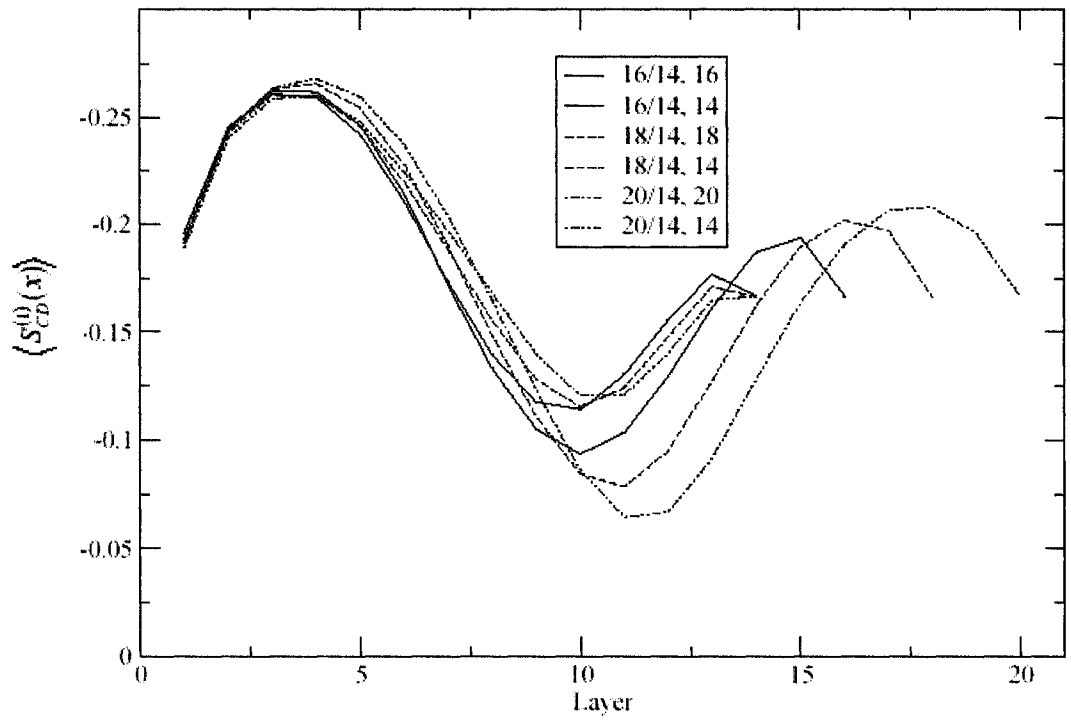

Figure 6.18

The average orientational order parameter on each layer for chains attached to the left side of equimolar binary bilayers of DPPC/DMPC, DSPC/DMPC, and DAPC/DMPC. The temperature is 338 K, and the pressure is the ambient pressure.

The results in Figure 6.18 show that at the same composition, when the chain length difference is larger, the difference between the maxima and the minimum of $\left|\left\langle S_{CD}^{(1)}(x)\right\rangle\right|$ will also be greater. This may have some relationship with the observation of larger chain length difference will lead to more prominent second plateau.

6.6 Gauche Isomers

Figure 6.19 shows the average number of gauche isomers as a function of the C–C bond number, $\eta(m)$, for the various 18/14 systems at temperature 338 K. There is some similarity between the structure of the curves in this figure and that of the curves in Figure 6.8. For $2 \le m \le 5$, the curves in both figures show a plateau-like structure. After $m \approx 5$, with increasing m, $\eta(m)$ increases, while the order parameter decreases. Both show a decreasing order toward the ends of the chains. For the long chains, after $m \approx 12$, the gauche isomer curves all show a plateau and there is a weak maximum at $m = 15$. Besides, for most m, $\eta(m)$ increases with decreasing fraction of long chains. However, after $m \approx 12$, the influence of composition on $\eta(m)$ tends to become less with increasing m. Especially for $m > 14$, $\eta(m)$ for the long chains in pure long chain bilayer becomes less than that in 50:50 mixture, or even less than that in 100:0 mixture. One can find some similarity between the behaviors described above and those shown in Figure 6.8.

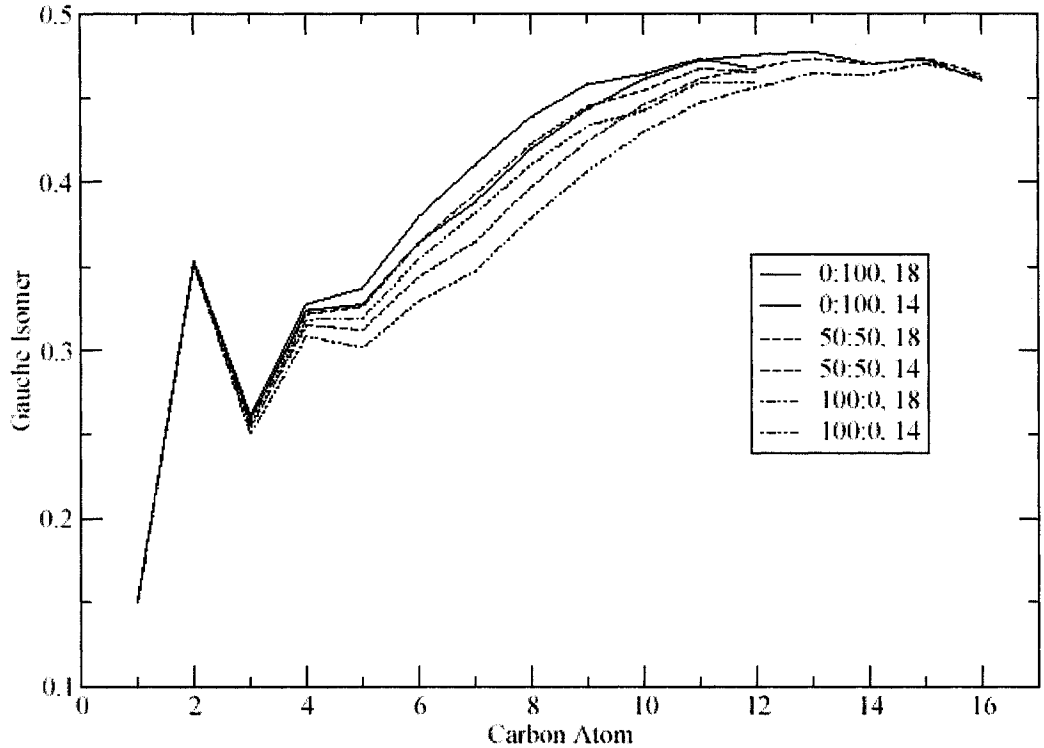

Figure 6.19

The gauche isomer profiles for binary mixtures of DSPC and DMPC. The temperature is 338 K, and the pressure is the ambient pressure. Here 0:100 means one DSPC in a bilayer of DMPC, 50:50 means equimolar mixture of DSPC and DMPC, and 100:0 means one DMPC in a bilayer of DSPC.

6.7 Experimental Comparison

Lu et al. [2] studied mixtures consisting of small concentrations of N-stearol galactosyl ceramide and N-lignoceroyl galactosyl ceramide in SOPC. N-stearol galactosyl ceramide is usually written as 18:0 GalCer or 18:0 GC; N-lignoceroyl galactosyl ceramide is usually written as 24:0 GalCer or 24:0 GC. Both 18:0 GC and 24:0 GC are glycosphingolipids, which have a single acyl chain, attached by an amide linkage to a sphingosine backbone. The length of the acyl chain of 18:0 GC is 18, and the length of the acyl chain of 24:0 GC is 24. The acyl chains of both 18:0 GC and 24:0 GC have no

double bonds. The chain length of SOPC is 18, and there is one double bond per SOPC molecule.

In Figure 6.20, there are two experimental systems, one is 10 mol% 24:0 GC in SOPC; the other is 10 mol%18:0 GC in SOPC; the temperatures for the experiments are 325 K. The theoretical system in Figure 6.20 is 24/18 mixture with 5% long chains. We make such choice of composition because there is only one acyl chain of length 24 per 24:0 GC and the chain length of the sphingosine is 18 or near 18.

In Figure 6.20, we show the orientational order parameter profile for the single acyl chain of glycosphingolipids of both 24:0 GC and 18:0 GC in the experiments, and show the profiles for both DLPC and DSPC in the theoretical system. The gel/liquid main transition temperature of SOPC is 6 ^{o}C, so the experimental temperature is 46 ^{o}C above the transition temperature. The theoretical gel/liquid transition temperature for DSPC is about 48 ^{o}C, so we conduct calculation at 48 + 46 = 94 ^{o}C, which is 367 K.

In the thesis of Lu [27], it was first argued that the order parameter profile for the single acyl chain of glycosphingolipid of 18:0 GC in Figure 6.20 can be used to approximate that of SOPC in the 24:0 GC/SOPC experiment. The following three conclusions were then drawn for 24:0 GC and SOPC in the 24:0 GC/SOPC experiment shown in Figure 6.20:

1. Their order parameters are very close to each other from C(2) to C(15);
2. For each segment from C(16) to C(18), the magnitude of the order parameter of 24:0 GC is greater than that of SOPC;

3. The $|S_{CD}(m)|$ from C(19) to C(24) for 24:0 GC are all smaller than $|S_{CD}(17)|$ for SOPC, which leads to the second plateau in the profile of 24:0 GC.

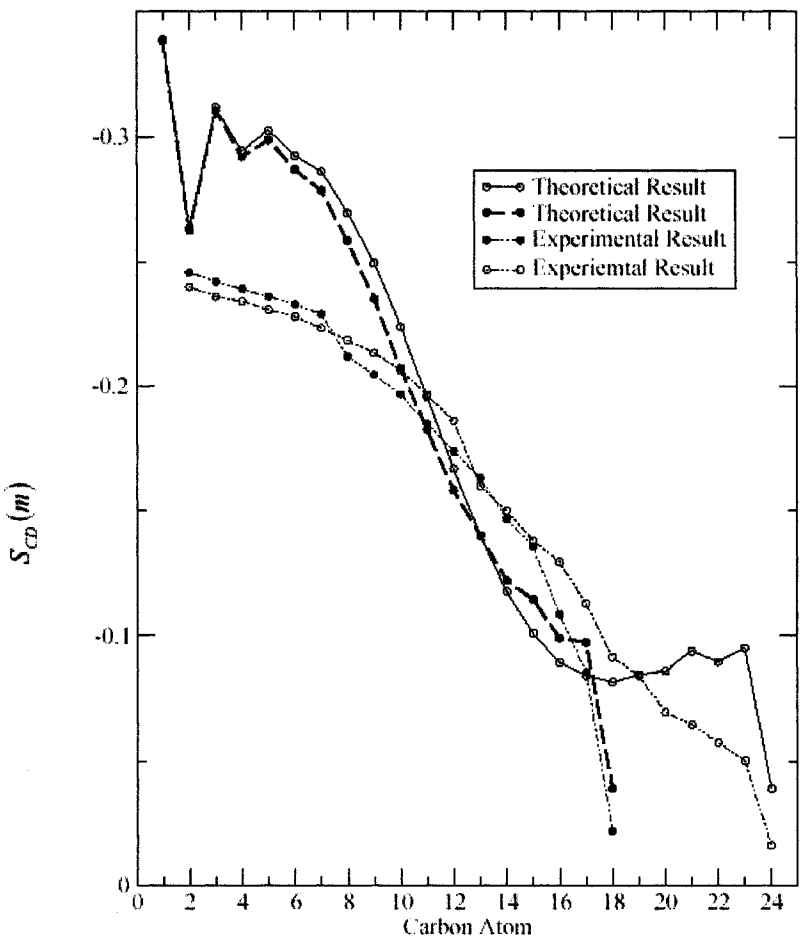

Figure 6.20

The orientational order parameter profiles. There are two experimental systems: one is 10 mol% 24:0 GC in SOPC, and the other is 10 mol% 18:0 GC in SOPC; the temperatures for the experiments are 325 K. The theoretical system is binary mixture of DLPC and DSPC with 5% DLPC, at a temperature of 367 K. The green line is for the single acyl chain of glycosphingolipids 18:0 GC, the blue line is for the single acyl chain of glycosphingolipids 24:0 GC, the red broken line is for DSPC, and the black line is for DLPC.

These conclusions can be compared with the calculation results shown in Figure 6.20.

For conclusion 1, the calculation results also show that orientational order parameter profiles of the short and long chains are about the same over the length of short chains. The calculation does not agree with conclusion 2. For conclusion 3, the calculated $|S_{CD}(m)|$ from C(19) to C(24) for the long chains are also smaller than $|S_{CD}(17)|$ for the short chains, and the long chains have also the second plateau, but the nature of the second plateau is different: there is a monotonic decrease in the experiment, but an increase in the theoretical results.

There are double bonds on the lipids in majority, SOPC, in the above experimental system, which will considerably lower the gel/liquid main transition temperature, and influence the environment. Because our present model does not consider double bond, we will next make comparison with the experimental systems that have no double bonds.

Figure 6.21 shows the calculated orientational order parameter profiles for DSPC/DMPC blends of various compositions at 333 K. Lu, Vavasour and Morrow have done the experiments for the same systems at the same temperature [3]. Their smoothed profiles are shown in Figure 6.22. The chain length difference is four for the present system.

In all the panels of Figure 6.22, the filled squares and circles are, respectively, the smoothed orientational order parameter profiles of DSPC in single component bilayers of DSPC, and DMPC in single component bilayers of DMPC. In panel (a), the open squares and circles are, respectively, the smoothed orientational order parameter profiles of DSPC and DMPC in binary bilayers of DSPC and DMPC with 25 mol% DSPC. In panel (b), the open squares and circles are, respectively, the smoothed orientational order

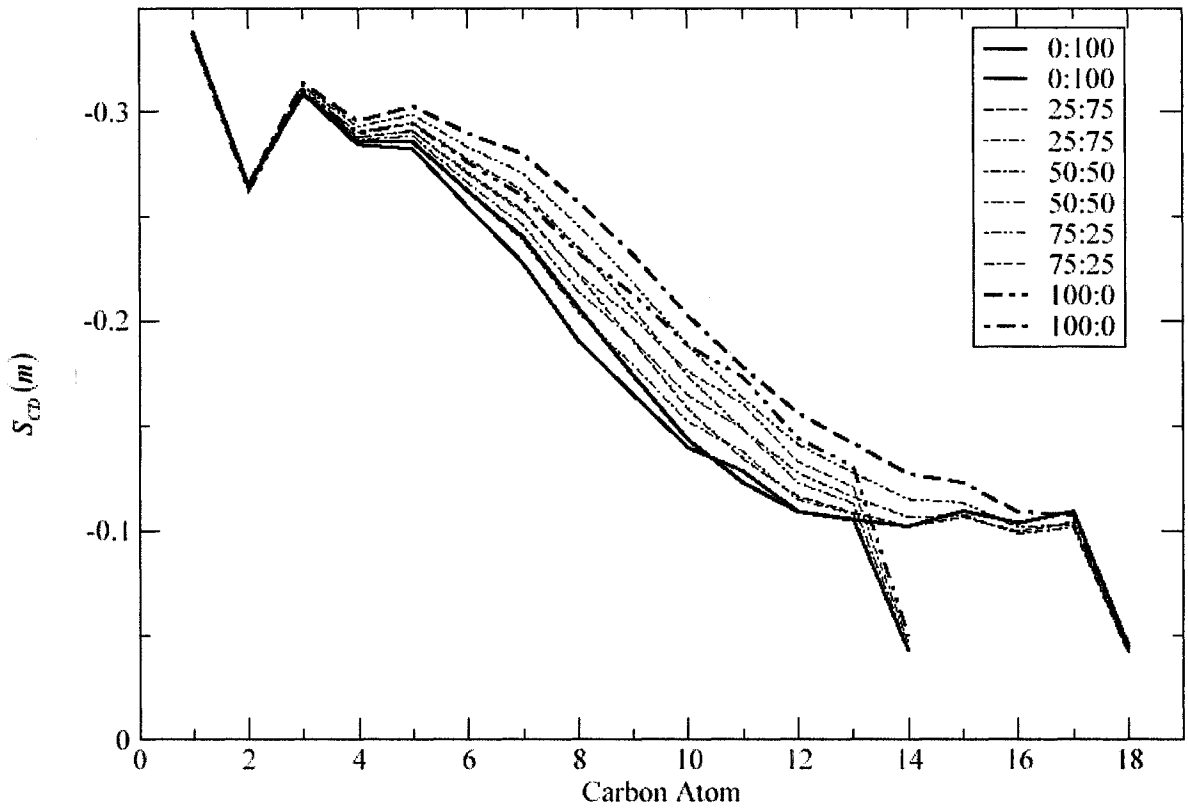

Figure 6.21

Calculated orientational order parameter profiles for mixtures of DSPC and DMPC. The temperature is 333 K, and the pressure is the ambient pressure. Here 0:100 means one DSPC in a bilayer of DMPC, 100:0 means one DMPC in a bilayer of DSPC, 25:75 means mixture with 25% DSPC, and etc.

parameter profiles of DSPC and DMPC in bilayers of equimolar DSPC and DMPC. In panel (c), the open squares are the smoothed orientational order parameter profile of DSPC in bilayers of DSPC and DMPC with 75 mol% DSPC. The open circles are the smoothed orientational order parameter profile of DMPC in bilayers of DSPC and DMPC with 70 mol% DSPC. The experimental results show a plateau for $m \leq 8$, then $|S_{CD}(m)|$ decreases quickly with m. In panel (a), except for the last carbon atom, the order

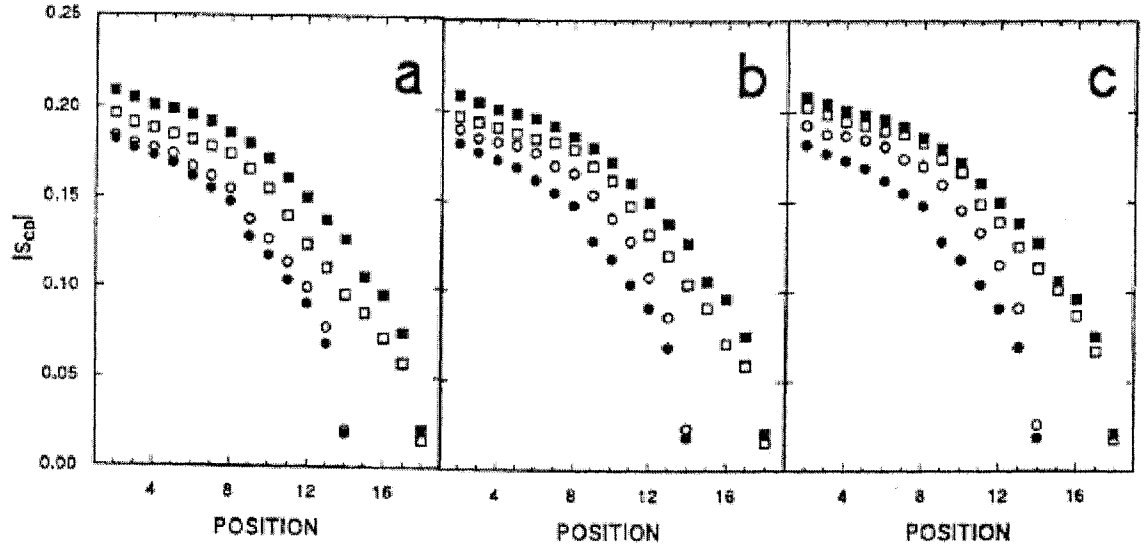

Figure 6.22

Experimental smoothed orientational order parameter profiles at 333 K. (*a*) DSPC-d_{70} (■), DMPC-d_{54} (●), DMPC-DSPC-d_{70} at f_{DSPC} = 0.25 (□), DMPC-d_{54}-DSPC at f_{DSPC} = 0.25 (○). (*b*) DSPC-d_{70} (■), DMPC-d_{54} (●), DMPC-DSPC-d_{70} at f_{DSPC} = 0.50 (□), DMPC-d_{54}-DSPC at f_{DSPC} = 0.50 (○). (c) DSPC-d_{70} (■), DMPC-d_{54} (●), DMPC-DSPC-d_{70} at f_{DSPC} = 0.75 (□), DMPC-d_{54}-DSPC at f_{DSPC} = 0.70 (○). Here f_{DSPC} is the fraction of DSPC.

parameter profile for DSPC in bilayers with 25 mol% DSPC is considerably closer to the order parameter profile for DMPC in pure DMPC bilayer than is the profile for DSPC in pure DSPC bilayer. However, the ending points of both the two DSPC profiles are very close. Consequently, compared with the order parameter profile of DSPC in pure DSPC bilayers, the magnitude of the order parameter profile of DSPC in bilayers of 25 mol% DSPC has a lower starting point, and decreases faster from C(9) to C(12), then decreases more slowly after C(12), and reaches an ending point closer to that of pure DSPC bilayers. So we can notice that, from C(14) to C(17), the order parameter profile of DSPC in bilayers of 25 mol% DSPC is not as steep as that in bilayers of pure DSPC. This phenomenon was called the appearance of a "second plateau" by Lu et al. [3]. In panel

(b), the percentage of DSPC is doubled, and the second plateau becomes less clear. In panel (c), the DSPC are in majority, and there is almost no such structure. If we compare the three panels, we can see that except the ending points, with the increase of DSPC percentage, the order parameter profile of DMPC becomes closer to that of DSPC in pure DSPC bilayer, and with the increase of DMPC percentage, the order parameter profile of DSPC becomes closer to that of DMPC in pure DMPC bilayer. The ending points seem to depend weakly on composition. The middle parts of the order parameter profiles are sensitive to composition change.

In our calculation results, $|S_{CD}(m)|$ fluctuates until $m \approx 7$, then decreases fast and monotonically until $m \approx 12$. Here, the $|S_{CD}(m)|$ of short chains continues its fast decrease, while that of the long chains shows the second plateau, especially in mixtures that the long chains are in minority.

One can also notice that in theoretical results the various orientational order parameter profiles all start at approximately the same point, and the ending points for the long chains and short chains separately are also similar. The largest differences for different compositions happen at the middle of the chains. Nagle has pointed out that [28] the orientational order parameter near the headgroup end of the acyl chains reflects the area per lipid molecule in the bilayer. The experimental results show that it is true only for very dilute binary mixtures that the orientational order parameter profiles for different compositions start at approximately the same point. But they also show, as do our theoretical results, that for long or short chains separately, after the middle of a chain, the

orientational order parameters for various compositions become progressively similar to each other until they have very close ending points.

In addition, both the theoretical and experimental results support that for a mixture with a high fraction of one component, the orientational order parameter profile of the major component becomes insensitive to composition change and is closest to that for single component bilayer of this major component, and the orientational order parameter profile of the minor component progressively approaches that of the major component.

The experimental results [3] show that with the increase of the long chain percentage, the plateau of the DMPC profile is extended, and with the increase of the short chain percentage, the phenomenon of the second plateau in DSPC profile become clearer, as we have described. From Figure 6.21, one can see that for DMPC, the $|S_{CD}(m)|$ values increase with increasing fraction of DSPC, and for the left half of the DMPC chain, the rate of the change of $|S_{CD}(m)|$ with composition increases with m. This extends the plateau region of the orientational order parameter profile of DMPC with increasing fraction of DSPC. For the right half of the DSPC chain, as discussed in section 6.4.2, with the increasing percentage of DMPC, the second plateau in the orientational order parameter profile of DSPC appears and becomes more clear. All these observations are in agreement with the experiment [3].

The experiment [3] also tells us that the difference between the DSPC and DMPC in mean chain extension at a given temperature is almost independent of composition. The theoretical results of the average orientational order parameter vs. composition for the above DSPC/DMPC system are shown in Figure 6.23. One can see that the lines for

DSPC and DMPC are almost parallel. At the left end, i.e., one DSPC in DMPC bilayer, the difference, which may be the largest among all compositions, is 0.019; while at the right end, i.e., one DSPC in DMPC bilayer, the difference, which may be the smallest among all the compositions, is 0.017. The difference between these two values is only 10%. This means that at a certain temperature the difference in average orientational order parameter of long and short chains is only weakly dependent on composition. The mean chain extension can be approximately related to the average order parameter by the following formula [38].

$$\langle l \rangle = l_0 n(0.5 - \bar{S}_{CD}) \tag{6.7}$$

where $l_0 = 1.25\,\text{Å}$, and n is the number of bonds per chain. In the derivation of this equation, it is assumed that the bonds not pointing towards the bilayer center are rare and can be neglected. With this equation, we can calculate the mean chain extensions for both the long and short chains. They are shown in Table 6.2.

Table 6.2

The calculated mean chain extensions for various binary mixtures of DSPC and DMPC. The temperature is 333 K. the pressure is the ambient pressure.

Percentage of DSPC	Mean Chain Extension (Å)		Difference of the Mean Chain Extensions (Å)
	DSPC	DMPC	
0	15.40	12.30	3.10
25	15.50	12.40	3.10
50	15.62	12.49	3.13
75	15.77	12.59	3.18
100	15.95	12.70	3.25

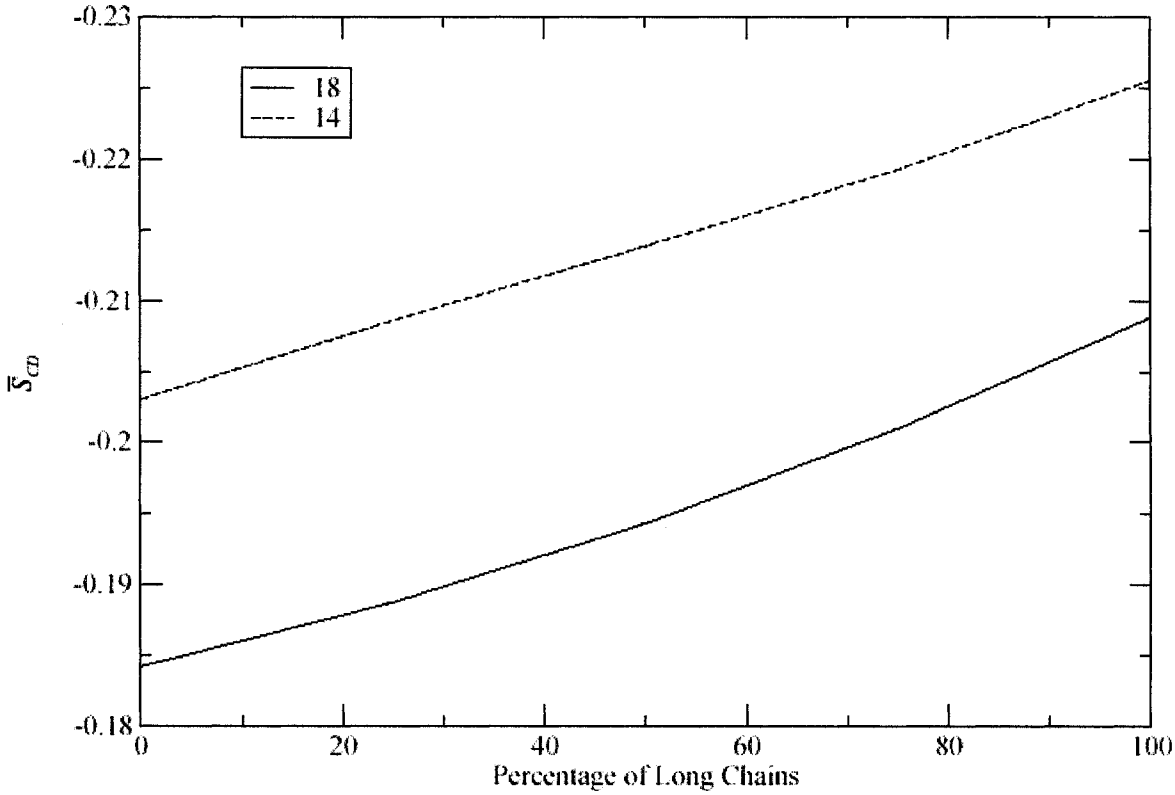

Figure 6.23

The relationship between the calculated average orientational order parameter and the percentage of DSPC, for mixtures of DSPC and DMPC. The temperature is 333 K, and the pressure is the ambient pressure.

The smallest difference between the mean chain extensions of DSPC and DMPC is about 3.1 $\mathring{A}$, which happens at one DSPC molecule in a DMPC bilayer, and the largest difference is about 3.3 $\mathring{A}$, which happens at one DMPC molecule in a DSPC bilayer. The change is only about 5%. This means that at a given temperature, the difference in mean extensions of the long and short chains depends only weakly on composition. Using Equation 6.7, Lu et al. [3] found that DSPC chain extends about 3.1 $\mathring{A}$ further than the

DMPC chain for all the experimental results shown in Figure 6.22. This is in good agreement with our calculation results.

Whitmore et al. [1] have mentioned several possible reasons for large order parameter values near the headgroup such as sharp headgroup/hydrocarbon interface, failure to exclude all $g^{\pm}g^{\mp}$ bond sequences (Here g^{+} and g^{-} denote gauche isomers rotating in the opposite direction. Because $g^{+}g^{-}$ and $g^{-}g^{+}$ sequences can lead to extremely strong overlap between hydrogen atoms bonded to carbon atoms, they should be eliminated in statistical-mechanical calculations), and the ordering effect introduced by placing all the chains on a lattice. Another possible reason may be the neglect of the headgroup movement. The headgroups can rotate and tilt about the bilayer normal, and there are also conformational fluctuations in headgroups. These can also decrease the order of the hydrocarbon units near the headgroups. However, the model does not include them. Besides, Seelig et al. have pointed out that the smoothed profiles may be not an accurate reflection of the detailed behavior near the headgroup end of the chain [29]. Several experiments [30, 31] also show that there exists variation in the plateau region of the smoothed profile, although it may not be big enough to fully explain the discrepancy.

For the composition independence of the plateau value in our model, one explanation may be that since the plateau value is relevant to the difference between the temperature and the main transition temperature, while our model predicts a weaker dependence of the main transition temperature on the chain length, consequently the calculated plateau value will also have weaker dependence on the chain length, and thus similar plateau values for long and short chains and their mixtures.

Chapter 7

Conclusions

In this thesis, we made calculations for DPPC/DMPC, DSPC/DMPC and DAPC/DMPC at various compositions, at a temperature of 338 K, and ambient pressure. The temperature and pressure ensure that all these systems are in liquid crystal phase. The chain lengths of DMPC, DPPC, DSPC and DAPC are respectively 14, 16, 18 and 20.

In section 4.2, for the model of binary bilayers, we re-derived the stability criteria: a mixture will be unstable, metastable, and stable, respectively, in the regions between neighboring spinodals, between a spinodal and neighboring binodal, and the other regions. If the second derivative of the partial relative Gibbs free energy $\Delta G_l / N_l$ is not negative for all the compositions, the mixtures under constant pressure have no phase separation. We plotted the curves of $\Delta G_l / N_l$ vs. composition for all these binary mixtures and saw positive curvature for all the compositions, which ensures that there is no phase separation in all of them. We also found that, under the same environment, the partial Gibbs free energy of single-component bilayers increases with chain length, so the transition temperature also increases with chain length, and at a given composition, mixing with lipids with longer chains will result in higher Gibbs free energy, and thus will lead to higher phase transition temperatures.

For the average order parameter, our results give the following conclusions. For single-component bilayers, the average order parameter increases with chain length. In binary mixtures, at any composition, the average order parameter of the short chains is

always larger in magnitude than that of the long chains. This shows that in order to be accommodated, the long chain has to be more disordered than the short chain. With the increase of short-chain percentage, the magnitude of the average order parameter of both long and short chains will decrease; one reason for this may be that the chains have to be more disordered to adapt to a thinner bilayer since the thickness also decreases with the increase of short-chain percentage.

From our calculated results for order parameter profiles, one can obtain the following conclusions. Except very near the headgroup, the order parameter for pure long-chain bilayer is larger at each unit than that for pure short-chain bilayer, and this difference increases with the chain length difference. With the decrease of the long-chain percentage, the order parameter profile of the long chain will move close to that of short chain in pure short-chain bilayer until they overlap in dilute long-chain mixture. With the decrease of the short-chain percentage, the order parameter profile of the short chain will move close to that of long chain in pure long-chain bilayer, but their difference remains even in dilute short-chain mixture, and this difference also increases with the chain length difference. When the long chains are in minority, a second plateau appears, and it becomes more prominent with the increase of short-chain fraction and chain length difference. The starting and ending points of order parameter profile seem to depend only weakly on chain length and composition.

The second plateau may be due to the penetration of bilayer midplane by the long chains. With this assumption in mind, we first plotted the thickness/composition curves

for all the above systems, and found that the bilayer thickness increases almost linearly with long-chain percentage.

After knowing the thickness for each system, the penetration of the bilayer midplane can be seen directly from the distribution of the last segment. Our results show that the maxima of the distribution profiles for the long chains occur at approximately the bilayer midplane and the long chains have considerable probability of reaching beyond the bilayer midplane. For short chains, if they are in minority, the maximum in the distribution of its last segment occurs before the midplane, especially when the chain length difference is large.

We then turned to the average order parameter on each layer, $\langle S_{CD}(x) \rangle$, which reflects the inner environment of bilayers. Our results show that $|\langle S_{CD}(x) \rangle|$, which is symmetric about the midplane, has a maximum a distance of about 1/6 thickness from each side, and a minimum at the center. When we compared the distribution of the last segment to $\langle S_{CD}(x) \rangle$, things became clearer: the lower the long-chain percentage, the thinner the bilayer is, and the farther the long chains penetrate into the opposite side. This increases the probability that the long chains sample the maximum of $|\langle S_{CD}(x) \rangle|$ at the other side. This can be explained in more detail as follows. The maxima in the segment distributions of the long chains are at about the same position, the midplanes of bilayers, as the corresponding minima in $|\langle S_{CD}(x) \rangle|$. The distributions to the left of the bilayers are approximately the same in all cases. The important difference is in the right side of the bilayers. The end segment of a long chain in pure short-chain bilayers has a relatively

high probability of sampling the region of higher $\left|\left\langle S_{CD}(x)\right\rangle\right|$ near the opposite side and even reaching the layers near and beyond the maximum in $\left|\left\langle S_{CD}(x)\right\rangle\right|$. This is not the case for long chains in pure long-chain bilayer where the end-segment distribution decays relatively quickly beyond the minimum of $\left|\left\langle S_{CD}(x)\right\rangle\right|$ in the midplane, so does not sample layers of higher $\left|\left\langle S_{CD}(x)\right\rangle\right|$. This suggests that the increase in $S_{CD}(m)$ for segments near the free end, and consequently the second plateau, are because these segments penetrate well beyond midplane to layers of large $\left|\left\langle S_{CD}(x)\right\rangle\right|$.

We probed this further by calculating the average order parameter on each layer of the segments on long or short chains anchored to the left side, $\left\langle S_{CD}^{(1)}(x)\right\rangle$. It qualitatively follows $\left\langle S_{CD}\langle x\rangle\right\rangle$ instead of $S_{CD}(m)$, although the right maximum of $\left|\left\langle S_{CD}^{(1)}(x)\right\rangle\right|$ is lower than its left maximum. With the increase of the short-chain percentage, the bilayer becomes thinner, and the minimum and maxima shift left. Meanwhile, the left maximum becomes lower because the chains become more disordered to adapt to a thinner bilayer, while the right maximum becomes higher because the end segments can sample region of second maximum in $\left|\left\langle S_{CD}(x)\right\rangle\right|$. We also found that at the same composition, when the chain length difference is larger, the difference between the maxima and the minimum of $\left|\left\langle S_{CD}^{(1)}(x)\right\rangle\right|$ will also be greater. This may have some relationship with the observation of larger chain length difference will lead to more prominent second plateau. Another interesting observation about $\left\langle S_{CD}^{(1)}(x)\right\rangle$ is that they all end at the same value of -1/6,

which is because the only contribution to $\langle S_{CD}^{(1)}(l)\rangle$, where l is the chain length, is that of the terminal unit of a fully extended chain.

There is some similarity between the gauche isomer profile and the order parameter profile, which may be because the larger gauche isomer number means the more disordered states, and thus the lower order parameter.

To compare with the experiment on GalCer in SOPC by Lu et al. [2], we made calculations for 24/18 mixture with 5% long chains at 367 K. Consistent with the experiment [2], the calculations give the orientational order parameter profiles for the short and long chains that are about the same over the length of short chain, the calculated $|S_{CD}(m)|$ from C(19) to C(24) for the long chains are also smaller than $|S_{CD}(17)|$ for the short chains, and the long chains also have a second plateau. However, the nature of the second plateaus is very different: there is a monotonic decrease in experiment, but an increase in the theoretical results.

To compare with the experiment on DSPC/DMPC mixture at 333 K by Lu et al. [3], we made calculation for 18/14 mixtures of various compositions at 333 K. The chain length difference is four for this system. The experimental results show a plateau for $m \leq 8$, then $|S_{CD}(m)|$ decreases quickly and monotonically with m; for the mixtures that the long chains are in minority, there is a modest second plateau near the free end of the long chains. In our calculations, $|S_{CD}(m)|$ fluctuates until $m \approx 7$, then decreases fast and monotonically until $m \approx 12$. Here the $|S_{CD}(m)|$ of short chains continues its fast decrease,

while that of the long chains shows the second plateau, especially in mixtures that the long chains are in minority.

In the theoretical results, the various orientational order parameter profiles all start at approximately the same value, and the ending points for the long chains and short chains separately are also similar. The largest differences for different compositions happen in between. The experimental results show that it is true only for very dilute binary mixtures that the orientational order parameter profiles for different compositions start at approximately the same point. But they also show, as our theoretical results, that for long or short chains separately, after the middle of a chain, the orientational order parameters for various compositions become progressively similar to each other until they have very close ending points.

Besides, both the theoretical and experimental results show that, for a mixture with a high fraction of one component, the orientational order parameter profile of the major component becomes insensitive to composition change and is close to that for single component bilayer of this major component, and the orientational order parameter profile of the minor component progressively approaches that of the major component.

Both the theoretical and the experimental results [3] show that with the increase of the long chain percentage, the plateau of the DMPC profile is extended, and with the increase of the short chain percentage, the DSPC profile begins showing clearer second plateau.

At any given temperature, in agreement with the experiment [3], the difference in the mean extensions of the long and short chains depends only weakly on composition.

In the future, the following two problems should be addressed:

1. The theoretical results give more prominent second plateaus than experimental results do;
2. The theoretical results give larger order parameter value near the headgroup than experimental results do.

The first problem, within the present model, according to the argument in section 6.5, could be due to penetration, i.e., the theory may predict greater penetration than the true bilayers do. However, it is also possible that we obtain the correct description of penetration, but higher maxima of $\left|\langle S_{CD}(x)\rangle\right|$ near headgroups than true bilayers. After all, the present theory indeed predicts higher order parameter values near the headgroups, which is the second problem noted above. So in the near future we should manage to decide which one is the dominant reason.

For the second problem, in section 6.6, we have mentioned the possible reasons such as sharp headgroup/hydrocarbon interface, failure to exclude all $g^{\pm}g^{\mp}$ bond sequences, the ordering effect introduced by placing all the chains on a lattice, and the neglect of the headgroup movement. So we can next attempt a more detailed model of headgroup, headgroup movement and fluctuation, and headgroup/solvent interactions, and see what changes to the results can be brought about. The progress in the second problem may also bring down the maxima of $\left|\langle S_{CD}(x)\rangle\right|$, and thus help the solution of the first problem.

Bibliography

1. M. D. Whitmore, J. P. Whitehead, and A. Roberge. *Can. J. Phys.* **76**, 831 (1998).
2. Dalian Lu, D. Singh, M. R. Morrow, and C. W. M. Grant. *Biochemistry*, **32**, 290 (1993).
3. Dalian Lu, I. Vavasour, and M. R. Morrow. *Biophys. J.* **68**, 574 (1995).
4. G. Cevc and D. Marsh. *Phospholipid Bilayers: Physical Principles and Models.* Wiley-Interscience, New York. 1987
5. M. R. Morrow, R. Srinivasan, and N. Grandal. *Chemistry and Physics of Lipids*, **58**, 63 (1991).
6. M. Bloom, J. H. Davis, and A. L. MacKay. *Chem. Phys. Lett.* **80**, 198 (1981).
7. E. Sternin, M. Bloom, and A. L. MacKay. *J. Magn. Res.* **55**, 274 (1983).
8. Y. Lee and S. I. Chan. *Biochemistry*, **16**, 1303 (1977).
9. M. E. J. Newman and G. T. Barkema. *Monte Carlo Methods in Statistical Physics.* Oxford University Press Inc., New York. 1999.
10. F. A. M. Leermakers and J. M. H. M. Scheutjens. *J. Chem. Phys.* **89**, 3264 (1988).
11. F. A. M. Leermakers and J. M. H. M. Scheutjens. *J. Chem. Phys.* **89**, 6912 (1988).
12. L. A. Meijer, F. A. M. Leermakers, and J. Lyklema. *Recl. Trav. Chim. Pays-Bas*, **113**, 167 (1994).
13. L. A. Meijer, F. A. M. Leermakers, and J. Lyklema. *J. Chem. Phys.* **99**, 17282 (1995).
14. J. Geehan. *Self-Consistent Field Theory of Compressible Bilayers: Mixtures of Two Different Chain Length Phospholipids, B.Sc. Thesis*, Memorial University of Newfoundland, St. John's, Canada (2002).

15. S. Marčelja. *Nature*, **241**, 451 (1973).

16. S. Marčelja. *Biochim. Biophys. Acta*, **367**, 165 (1974).

17. J. –P. Meraldi and J. Schlitter. *Biochim. Biophys. Acta*, **645**, 183 (1981).

18. J. –P. Meraldi and J. Schlitter. *Biochim. Biophys. Acta*, **645**, 193 (1981).

19. D. W. R. Gruen. *Biochim. Biophys. Acta*, **595**, 161 (1980).

20. D. W. R. Gruen. *J. Phys. Chem.* **89**, 146 (1985).

21. D. W. R. Gruen. *J. Phys. Chem.* **89**, 153 (1985).

22. F. Schmid and M. Schick. *J. Chem. Phys.* **102**, 2080 (1995).

23. P. J. Flory. *Statistical Mechanics of Chain Molecules*. Wiley, New York. 1969.

24. E. A. Dimarzio. *J. Chem. Phys.* **66**, 1160 (1976).

25. P. J. Flory. *Principles of Polymer Chemistry*. Cornell University Press, London. 1953.

26. M. R. Morrow, J. P. Whitehead, and D. Lu. *Biophys. J.* **63**, 18 (1992).

27. Dalian Lu. *Effects of Chain Length and Chain Length Mismatch on Orientational Order in Fluid State Lipid Bilayer Membranes, Ph.D. Thesis*, Memorial University of Newfoundland, St. John's, Canada (1995).

28. J. F. Nagle. *Biophys. J.* **64**, 1476 (1993).

29. J. Seelig and A. Seelig. *Q. Rev. Biophys.* **13**, 19 (1980).

30. A. Seelig and J. Seelig. *Biochemistry*, **13**, 4839 (1974).

31. M. R. Morrow and D. Lu. *Chem. Phys. Lett.* **182**, 435 (1991).

32. A. J. Robinson, W. G. Richards, P. J. Thomas, and M. M. Hann. *Biophys. J.* **67**, 2345 (1994).

33. R. Mendelsohn, M. A. Davies, J. W. Brauner, H. F. Schuster, and R. A. Dluhy. *Biochemistry*, **28**, 8934 (1989).

34. E. Oldfield, M. Meadows, D. Rice, and R. Jacobs. *Biochemistry*, **17**, 2727 (1978).

35. Z. –C. Xu and D. Cafiso. *Biophys. J.* **49**, 779 (1986).

36. J. F. Nagle. *Biophys. J.* **64**, 1476 (1993).

37. A. Brown, I. Skanes, and M. R. Morrow. *Phys. Rev.* **E69**, 011913 (2004).

38. H. Schindler and J. Seelig. *Biochemistry*, **14**, 2283 (1975).

39. J. Stamatoff, D. Guillon, L. Powers, and P. Cladis. *Biochem. Biophys. Res. Commun.* **85**, 724 (1978).

40. L. F. Braganza and D. L. Worcester. *Biochemistry*, **25**, 2591 (1986).

41. R. Winter and W. –C. Pilgrim. *Ber. Bunsenges. Phys. Chem.* **93**, 708 (1989).

42. I. P. Sugár, T. E. Thompson, and R. L. Biltonen. *Biophys. J.* **76**, 2099 (1999).

43. E. I. Michonova-Alexova and I. P. Sugár. *Biophys. J.* **83**, 1820 (2002).

44. T. Zaraiskaya and K. R. Jeffrey. *Biophys. J.* **88**, 4017 (2005).

45. A. A. Gurtovenko, M. Patra, M. Karttunen, and I. Vattulainen. *Biophys. J.* **86**, 3461 (2004).